MONITORING AND CONTROL OF LOW FREQUENCY OSCILLATIONS IN POWER SYSTEM

Ph.D. Thesis

ABHILASH KUMAR GUPTA
I.D. No. 2014REE9517

DEPARTMENT OF ELECTRICAL ENGINEERING

MALAVIYA NATIONAL INSTITUTE OF TECHNOLOGY JAIPUR

JUNE 2019

MONITORING AND CONTROL OF LOW FREQUENCY OSCILLATIONS IN POWER SYSTEM

Submitted in

fulfilment of the requirements for the degree of

Doctor of Philosophy

by

ABHILASH KUMAR GUPTA
ID: 2014REE9517

Under the Supervision of

Dr. Kusum Verma and Prof. K. R. Niazi

DEPARTMENT OF ELECTRICAL ENGINEERING

MALAVIYA NATIONAL INSTITUTE OF TECHNOLOGY JAIPUR

JUNE 2019

DECLARATION

I, **Abhilash Kumar Gupta**, declare that this thesis titled, **"Monitoring and Control of Low Frequency Oscillations in Power System"** and the work presented in it, are my own. I confirm that:

- This work was done wholly or mainly while in candidature for a research degree at this university.
- Where any part of this thesis has previously been submitted for a degree or any other qualification at this university or any other institution, this has been clearly stated.
- Where I have consulted the published work of others, this is always clearly attributed.
- Where I have quoted from the work of others, the source is always given. With the exception of such quotations, this thesis is entirely my own work.
- I have acknowledged all main sources of help.
- Where the thesis is based on work done by myself, jointly with others, I have made clear exactly what was done by others and what I have contributed myself.

Date:

Abhilash Kumar Gupta
(2014REE9517)

CERTIFICATE

This is to certify that the thesis entitled **"Monitoring and Control of Low Frequency Oscillations in Power System"** being submitted by **Mr. Abhilash Kumar Gupta (2014REE9517)** is a bonafide research work carried out under our supervision and guidance in fulfillment of the requirement for the award of the degree of **Doctor of Philosophy** in the Department of Electrical Engineering, Malaviya National Institute of Technology, Jaipur, India. The matter embodied in this thesis is original and has not been submitted to any other University or Institute for the award of any other degree.

Place:
Date:

(Dr. Kusum Verma) (Dr. K. R. Niazi)
Associate Professor Professor
Department of Electrical Engineering
MNIT Jaipur

This Thesis is dedicated to
My Dear Parents

ACKNOWLEDGEMENT

I started writing this thesis with the "simple" purpose of digesting the work of four years of my doctoral studies. Almost immediately, I realized that I was not the only contributor to this work. In the following few paragraphs I will try to acknowledge the people that played a role, smaller or bigger, in making this PhD a reality.

First and foremost, I would like to extend my sincerest and heartfelt gratitude to my supervisors, ***Dr. Kusum Verma*** (Associate Professor, Department of Electrical Engineering, MNIT Jaipur) and ***Dr. K. R. Niazi*** (Professor, Department of Electrical Engineering, MNIT Jaipur) for their constant encouragement and guidance which helped me to conceptualize the research plan for my thesis work. When I got admission in doctoral program in January 2015, I had little knowledge of what research is. Over the next years, they help me develop valuable skills as a researcher and as an academic and devoted their time to transfer their theoretical and practical understanding of power systems to me. They have always encouraged and trusted me to venture on new ideas, which incented me to widen my research from various perspectives. I am highly indebted to them for their supervision and valuable suggestions for successful completion of my PhD work. It was a great opportunity to complete my doctoral study under their guidance.

I wish to express my gratitude to each member of the Departmental Research Evaluation Committee (DREC), ***Prof. Rajesh Kumar***, ***Prof. Vikas Gupta*** and ***Prof. Rajive Tiwari*** for their valuable comments and suggestions during the course of my doctoral work. Throughout the process, I have been greatly benefited from the feedbacks of DREC members.

My sincere thanks to ***Prof. Udaykumar R Yaragatti***, Director, MNIT Jaipur, ***Prof. Rajesh Kumar***, HOD, Department of Electrical Engineering, MNIT Jaipur and ***Prof. Harpal Tiwari***, DPGC Convener, Department of Electrical Engineering, MNIT Jaipur for providing the required infrastructural facilities. I am also thankful to all the faculty members and staff of the Electrical Engineering Department, MNIT Jaipur for promptly offering their support and advice whenever needed.

I would also like to thank my colleagues, ***Dr. Nand Kishor Meena, Dr. Saurabh Ratra, Dr. Dhanraj Chitara, Dr. Sujil A., Mr. Ajeet K Singh, Mr. Pranda Prasanta Gupta, Mr. Jay Prakash Keshri, Mr. Vikram Singh, Mr. Rayees A Thokar, Mr.***

Sachin Sharma, Ms. Vishu Gupta *and* ***Mr. Tanuj Rawat***, for their help and encouragement which enabled me to complete my PhD work.

My four years at MNIT Jaipur were nothing less than wonderful despite the hardships PhD offers, only because of constant support of some awesome friends I made during my doctoral studies. I feel profound pleasure to thank ***Mr. Pradeep Singh, Ms. Akanksha Shukla*** and ***Ms. Venu Sangwan*** for giving me the moments to cherish for life and making my stay at MNIT memorable. My heartiest thanks to ***Akanksha*** and ***Pradeep*** for being my pillars of strength in my ups and downs. I treasure the shared precious moments.

I would like to thank my father, ***Mr. Shyam Sunder Gupta***, my mother, ***Mrs. Komal Gupta*** and my sister, ***Ms. Aparna Gupta*** for their continuous support, patience, understanding and firm belief in me throughout this period. Thank you for everything.

Also, I would like to take this opportunity to convey my thanks to all those individuals who have directly or indirectly provided me with invaluable assistance for completion of this PhD.

Above all, I am thankful to the Almighty ***God*** for showing me the right path and showering his blessings towards me in all walks of my life.

Thank you everyone.

(Abhilash Kumar Gupta)

ABSTRACT

The dynamics of modern power grids are becoming increasingly complex as they are hugely interconnected and working in highly stressed operating conditions. The increasing energy demand, utilities deregulation, environmental concerns, increasing renewable penetration and limited investment in new transmission facilities is forcing the modern power systems to utilize their existing resources to the maximum limits. This further brings the system closer to its stability limits. For the power systems operating in such stressed and complex operating conditions, maintaining system stability is a challenging task. In power systems, instability or collapse can occur when the system is subjected to unusually high stress. The electromechanical oscillations are inherent to interconnected power systems and the poorly damped and/or unstable Low Frequency Oscillations (LFOs) in particular often limits the power transfer capacity of tie-lines. In these severe cases, the system collapse may occur leading to blackout. Thus, ensuring acceptable system damping is one of the major challenges of modern power systems. There is an urgent need to develop methods to monitor and control the system oscillatory stability under highly varying operating conditions. Therefore, this thesis attempts to address major issues of LFOs monitoring, the impact of renewable integration on LFOs and control strategy for damping improvement of LFOs. A detailed literature survey pertaining to these areas has been carried out and on the basis of that research objectives are framed.

For performing LFOs monitoring, optimal Phasor Measurement Unit (PMU) placement has been performed using a multi-criteria contingency constrained methodology and solved using Integer Linear Programming (ILP). The application of Artificial Neural Network (ANN) has been investigated for the online and real-time monitoring of oscillatory stability. The two different ANN architectures, Feed Forward Neural Network (FFNN) and Radial Basis Function Neural Network (RBFNN) are trained using synchronously sampled data to predict the oscillatory stability status and coherent groups in real-time. The results obtained using the two architectures are compared and presented. The proposed real-time PMU-ANN based approach is tested on IEEE 39-bus New England test system for different contingencies and varying load conditions. The results show that the proposed approach gives very small error and testing time/sample values and has very less

computational requirement. Therefore, the proposed method may serve as a promising tool for real-time oscillatory stability monitoring of power system.

The rapidly increasing integration of renewable energy sources into the grid, having very less or no inertia, can change the way power systems operate and respond to system disturbances. The increasing integration of wind turbines mainly doubly fed induction generators (DFIGs) introduces dynamic interaction with the conventional synchronous generators (SGs) affecting the damping of LFOs in the system. This may further complicate the system stability. Thus, a complete impact analysis of DFIG integration on system damping has been carried out in this work. The DFIGs are integrated by two ways – by replacing existing SGs and by adding them directly to non-generator buses without replacing existing SGs. A Damping Ratio Sensitivity Index (*DRSI*) based method is proposed for impact analysis of DFIG integration in former case while eigenvalue analysis and dynamic sensitivity analysis are used in latter case. The individual impact on dynamic performance of the system due to removal of SGs and addition of DFIGs is investigated. The DFIG penetration is increased on the basis of sensitivity analysis results and participation of SGs in critical modes. The effectiveness of the proposed methods is tested on IEEE 39-bus New England test system. In both the studies, the location of DFIG proved to be one of the key factors that impact the oscillatory stability of the system.

With the inclusion of renewable sources into the grid, conventional PSSs alone are not effective in controlling the LFOs. In this thesis, the damping improvement of LFOs has been presented for a high wind penetration power system by a robust coordinated control strategy of the Power System Stabilizer (PSS) and Power Oscillation Damper (POD) of DFIG. The control strategy is achieved using an improved eigenvalue based objective function, and optimized using Grey Wolf Optimizer (GWO). The wide-area based PMU signals are used as PODs input selected using modal observability criterion. The eigenvalue analysis, time-domain simulations and robustness analysis are performed to verify the efficacy of the proposed control strategy on a modified IEEE 39-bus New England system. The simulation results show the improvement in LFO damping with the proposed control strategy for a wide range of operating scenarios including faults and line outages at different loading conditions. The proposed method can be used for planning studies in modern power grids to augment LFO damping with high renewable integration.

TABLE OF CONTENTS

LIST OF TABLES

Continued…

LIST OF TABLES (Continued…)

LIST OF FIGURES

Continued…

LIST OF FIGURES (Continued…)

LIST OF SYMBOLS

CHAPTER 3

P_{ij}	Power flow in the line *i-j*
T_L	List of Critical Tie Line buses
ε_t	Threshold on Tie line power flow
N_L	Total number of transmission lines in the system
p_{ki}	Normalized participation factor of k^{th} generator in i^{th} mode
ε_t	Threshold on participation factor value
T_G	List of Critical Generator buses
H_i	Inertia time constant of i^{th} generator
N_g	Total number of generators
δ_i	i^{th} bus angle
$\theta_{i,COI}$	Phase angle at i^{th} bus with respect to the centre of inertia
$\theta_{i,dev}$	phase angle deviation at any bus
$\theta_{i,COI}^{max}$	Maximum deviation in bus phase angle for i^{th} bus
$\theta_{i,COI}^{min}$	Minimum deviation in bus phase angle for i^{th} bus
θ_v	Threshold on phase angle deviation value
T_V	List of Vulnerable buses
C_B	Complete list of Critical buses
N	Number of buses in the system
A	System connectivity matrix
P	Permutation matrix
$\zeta_{\min}$	Minimum required damping
n	index norm
ζ_{abs}	Absolute damping limit
$\delta_{j,COI}$	Relative rotor angle difference between the j^{th} generator and COI
ρ	Approximation Precision
y_i	Input set to ANN
y_o	Output set of ANN
f_i	Frequency of i^{th} mode
pf_i	Participation Factor valued for i^{th} mode
CG_j	Coherent Group information for j^{th} generator

CHAPTER 4

v_{sd} and v_{sq}	*d*- and *q*-axis stator voltages of DFIG
v_{rd} and v_{rq}	*d*- and *q*-axis rotor voltages of DFIG
i_{sd} and i_{sq}	*d*- and *q*-axis stator currents of DFIG
i_{rd} and i_{rq}	*d*- and *q*-axis rotor currents of DFIG
r_s	Stator resistance of DFIG
r_r	Rotor resistance of DFIG
x_s	Stator reactance of DFIG
x_m	Magnetizing reactance of DFIG
x_r	Rotor reactance of DFIG
ω_m	Rotor speed of DFIG

p_i and q_i	Real and Reactive powers injected in the grid
v_i	DFIG Bus voltage
T_e	Electromagnetic Torque of DFIG
ω_b	System frequency rate in rad/s
H_m	Inertia constant in kWs/kVA
T_m	Mechanical Torque
P_w	Mechanical power extracted from the wind
n_g	Number of machines that compose the wind park
S_n	Total power in MVA of the single or aggregated wind turbine
ρ	Air Density
v_w	Wind Speed
C_p	Performance Coefficient
κ	Tip speed ratio
A_r	Area swept by the rotor
V_{ref}^0	Initial reference voltage
V_s^{POD}	Additional signal of the POD
$P_w^*(\omega_m)$	Power-speed characteristic of DFIG
ζ_{gi}	Damping ratio when SG is modelled as constant power source
ζ_{wi}	Damping ratio when SG is replaced by DFIG
P	Total generation in base case

CHAPTER 5

A, B, C, D	State, Input, Output and Feed-forward matrices respectively
K	Stabilizer Gain
T_W	Wash-out Time Constant
$T_{1,2,3,4}$	Lead-lag time constant of controllers
N_G	Total number of SGs in the system
T	Total simulation time
N	Total number of data samples recorded
ω_{mn} , $\omega_{COI,n}$	SGs rotor speed and rotor COI speed at the n^{th} instant
λ_i	Eigenvalue of i^{th} mode
σ_i	Real part of eigenvalue of i^{th} mode
ξ_i	Damping Ratio of i^{th} mode
$\sigma_{i,k}$	Real part of the i^{th} eigenvalue for the k^{th} operating condition
$\xi_{i,k}$	DR of the i^{th} eigenvalue for the k^{th} operating condition
ϕ_i	Right eigenvector
ψ_i	Left eigenvector
δ	Rotor Angle
ω	Rotor Speed
oc	No. of operating conditions
ξ_{spec}	Specified damping ratio
$\sigma_{i,k}$	Specified real part of eigenvalue

LIST OF ABBREVIATIONS

AI	Artificial Intelligence
ANN	Artificial Neural Network
AVR	Automatic Voltage Regulator
COI	Centre of Inertia
DFIG	Doubly Fed Induction Generator
DI	Damping Index
DR	Damping Ratio
DRSI	Damping Ratio Sensitivity Index
EMS	Energy Management System
ERA	Eigensystem Realization Algorithm
FACTS	Flexible Alternating Current Transmission System
FFNN	Feed-Forward Neural Network
FFT	Fast Fourier Transform
GSC	Grid Side Converter
GWO	Grey Wolf Optimizer
ILP	Integer Linear Programming
LFO	Low frequency oscillation
LV	Less Vulnerable
MI	Mode Index
MSE	Mean Square Error
MT	Model Tree
MV	More Vulnerable
OPP	Optimal PMU Placement
PI	Performance Index
PCA	Principal Component Analysis
PMU	Phasor Measurement Unit
POD	Power Oscillation Damper
PSO	Particle Swarm Optimization
PSS	Power System Stabilizer
RAS	Relative Rotor Angle Dynamic Sensitivity
RBFNN	Radial Basis Function Neural Network
RHP	Right-Half Plane
RI	Robustness Index
ROCOF	Rate of Change of Frequency
RSI	Rotor Angle Sensitivity Index

RSC	Rotor Side Converter
SCADA	Supervisory Control and Data Acquisition
SG	Synchronous Generator
VSWT	Variable Speed Wind Turbine
WADC	Wide-Area Damping Controller
WAMS	Wide Area Measurement System
WAMCS	Wide Area Measurement and Control System
WOA	Whale Optimization Algorithm
WTG	Wind Turbine Generator

CHAPTER 1

INTRODUCTION

1.1 BACKGROUND

The power grids around the world are evolving very rapidly becoming more and more interconnected and complex with time. The rising electricity demand, restructuring and deregulation of electric utilities, change in loading patterns, compelled the utilities to run the power system very close to its stability limits in highly stressed conditions. Under such conditions, it becomes very difficult to ensure reliable power system operation. Also, due to the growing environmental concerns, the renewable integration is increasing in the system, having very less or no inertia. The rapidly increasing integration of renewable energy sources into the grid can change the way power systems operate and respond to system disturbances. This may further complicate the system stability and reliable system operation. The stressed operating conditions are more prone to disturbances leading to vulnerability and insecurity of power systems. Under such fragile conditions, even small disturbances may pose instability problems.

The stability studies are usually classified as small signal stability and large signal stability. Small signal stability is concerned with the ability of the power system to maintain synchronism under small disturbances. The change in electrical torque of a synchronous machine following a perturbation can be resolved into two components: synchronising torque component which is in phase with rotor angle deviation and damping torque component which is in phase with the speed deviation. The instability that may result can be due to increase in rotor angle due to lack of synchronizing torque, or rotor oscillations of increasing amplitude due to lack of sufficient damping torque.

The power system's response to small disturbances is usually oscillatory as the use of modern continuous acting voltage regulators reduces the risk of aperiodic stability to a great extent. These Low Frequency Oscillations (LFOs) in power systems are triggered by sudden variations in load demand, the action of voltage regulators due to faults, etc. Basically, LFOs are of two types: local-area modes and inter-area modes. Local modes (0.8 to 2 Hz) involve the swinging of units at a generating station with respect to the rest of the power system. Inter-area modes (0.1

to 0.8 Hz) are associated with the swinging of many machines in one part of the system against machines in other parts. The LFOs are inherent to the power system and any unexpected events, contingencies etc. may cause increasing oscillations leading to loss of synchronism and consequent blackout.

The power system damping plays a very important role in the enhancement of power transfer capability and stabilizes the system. To improve the system damping, conventional Power System Stabilizers (PSSs) are employed. The PSSs are feedback controllers which injects an additional stabilizing signal to the Automatic Voltage Regulator (AVR) in the excitation system.

All around the globe the concept of smart grids is taking shape. With the emergence of Phasor Measurement Units (PMUs), the wide-area monitoring and control of power system becomes easier to implement.

1.2 CHALLENGES ASSOCIATED WITH LFOS

Power system LFOs monitoring is a critical issue to be taken into consideration in operation of modern interconnected power systems. The monitoring involves identification of critical LFO modes present in the system having very low damping and also identifying the key source of these LFOs. Thus, complete monitoring and control of LFOs needs to be carried out in real time to ensure the secure operation of the system.

Due to the slow scan rate of current Supervisory Control and Data Acquisition (SCADA) systems, they are not suited for tracking the dynamic behaviour of modern grids in real-time. So, they are progressively replaced by synchrophasor-based Wide Area Monitoring and Control Systems (WAMCS) employing PMUs. Thus, monitoring and control systems based on synchrophasors lead to improved awareness of the behaviour and constraints of power systems, and to prepare better remedial actions for future implementations. However, it is not possible to install a PMU at every bus of the system due to the high cost associated with it, the absence of communication facility at certain buses and limited channel capacity. So the optimal placement of PMUs needs to be performed for complete system observability.

The wind energy is emerging as one of the most prominent renewable energy resource to augment present generation and in some cases replace the fossil-based generation. The high penetration of renewables can affect the rotor angle stability and small signal stability of power systems. Thus, it is imperative to analyse their impact on damping of LFOs in the system.

The synchronous generators (SGs) are equipped with PSSs to enhance the oscillatory stability of the system, but they often have limited effect on the low frequency interarea modes. Conventional controllers are designed to operate on some specific system conditions. However, the present power system is highly non-linear and dynamic in nature, and the operating scenario keeps on changing every instant. With the inclusion of renewable sources into the grid, the system behaviour becomes even more complex. In such conditions, conventional PSSs are not effective in controlling the LFOs. They need to be supported using some supplementary controllers to have acceptable system damping under widely varying operating conditions. Recent researches propose the use of Power Oscillation Dampers (PODs) employed with Doubly Fed Induction Generators (DFIGs) to improve damping in wind integrated systems. The PODs when designed in coordination with PSSs are found to be more effective in damping the LFOs. This coordinated controlling of controllers is a very significant problem in power system. The realization of the coordinated tuning of multiple controllers simultaneously for high penetration of wind in the system for damping improvement is a challenging task.

1.3 MOTIVATION

Oscillatory stability is one of the major concerns for modern power systems. The information regarding the frequency, damping ratio of LFO modes and the critical generators having high participation in these modes must be known to the operator for proper application of control actions. Thus, there is a need for proper monitoring and control of low frequency oscillations in real time to ensure the secure operation of the system. The impact of DFIG integration on LFOs carried out by many researchers reports both favourable and adverse effects of DFIG integration on LFO modes. It is necessary to systematically analyse the influence of wind power integration on power system oscillation modes and their damping characteristics.

The tuning of controllers parameters is usually obtained using analytical, numerical, meta-heuristic techniques, etc. However, out of them, metaheuristic techniques are preferred as they do not require past knowledge of the problem. They are independent of system complexity, the number of devices to be tuned and gives a faster solution. Thus, there is a need to carry out the controllers tuning effectively to integrate more renewables in the system.

The observation of the LFO has been reported by many utilities throughout the world and prompts the development of specialized tools for the small signal stability

analysis of the power system. Thus, there is a need to investigate the LFOs problem, its effect on system stability and how to control or damp these oscillations. Therefore, this research work attempts to address the major issues of monitoring and control of low frequency oscillations, and the impact of renewable integration on LFOs in power system.

1.4 THESIS ORGANIZATION

The research work essentially focused on three main objectives: wide area monitoring of LFO modes in power systems in real-time; dynamic impact analysis of wind power integration and their location on LFOs; and control strategy for damping LFOs in a high wind penetration power system.

The thesis is divided into six chapters. In this chapter, a brief introduction of the proposed research work is presented.

Chapter 2 presents a comprehensive literature survey of significant works in the areas of OPP, LFOs monitoring, coherency determination, impact analysis of wind integration and control of LFOs as inferred from textbooks, technical reports and research publications. On the basis of literature survey, the research objectives formed are also presented.

In chapter 3, a multi-criteria contingency constrained methodology is proposed for OPP problem. A real-time PMU-ANN based approach is also proposed to determine the oscillatory stability of the system and generator coherency following disturbance using synchronously sampled data from PMUs. Simulation and results obtained using the proposed method are also presented and discussed in detail.

In Chapter 4 of this thesis, a dynamic impact analysis of DFIG-based wind generators integration on LFOs is presented. The impact of DFIG location on LFOs damping is studied and analysed using different techniques, and the simulation results are presented.

In Chapter 5, LFOs damping improvement is presented by a robust, coordinated control strategy of the PSS and POD of DFIG. The implementation and illustration of the proposed method on the standard test system are carried out.

In Chapter 6, finally, conclusions of the research work are presented with a brief description of the future scope of this research work.

CHAPTER 2

LITERATURE SURVEY

Oscillatory stability is one of the major concerns in present highly interconnected power systems. The lack of sufficient damping torque results in oscillatory instability. Due to substantial power transfers and weak tie-lines, interarea oscillation arises. The growing electricity demand and increasing concern to reduce carbon emission is leading to an increase in renewable integration in the modern grids. The renewable integration however causes a reduction in overall system inertia and further complicates the oscillatory stability problems in the system. Though low frequency oscillations (LFOs) are inherent in the power system, but if not appropriately controlled could lead to a partial or complete blackout of the system as reported for many practical power systems. Modern power system requires fast and accurate estimation of these oscillations to timely mitigate the problem. Hence, a complete understanding of the problem would help in finding effective remedial measures, ways and means to control them.

As Wide Area Monitoring and Control Systems (WAMCS) are now available, new ways to more effectively tackle this problem need to be explored. Over the last four decades, many power system researchers and engineers have contributed to the understanding and solution of the problem of low frequency oscillations in power system. A brief literature survey of the significant works in this research area is presented in the following sections. The critical review is presented and the research gaps are identified in this chapter. On the basis of these, the research objectives are then formulated and attempted in this thesis.

2.1 OPTIMAL PMU PLACEMENT (OPP) [1]–[27]

The first and most important assignment in WAMCS deployment is the decision about the locations where PMUs needs to be installed. Due to the high cost of installing PMUs and other accompanying technical restrictions, it is not feasible to install PMUs at every bus of the system. Therefore, obtaining the optimum number of PMUs and their location in the system is propounded as a considerable challenge called OPP problem. Mainly, there are two approaches for this – one based on topological aspects and other on the system behaviour.

Earlier the OPP problem revolved around minimising the number of PMUs while maintaining the complete observability of the system and was based on topological characteristics. However, it does not consider system behaviour. Lot of research has been carried out in this field and several methods have been proposed in the literature based on topology reported in [2], [6]-[24]. Different optimisation techniques have been presented in the literature to solve the OPP problem which can be divided into two main groups of conventional techniques [8]-[13] and heuristic algorithms [14]-[23].

PMU placement scheme using bisecting search and simulated annealing [8] reported that PMUs need to be installed at 1/5 to 1/3 of the number of system buses for the system to be completely observable. The conventional techniques like Binary Search [9], Integer Linear Programming (ILP) [10]-[12], provide good results. A three-stage OPP method is presented in [13] using network connectivity information. Various heuristic algorithms like Genetic Algorithm [14], Tabu Search [15], Simulated Annealing [10],[16], Differential Evolution [17], Particle Swarm Optimization [18],[19], Immune Algorithm [20], Iterated Local Search [21], Spanning Tree Search [16], Greedy Algorithm [22], Decision Tree [23], are also employed for optimally placing the PMUs. Various constraints have also been added to OPP problem to make it more practical like OPP with and without conventional measurements [9], [10], [18], maximizing redundancy [15], [18], with single or multiple PMU loss contingency [11], [14], [18], [23], single branch outage contingency [11], [14], [18], [23], and with channel constraints [24].

Recently, a few papers have considered the aspect of system behaviour also for OPP problem [1], [25]-[27]. The various system aspects considered are voltage stability, transient stability, state estimation, coherency, etc. It is logical to consider both topological and system behaviour or stability aspects while solving OPP problem, especially during the early stage of PMU deployment where a few units need to be installed. Preferably, the selection of location should be based on the planned purpose [27].

2.2 MONITORING OF LOW FREQUENCY OSCILLATIONS

The first step in the analysis of oscillations is to determine the electromechanical modes present in the system and to identify the poorly damped or critical modes from them. The report in [28] gives an account of various identification techniques of

electromechanical modes in power system. The various methods for mode identification can be categorized as conventional [29]-[38], response based [39]-[41], AI-based [42]-[48] and WAMS based methods [49]-[62].

A. Conventional Methods

Modal Analysis is one of the most used and well-established conventional approaches for mode identification. It depends upon linearization of the power system and identifies the individual modes by the eigenvalues [29]. It also provides information about mode shapes and sensitivities to parameter changes [30], [31]. This technique is subdivided into full and partial modal analysis technique. The QR method and BR method [32] are full modal analysis techniques and are adequate for small systems. The partial modal analysis methods like AESOPS method [33] are used for large systems. Similarly, there are various other methods like inexact two-sided Jacobi–Davidson [34] and eigen function analysis [35] for the large power systems. However, determining oscillation modes and their participation factors using conventional methods is a challenging and time-consuming task which is not appropriate for online applications. Some indices are also used for oscillations monitoring. An index is proposed in [36] to rank all modes according to their localness based on participation factor. In [37], a three-layer index based on damping ratio is proposed to provide a measure related to the stability of the system. A performance index based on damping ratio is introduced in [38] which reports about changes in mode stability with changing system conditions. However, they are employed for offline analysis only and no topological variations are considered.

B. Response Based Methods

Response based methods process the time domain records such as simulation results or measured data and are not bounded by the system size. Their performance is influenced by the availability and the quality of the time-domain signals. It includes ringdown analysis [39], mode-meter analysis [40] and nonlinear and non-stationary analysis methods [41]. Ringdown analysis method typically used to process ringdown signals, i.e., signals that arise following a transient event. The Prony method, ERA, the Pencil Method, etc. are some of the employed techniques [39]. The measurement or communication noise severely affects the performance of this method. Mode-Meter analysis method like Yule-Walker based algorithm [40] can be applied to any portion of the response: ambient; transient; or combined ambient/transient. However, this method only allows for the computation of those modes present in the signals used to

perform the identification. Recently nonlinear and non-stationary analysis methods like Hilbert-Huang Transform [41] are also employed for mode identification. These methods suffer from the problem of computational burden.

C. AI-Based Methods

The subject of oscillation monitoring by machine learning techniques has been addressed in various papers. Use of Artificial Neural Networks (ANN) for power system oscillation analysis has increased in last few years. ANN is capable of solving complex and non-linear problems in a very efficient manner. The state of art of ANN applications in power systems is presented in [42]. In [43], the multilayer feedforward ANN is employed to evaluate system eigenvalues. In [44], a new method for eigenvalue prediction of critical inter-area stability modes of the European electric power system based on ANN is shown, but the analysis is performed offline. In [45], the prediction of participation factors is made using ANN for the online environment. In [46], three different neural network topologies are used to link the mode damping to the system conditions using the real system data. In [47], classification trees are used to predict mode damping, amplitude and mode control variables are highlighted. The oscillatory stability by eigenvalue region prediction of critical modes is proposed in [48] using Decision Tree and Genetic Algorithm.

D. WAMS based Methods

These methods are based on the application of PMU data in determining whether an evolving event will eventually be stable or unstable. In [49], the causes of poor damping of interarea oscillations are identified using PMU measurements. A stepwise-regression method for automatically selecting dominant modes from Prony analysis using phasor measurements is proposed in [50]. A new block processing technique for real-time estimation of the dominant interarea oscillation mode, based on synchronised wide area phasor measurements and the Newton Type Algorithm is introduced in [51]. A regression tree-based approach is used in [52] to predict the stability margins using synchrophasor measurements. The dominant interarea oscillation paths are found using three algorithms in [53]. In [54], various mode parameters are calculated using PMU data and spectral analysis technique. In [55], the damping and relative mode-shape are estimated in near real-time under transient condition using phasor approach using PMU measurements. The monitoring of interarea oscillation mode by synchronised phasor measurement is shown in [56]. A method of estimating the electromechanical modes and mode shapes from multiple

synchrophasors is presented in [57]. The mode shapes are estimated using synchrophasor measurements using spectral analysis in [58]. The oscillatory mode source identification is attempted in a few papers [29], [47], [59]-[62]. In [29], the mode shape values are used to find the dominant generators. In [59], PMU measurements are employed to find the disturbance source that excites the forced low frequency oscillation in the large power system. A method based on energy to locate oscillation sources in power systems which can be computed using WAMS data is proposed in [60]. A method utilising the differences in the damping contribution from different generators is employed in [61] to find the source of oscillations. A case study of an Indian grid is shown in [62] in which wide-area measurements are employed and oscillation sources are identified using Matrix pencil method.

2.2.1 Coherency Identification Methods

Following any disturbance, some generators tend to swing together. Such groups of generators are called coherent generator groups [63]. Coherency detection is necessary to establish wide-area control systems. If the system is in the insecure state following a disturbance, then coherency information is useful in applying emergency control measures like controlled islanding [64]-[66]. Coherency detection is mostly executed offline. However, with a change in system operating conditions the coherent groups of generators tend to alter. Also, for effective application of controlled islanding, the coherency information is required in real-time. Various methods have been reported in literature [67]-[71], for identifying coherent groups which involves the slow coherency [66], Principal Component Analysis (PCA) [67], Independent Component Analysis [68], continuation method [69], index-based method [70] and Support Vector Clustering [71]. However, most of these techniques are suitable for offline and online analysis only. A few schemes provide real-time identification [63]-[65], [72], [73], but they are either computationally burdensome or require long duration post-disturbance records to determine the coherent generators.

2.3 IMPACT OF DFIG INTEGRATION ON LOW FREQUENCY OSCILLATIONS

The wind energy is emerging as one of the most prominent renewable energy resource to augment present generation and in some cases replace the fossil-based generation [75]. Among various Wind Turbine Generators (WTGs) used, Doubly Fed Induction Generator (DFIG) [76] is the most popular one due to their improved

efficiency, superior control and smooth grid connection as compared to others. However, the WTG technology differs considerably from that of conventional Synchronous Generators (SGs). So, their proliferation affects many aspects of the dynamic and operational characteristics of SG dominated power system. Thus, it is imperative to analyse their impact on system stability, reliability and security. One of the main concerns is their impact on the LFOs. The WTGs are usually located in remote areas resulting in long-distance power transmission which may significantly change the network power flow that affects system damping [74]. The change in the eigenvalue or the mode damping is caused by the change in load flow and system configuration and due to the addition of dynamic interaction between conventional SGs and DFIG [75]. Wind power has characteristics of randomness, volatility and intermittence which affect the small signal stability of the system. The power electronics based coupling decouples DFIG's inertia from the system [76]. Being asynchronous machines, DFIGs do not inherently participate in LFO, but the interaction of their dynamics with LFO modes of nearby SGs may change the characteristics of oscillations [77].

A lot of research has been carried out to evaluate the impact of wind penetration on the power system oscillations. Most of the papers have presented both favourable and adverse effects on modes damping. The author in [78] presented a review of several issues associated with DFIG integration in the system. In [74], a sensitivity based ranking of generators to be used to insert wind by replacing them is determined. The impact of increased converter control based generators penetration on oscillation modes and the presence of new modes involving converter control based generators state variables is studied in [76]. The author in [77] proposed a separate analysis of different factors affecting the small signal stability of the system. A new approach based on the sensitivity of SGs eigenvalue with respect to variations in the Jacobian matrix is proposed to study the interaction of DFIGs with modes. The eigenvalue sensitivity analysis with respect to inertia is used in [79] to assess the impact of increased DFIG integration into the system. In [80], it is found that WTG improves damping due to a reduction in the size of SG involved in LFO. The impact of constant-speed WTG on LFO is studied in [81]. In [82], the effect of DFIG on the small signal stability of two-area power system with and without AVR and PSS is investigated. The tie-line power is introduced as an important parameter and its effect on LFO with wind integration is studied in [83]. The interaction of DFIGs with modes

is studied based on eigenvalue sensitivity with respect to the Jacobian matrix in [84]. In [85], impact analysis using modal analysis is presented on a seven-generator system integrated with 3.6 MW Siemens WTG. Tsourakis et al. in [86] suggested that the effect of increased wind penetration on system damping is favourable and some adverse interactions occurred can be avoided by appropriate tuning of control loop parameters of DFIG. Vittal et al. in [87], examined how the reactive power injection by wind can be utilised to support rotor angle stability of the system. It also inferred that replacing SGs by WTGs not only cause loss of inertia but also reduce the mitigation capabilities due to loss of AVRs, VAR support, etc. The critical WTGs locations for improved system stability are identified in [88]. In [89], the impact of wind integration on system oscillatory stability is examined using measurement-based methods. The authors in [90] have given survey of some representative works on the impact of WTGs on small signal stability.

2.4 CONTROL OF LOW FREQUENCY OSCILLATIONS

With high penetration of DFIGs in the system, network power flow and system configuration alters, dynamic interaction due to converters increases, and this escalates the LFOs problem in the system. In order to improve the system damping, conventional PSSs are employed [30]. The PSSs are feedback controllers which injects an additional stabilizing signal to the AVR in the excitation system. The SGs are equipped with PSSs to enhance the oscillatory stability of the system. However, the conventional PSSs are not effective under the high wind penetration condition. They need to be supported using some supplementary controllers to have acceptable system damping under widely varying operating conditions.

There might be some negative impact due to high DFIG penetration but if these DFIGs are properly controlled and equipped with supplementary controllers, they are capable of enhancing the system damping. Recently many researchers have proposed methods to improve damping in wind integrated systems using the PODs [91]-[105] employed with DFIGs. It is shown in [91] that WTG can contribute towards LFO damping. In [92], the damping of a single machine system is improved using the DFIG controller. The authors in [93] have shown that using conventional PSS inside voltage control loop of DFIG rotor side converter delivers damping improvement. A robust control approach is proposed in [94] to attain small signal stability and voltage regulation together. Non-linear POD controllers are designed in [95]. A wide-area

PSS to damp the LFO is suggested in [96]. The authors in [97] proposed a robust centralized PODs design of DFIG.

The PODs, when designed in coordination with PSSs are found to be more effective in damping the LFOs as suggested in recent literature [98]-[104]. The probabilistic theory based method is used for coordinating the PSS for DFIG and SG in [98]. A two-level hierarchical control strategy for PSS, DFIG and FACTS for frequency regulation and damping improvement is employed in [99]. In [100], an observer based state-feedback methodology is suggested to design a POD and results show that stability is improved by using wide area measurements. The simultaneous coordinated control of DFIGs with wide-area based controllers is obtained in [101]-[103]. In [104], PODs and PSSs are coordinately controlled along with optimally controlling the plant dynamics. The authors in [105] explained that the damping effect of DFIG Rotor Side Converter (RSC) reactive power controller is much higher as compared to Grid Side Converter (GSC). In [106], a review of wind power contribution to power oscillation damping is evaluated and presented. Various wide-area damping control methods for interarea modes damping with increasing renewable penetration are reviewed in [107].

A number of papers mention about the proper control signal selection mainly on two basis; one to improve the controllability/observability of interarea modes and other to minimize interactions between the controllers [108]. Farsangi et al. [109] presents a method which uses the Minimum Singular Values, the Right-Half Plane zeros, the Relative Gain Array, and the Hankel Singular Values as indicators to find stabilizing signals. Many papers have employed the transfer function residue method. In [110], the importance of phase of residues in addition to magnitude in selecting control signals has been shown. Geometric measures of controllability/observability are used to select the most effective stabilizing signals and control locations in [111]. Kamwa et al. [112], compared the two different approaches of signal selection – residue method and geometric approach. The minimum variance of the modal residue has been utilised to select a robust signal for damping purpose in [113]. A hybrid method to assess and select suitable control inputs for multiple Wide-Area Damping Controllers (WADCs) is proposed by Li et al. in [114], where residue analysis is performed along with Relative Gain Array method. The interarea oscillations involve many machines swinging against each other in different areas. Thus, they are more observable in wide-area signals as compared to local signals. The feedback signal

should be chosen to give high modal observability of the critical mode(s), as this helps in simplifying the design of controller and also establishes a robust damping performance over a wide range of operating conditions [115].

2.5 CRITICAL REVIEW

It is clear from the literature survey presented that wide area measurements obtained from PMUs can play a very important part in monitoring and control of power system oscillations. In most of the literature, PMU placement is performed giving equal consideration to all the buses. However, in power system some buses or generators are more critical and their visibility is very important for stability studies. Thus, placement should be done giving more importance to those buses or generators. The literature survey shows that the OPP should be performed keeping in mind the purpose of deployment and the system characteristics. At the same time, the number of PMUs should be kept minimum while maintaining the system's complete observability. Also, the placement must ensure continuous monitoring even in the event of a line outage or PMU loss. The purpose of present study is monitoring and control of LFOs. For understanding the nature of the oscillatory modes, PMUs must be placed at those buses which are critical for oscillation monitoring. So the OPP problem should be solved such that the LFO can be monitored in the system with high observability in all the cases and with minimum number of PMUs. Nonetheless, the placement can also be performed on the basis of operators experience and past history of critical buses that needs efficient monitoring.

The analysis of interarea modes of a large power system by the conventional methods like modal analysis is time consuming, expensive and complex. The response based methods operate directly on the system output, thus size limitation for the studied power systems is completely removed. However, these methods require several time domain simulations to excite and identify all the modes in the system. This is a trial-and-error approach, and some of the modes may remain undetected. The use of machine learning techniques for modal analysis provides fast and better results but require offline training. Decision Tree based solutions are fast with better interpretability, but they lack adaptability as these methods provide rule based solutions that are system specific. ANN produces good results but success depends on the choice of input variables. As there is lot of data available through PMUs, finding an appropriate feature set for training is important. There is need to apply suitable

data fusion methods to exploit a proper attributes for training the ANN. It is evident from the literature that using ANN for the power system monitoring and control can provide higher speed, accuracy and efficiency compared to its conventional counterparts. The ANN has capability to extract complex mapping of inputs parameters and output results. It can extract hidden relationship of system parameters and system behavior. ANN should be taken as an additional tool, instead of a replacement for conventional or other AI-based power system techniques. Some indices are also proposed in literature to assess the oscillatory stability of power system. However, most of the indices are utilized for offline analysis only. Therefore, more investigations are needed on using indices to analyse and monitor oscillatory stability in real-time.

From literature survey of the coherency analysis, it is inferred that it is mostly executed offline. However, with the changes in system operating condition and network configuration, the groups of coherent generators tend to vary. Furthermore, the accuracy of the system parameters (generator, loads and networks) influences the accuracy of the technique to obtain coherent islands in the system. Therefore, involving real-time operation to define the system coherency is better than identifying coherency based on offline studies. A few real-time schemes are employed, but they are either computationally inefficient or require long duration post disturbance data to determine the coherent groups. Therefore, further investigations are needed to explore a computationally efficient method which require less duration data to obtain coherency in real-time.

The literature survey reveals that the wind integration affects oscillatory stability in two ways: (a) by changing the damping of the already present low frequency critical mode(s) in the system, and/or (b) by addition of new modes of low damping in the system. If the damping of critical mode(s) improves and no new low damping mode shows up by wind integration, then it is beneficial for oscillatory stability of the system, otherwise not. The literature reports both favorable and adverse effects of DFIG integration on LFO modes. Therefore, it is necessary to systematically analyse the influence of wind power integration on power system oscillation modes and their damping characteristics.

Also, as identified in many papers that the actual impact of DFIGs on the system damping can only be realized for higher penetration (>15-20%) of wind in the transmission system. However, most of the damping improvement strategies are

designed and verified for small penetration of DFIGs in the system, which may not provide the effective damping for higher wind penetration. The conventional PSSs are not effective under these conditions. They need to be supported using some supplementary controllers to have acceptable system damping under widely varying operating conditions.The realization of the coordinated tuning of multiple controllers simultaneously for high penetration of wind in the system for damping improvement is a challenging task.

Practically, wind locations depend on the wind power resource and cannot be optimized. Thus, those locations could be either beneficial or detrimental to system damping. The control methodology should be able to neutralize the detrimental effect of wind penetration if they are negatively affecting system damping at certain locations. Thus, further investigations are needed to develop a robust control methodology for damping low frequency oscillations with high wind penetration in the power system. There is a need to resolve this LFO problem effectively in order to integrate more renewables in the system.

2.6 RESEARCH OBJECTIVES

On the basis of the literature survey and the critical review, following research objectives have been formulated in this thesis work:

1. To carry out a comprehensive literature survey on monitoring and control of low frequency oscillations in power system and perform critical analysis of the survey.
2. To develop a suitable method for optimal PMU placement for complete observability of the system.
3. To develop an efficient methodology for wide area monitoring of low frequency oscillation modes in power systems under wide range of operating conditions.
4. To investigate the impact of DFIG integration on low frequency oscillations in power system.
5. To develop suitable control methodology for damping low frequency oscillations in power system having high level of wind penetration.

2.7 SUMMARY

In this chapter, an exhaustive literature survey of low frequency oscillations monitoring and control has been carried out. The critical analysis of literature survey

has been performed related to these aspects and on that basis research objectives have been framed for the present research work.

CHAPTER 3

MONITORING OF LOW FREQUENCY OSCILLATIONS IN POWER SYSTEMS

3.1 INTRODUCTION

The modern power system due to continuously increasing power demand, complexity of interconnections, large power transfers closer to limits, are prone to low frequency oscillation problems. These low frequency electromechanical oscillations are the results of small disturbances such as sudden load change, change of system configuration, switching off / on of one of the parallel lines etc. The basic cause of small signal stability is lack of sufficient damping at particular operating condition. The low frequency oscillations may lead to decrease in power transfer capability and if these oscillation are allowed to build up they may possibly cause a system to collapse. Therefore, there is a need to continuously monitor the oscillatory stability of the power system under all operating conditions and apply appropriate remedial control measures before the system goes out of step. The information about oscillatory instability and their source should be known to the operator in real-time to initiate appropriate control actions. To detect approaching oscillatory instability in real-time, fast and accurate monitoring approaches needs to be developed. Therefore, the aim of this chapter of the thesis is to explore suitable techniques for identification and analysis of low frequency oscillations under diverse operating conditions.

The oscillation monitoring in real-time however requires availability of various system parameters to the operators in real-time. This requires suitable devices to be placed in the system for collecting and sending such data in real-time. With the advent of PMUs in the power system, placed at key locations, operator can visualize the oscillations in the system more clearly on a wider geographical area [2]-[3]. Thus, the low frequency oscillations and their control issues can be dealt with more comprehensively in real-time employing these measurements.

For understanding the nature of the oscillatory modes, PMUs must be placed at those buses which are critical for oscillation monitoring. Also, the number of PMUs should be kept minimum while maintaining the system's complete observability. The placement must also ensure continuous monitoring even in the event of a line outage or PMU loss. Therefore, the OPP problem needs to be solved in a way that the low

frequency oscillations can be monitored in the system with high observability for different operating conditions with minimum number of PMUs.

The real-time monitoring data obtained from PMUs can also be utilized in determining the generators coherency in the system. The coherency of synchronous generators is usually calculated on the basis of generators swing following any disturbance and thus can be determined along with oscillation monitoring procedure. Therefore, this chapter also explores a computationally efficient method which require less duration data to obtain coherency in real-time.

The prime objective of this chapter is to develop a suitable methodology for real-time low frequency oscillations monitoring in power system. For this, the system operator needs complete system observability in real-time for all given operating conditions including contingencies. Thus, a multi-criteria methodology is proposed for the optimal placement of PMUs in the system. This problem is solved using Integer Linear Programming (ILP). The proposed methodology ensures complete observability under N-1 contingency including the line outages and loss of PMUs for proper monitoring of low frequency oscillations.

For real-time monitoring of low frequency oscillations a PMU-ANN based approach is proposed. It is used to determine the oscillatory stability of the system and generator coherency following disturbance using synchronously sampled data from PMUs. The Feed Forward Neural Network (FFNN) and Radial Basis Function Neural Network (RBFNN) are two of the most commonly used ANNs for power system monitoring and control because of their effectiveness in such applications. The FFNN and RBFNN are used in proposed method to predict the oscillatory stability status and coherent groups in real-time and their results are compared. The dimensionality reduction of the data is performed using Principal Component Analysis (PCA). The oscillatory stability status is predicted with the help of two indices – Mode Index and Damping Index. Also, other mode related information like frequency, damping ratio and participation factor values are predicted at the same time. In case of any insecure condition, the critical generators responsible for low frequency oscillations and poor damping can be determined using the proposed method. With the help of these parameters and information about oscillatory stability, main sources of oscillations and coherency will be available in real-time and may be useful in supporting fast and accurate control measures to prevent the system from severe damages and blackouts.

3.2 PROPOSED METHOD FOR OPTIMAL PMU PLACEMENT

The first step in oscillatory stability analysis is monitoring of electromechanical modes present in the system. This requires the identification of the critical modes present in the system in real-time. To perform this analysis, the optimal PMU placement is performed in this chapter such that the monitoring of critical buses with respect to oscillatory stability is ensured in addition to system's complete observability, even in the event of N-1 contingencies or single PMU outage.

The system may become small-signal unstable either due to oscillations at some critical tie-lines or rotor angle oscillations at some high participating generators, or angular instability at some critical buses etc. The observability of buses prone to oscillatory instability is crucial and therefore, PMUs must be placed at these critical buses since the observability of oscillations is maximum at such buses. For identifying these critical buses, a list of such critical buses is formed by considering different operating criteria and included in the ILP based optimal PMU placement approach for real-time LFOs monitoring. This is performed in three steps:

(i) Determine the critical buses with respect to oscillatory stability,

(ii) Include these buses in optimal placement algorithm so as to ensure PMU placement on these buses with complete system observability and minimum number of PMUs. This to include both topological aspects and system behaviour in the study,

(iii) Ensure complete observability under N-1 contingencies (PMU or line loss).

The detailed multi-criteria contingency constrained approach is described below.

3.2.1 Criteria for Critical Buses Identification

The different criteria used for finding out the critical buses for monitoring the oscillations are critical tie-line identification, critical generators identification, and vulnerable bus identification.

A. Critical Tie-line Identification

The transmission lines in the system that transfers high amount of power are the tie-lines. It is beneficial to monitor the tie-lines, as in large systems power oscillations are generally detected through the dynamic changes in the tie-line power flows and phase angle difference at its two ends [1]. A PMU placement strategy should be adequate to ensure the monitoring of important tie-lines. The placement of PMU at either end of a

tie-line will make both the ends of tie-line observable. The algorithm to find critical tie-line buses is as follows:

(i) Run load flow to obtain the line flows.

(ii) Compute the power flow on the line *i-j*, and define list of critical tie-line buses (T_L) having high power flows, $P_{ij} \geq \varepsilon_t$ (value of ε_t varies with system).

(iii) From the two buses at either end of the critical tie-line, the bus with maximum connecting neighbouring buses is selected. The PMU placement at these critical buses will make more number of buses observable. The remaining buses are removed from T_L.

B. Critical Generators Identification

The generators having high participation in low frequency oscillation modes are considered as critical generators. The high participation factor of a generator in inter-area mode indicates that the observability of oscillations will be very high in the output of that generator and therefore, it must be continuously monitored using PMU. The steps involved in identifying such critical generators are as follows:

(i) For line y =1 to N_L, perform time domain simulation for 10 seconds with single line outages of each line at 1.0 second and execute small signal analysis (modal analysis) for each case; N_L is the total number of transmission lines in the system.

(ii) For each contingency, determine the rotor speed participation factor values for all generators in each inter-area mode and normalize them between 0 and 1.

(iii) For each case, find the generators having high normalized participation factor, $p_{ji} \geq \varepsilon_g$ (value of ε_g varies with system) and term them critical.

(iv) List the critical generator buses (T_G). The T_G contains the buses connected to critical generators identified in previous step.

(v) The buses are ordered in descending order in T_G, based on the number of times each generator bus is appearing for all the contingency cases.

(vi) Selecting top few buses based on the system and frequency of appearing in the list, remaining buses are deleted from the list.

C. Vulnerable Bus Identification

There are certain buses in the system where the phase angles vary widely when system is in stressed condition, following any faults, outages or other contingencies. The phase angles of such buses indicates closeness to instability in the system. Real-time

monitoring of these buses may be used for the purpose of stability monitoring. However, this criterion is more related to transient stability but it should also be considered for oscillatory stability monitoring.

The phase angles at buses are obtained with respect to the Centre of Inertia (*COI*) angle. The *COI* angle is given by

$$\delta_{COI} = \frac{\sum_{j=1}^{N_g} \delta_j \, . H_j}{\sum_{j=1}^{N_g} H_j} \tag{3.1}$$

where, H_j is the inertia time constant of j^{th} generator, N_g is the total number of generators and δ_j is the j^{th} generator rotor angle. The phase angles at i^{th} bus, θ_i, with respect to the centre of inertia and phase angle deviation at any bus for any given contingency is given by (3.2) and (3.3) respectively.

$$\theta_{i,COI} = \left|\theta_i - \delta_{COI}\right| \tag{3.2}$$

$$\theta_{i,\mathrm{dev}} = \left|\theta_{i,\mathrm{COI}}^{\max} - \theta_{i,\mathrm{COI}}^{\min}\right| \tag{3.3}$$

where, $\theta_{i,\mathrm{COI}}^{\max}$ and $\theta_{i,\mathrm{COI}}^{\min}$ are the maximum and minimum deviation in bus phase angle for i^{th} bus for any given contingency. The various steps followed to identify such vulnerable buses are as follows:

(i) For line y =1 to N_L, single line outages are performed of each line by opening the breakers at t =1.0 second. The value of *COI* angle is calculated using (3.1).

(ii) For each contingency, calculate the phase angle deviation for all the buses.

(iii) Compute the maximum angular deviation of each bus for all the contingencies.

(iv) Arrange the buses in descending order on the basis of maximum deviation values.

(v) Form two groups of buses - More Vulnerable (MV) and Less Vulnerable (LV). The buses having phase angle deviation values $\theta_{i,COI} \geq \theta_v$, are grouped as MV and remaining as LV (value of θ_v varies with system).

(vi) Now order the buses of MV group in descending order based on number of times each bus appears in MV group.

(vii) A few highest appearing buses are stored in vulnerable bus list (T_V).

The critical buses obtained using above three criteria are combined and stored in a separate list, C_B.

$$C_B = T_L \cup T_G \cup T_V \tag{3.4}$$

3.2.2 Objective Function Formulation

The objective of optimal PMU placement is to minimize the number of PMUs while keeping the system completely observable under N-1 contingencies. The optimal locations for placing PMUs in the system are determined using ILP method described in [10]. Using this method, the minimum number of PMUs can be obtained for the given system, but in the event of a transmission line loss or a PMU loss, some buses may become unobservable. For a robust PMU placement scheme for node monitoring, each node must be monitored using at least two PMUs [1]. This increases the reliability of the monitoring scheme. In addition, it is also to be ensured that critical buses contained in list C_B are directly monitored by PMUs. The effect of zero injection buses should also be taken into account to reduce the optimal number of PMUs required.

An ILP based method is proposed here to identify the optimal PMU locations taking into account all the above criteria, considering both the topological and oscillatory stability aspects. The locations obtained using the proposed approach ensures the prioritized observability of oscillatory critcal buses along with complete system observability. The OPP problem is formulated as follows:

$$\left.\begin{aligned} &Minimize \sum_{j=1}^{N} x_j \\ &\text{subject to } [T][P][A][X] \geq 2*[b] \\ &[A_{eq}][X] = [b_{eq}] \\ &x_i \in \{0,1\} \end{aligned}\right\} \tag{3.5}$$

where,

N – number of buses in the system;

A – system connectivity matrix such that $A_{i,j} = \begin{cases} 1, if\ \ i = j \text{ or } i \ \& \ j \text{ are connected} \\ 0, otherwise \end{cases}$;

X – vector containing binary decision variable, x_j ;

x_j =1 if PMU is placed at bus i, otherwise 0;

P – permutation matrix of size N x N ;

$[T] = \begin{bmatrix} I_{M\times M} & 0 \\ 0 & T_m \end{bmatrix}$, M are buses which are not zero injection buses;

A_{eq} - diagonal matrix given by $A_{eq}(i,i) = \begin{cases} 1, \text{for buses in list } C_B \\ 0, otherwise \end{cases}$;

b_{eq} - column matrix given by $b_{eq}(i,1) = \begin{cases} 1, \text{for buses in list } C_B \\ 0, otherwise \end{cases}$

The proposed PMU placement methodology is also shown using a flowchart in Fig. 3.1.

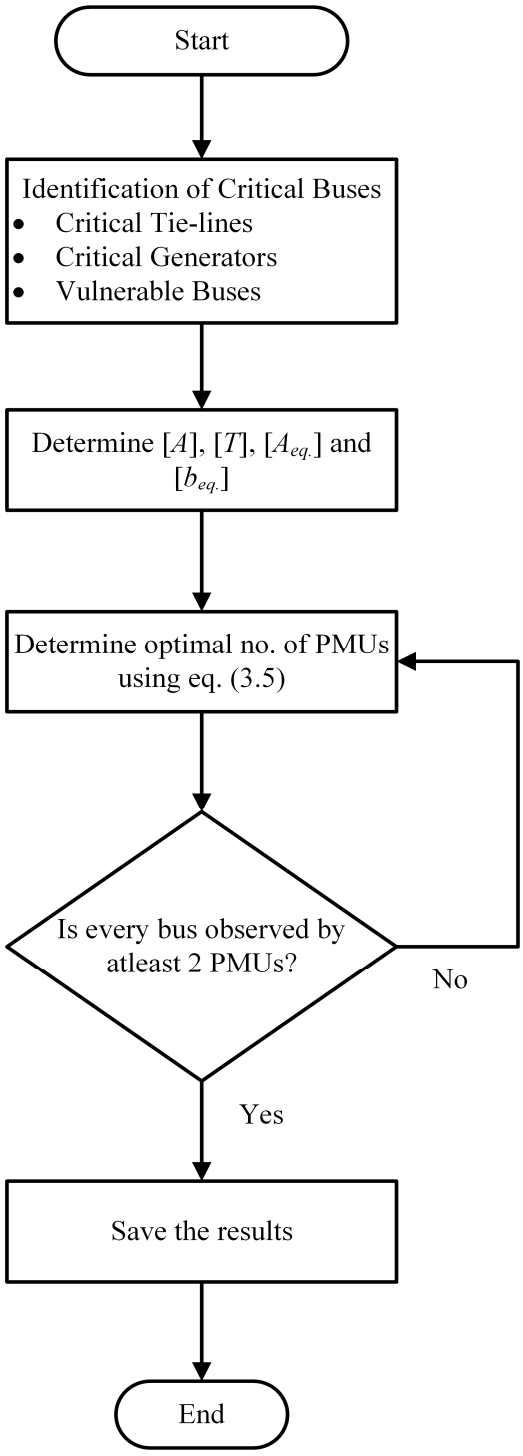

Fig. 3.1 Flowchart of proposed optimal PMU placement

The detailed explanation of some of these matrices with examples can be referred from [10]. The inequality constraint in eq. (3.5) ensures that each bus is monitored by at least two PMUs and thus keep the system observable in the event of a PMU outage. Also since each bus is observed by two PMUs, a line outage will not affect the complete observability. The monitoring of critical buses contained in list C_B is ensured by $[A_{eq}][X]=[b_{eq}]$. Thus above formulation provides the optimal PMU locations for any given system ensuring the PMU placement at critical buses and complete observability even in the case of line outage or PMU loss. The advantage of the proposed approach is that it is a generalized approach and any number of criteria can be included according to application requirement.

3.3 INDICES FOR LOW FREQUENCY OSCILLATIONS MONITORING

In this chapter, two indices have been employed to study the localness of various modes and to monitor the impact of disturbances on damping of modes.

***A. Mode Index* (*MI*)**

The distinction between the local/interarea modes is usually performed on the basis of frequency range and the participating generators. However, in large power systems it has been observed that it is difficult to define the most local or global mode. The mode index ranks all the modes according to their localness [36]. For the N_g generator system, the mode index of the i^{th} electromechanical mode is calculated from the normalized participation factor values of generator rotor speed variable as

$$MI_i = \sum_{j=1}^{N_g} (1 - p_{ji})^n \tag{3.6}$$

The exponent of each term, *n*, is chosen to give the property of clustering to the *MI*. The modes placed at base of this ranking table are inter-area modes and modes placed at upper part are local modes. It is proposed in [36] that the exponent *n* correspond to the number of synchronous generators in the system under consideration.

B. *Damping Index* (*DI*)

There is a need to monitor the damping of modes to monitor the oscillatory stability of the power system. The damping index is employed to monitor the effect of disturbances on the damping of modes [38]. It gives the severity status of each mode. The value of index for a mode is given as

$$DI = \begin{cases} \min\left(1, \left(\frac{\zeta}{\zeta_{\min}}\right)^{-n}\right), & if\ \zeta > \zeta_{abs} \\ 1, & if\ \zeta \le \zeta_{abs} \end{cases} \tag{3.7}$$

where $\zeta_{\min}$ is minimum required damping, n is index norm and ζ_{abs} is absolute damping limit. The minimum damping limit to categorize the critical modes is system dependent and usually in the range of 3-5% [38]. In this work, the threshold is taken as 2.5%. The value of *DI* varies from '0' when system is fully damped (ζ=100%) to '1' when damping reaches minimum admissible value ($\zeta = \zeta_{\min}$). If *DI* < 1 system is well damped and is in secure state, otherwise system is insecure or poorly damped. The sensitivity of index towards varying system conditions is taken care of by the norm. The norm value depends on experience or system-sensitivity studies. Here, norm is taken as 1.36 to have index value 0.5 at 5% damping and 1 at 2.5% ($\zeta_{\min}$ = 2.5%).

3.4 COHERENT GROUPS IDENTIFICATION

Coherency detection is necessary to establish wide area control systems [65]. For effective application of emegency control actions like controlled islanding, the coherency information is required in real-time. In this chapter, the coherent groups are determined based on the separation between the machine rotor angle and the inertial center. For this the swing curves of all the generators are observed. For a N_g generator system, the coherent groups are found by calculating the relative rotor angle difference between the j^{th} generator having rotor angle δ_j and the angle of inertial center δ_{COI} as

$$\delta_{j,COI} = \left|\delta_j - \delta_{COI}\right| \quad for\ j = 1\ to\ N_g \tag{3.8}$$

Based on the values of $\delta_{j,COI}$ obtained above, i.e., the separation between the machine rotor angles and inertial center, different generators are classified in separate groups. The rotor angle values are recorded at the 3 second instant in this study and generators are classified in 10 different coherent groups as shown in Table 3.1.

The separation between different generators in a group remains within a certain range and it is taken as 10° in this study. A tolerance limit of ±2° is also considered. All the angles measured are in degrees. These coherent groups are predicted by ANN using PMU-ANN based method detailed in coming subsections. The coherency information thus obtained in real-time for the insecure cases can be utilized for the application of emergency control measures in case a major disturbance occurs.

TABLE 3.1
COHERENT GROUPS CLASSIFICATION

Coherent Group	Value of $\delta_{j.coI}$ (at 3 second)
1	>100°
2	90°-100°
3	80°-90°
4	70°-80°
5	60°-70°
6	50°-60°
7	40°-50°
8	30°-40°
9	20°-30°
10	<20°

3.5 PMU-ANN BASED METHOD FOR OSCILLATIONS MONITORING

In this chapter, a PMU-ANN based approach is proposed for monitoring the oscillatory dynamics and the stability of power system in online and real-time environment. The source of oscillation responsible for creating insecure conditions is also found in real-time. By determining the main drivers of oscillation it is easy to implement control actions before the system goes out of step. The optimally placed PMUs provide the bus voltages and angles in real-time which are used as ANN inputs. ANN outputs are the values of indices and mode related information as shown in Fig. 3.2. Two different ANNs are employed and their results are compared. The proposed approach consists of data generation, feature selection using PCA and selection of neural network architecture.

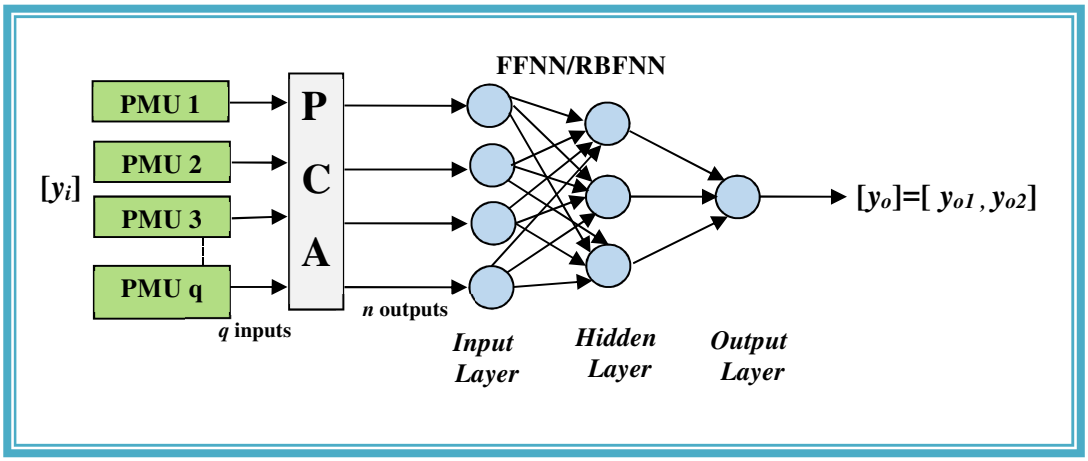

Fig. 3.2 Block diagram of proposed PMU-ANN based approach

3.5.1 Data Generation

The data set should be precise and should represent a wide range of possible operating conditions. Proper data generation is an important step to improve the efficiency of ANNs. The data is generated to create a large pattern vector by randomly varying the real and reactive loads on all the buses and shown by a flowchart in Fig. 3.3.

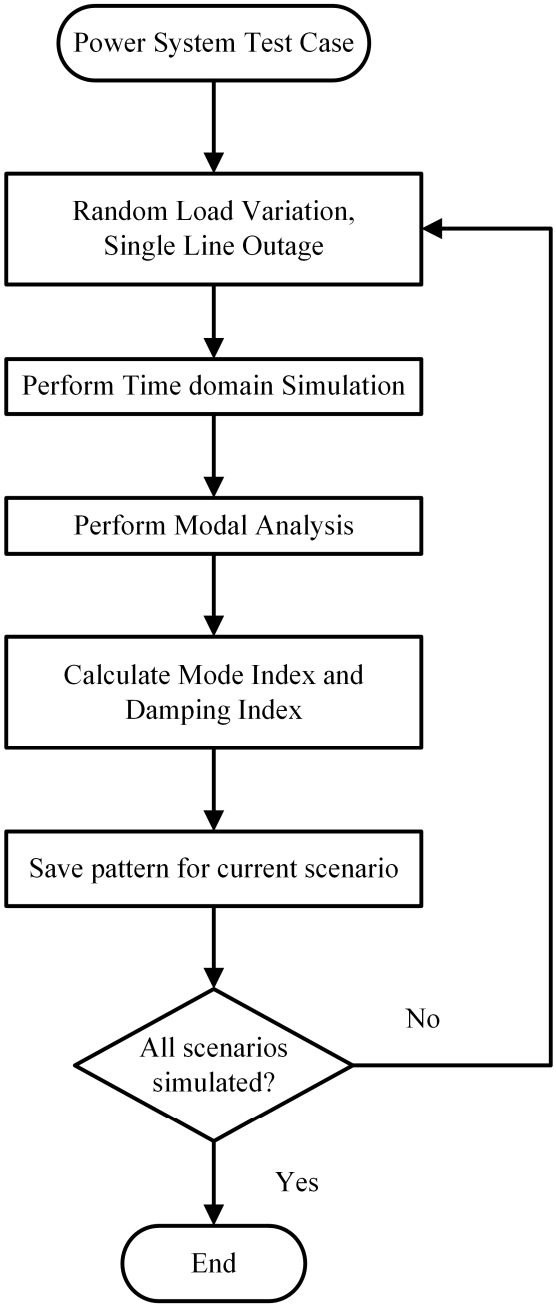

Fig. 3.3 Flowchart of data generation for PMU-ANN based approach for oscillation monitoring

Topological variations are also simulated considering various single line outages. The selection of critical contingencies depends upon the knowledge of the operator

about the probability of their occurrence and severity. For this study, data consists of 1500 patterns (operating conditions) that are normalized, shuffled and divided into two groups; one for training and the other for testing.

3.5.2 Feature Selection Using PCA

The selection of proper input variables for ANN is one of the important aspect of ANN training. It is required to select the optimum number of inputs, by selecting only the significant ones and discarding the insignificant ones. It gives better performance and also reduces the computational burden and training time of ANN.

PCA [67] is one of the best dimensionality reduction techniques for the large amount of data. PCA is a technique that transforms a set of q correlated variables to a new set of uncorrelated variables called principal components without losing much information [67]. Consider a data set Y of size pxq, where p is the number of operating conditions. First, the mean is calculated for each column vector and is subtracted from each corresponding input variable to create a normalized matrix. The covariance matrix is obtained from this normalized matrix which gives eigen values and eigen vectors (principal components). These eigen vectors are rearranged by arranging the eigen values in descending order. Out of these first n eigen vectors are selected, where ($n<q$) by providing a threshold ρ which denotes the approximation precision of the n largest eigenvectors.

$$\frac{\sum_{i=1}^{n}\lambda_i}{\sum_{i=1}^{q}\lambda_i} \geq \rho \tag{3.9}$$

The low-dimension data P of size pxn is calculated as

$$\mathrm{P} = \lambda^T Y^T \tag{3.10}$$

3.5.3 Selection of ANN Architecture

Two different ANN architectures – FFNN and RBFNN are employed in this work to determine the desired output and their results are compared. Both FFNN and RBFNN have been widely used for solving many power system problems. Here, FFNN consists of five layers: one input, three hidden and one output layer. RBFNN consists of three layers: one input, one hidden and one output layer. The number of PMU variables used determines the size of input layer. The input set to both the ANNs consists of bus voltage magnitudes and angles obtained from PMUs given by

$$\left[y_i\right] = \left[|V|, \angle V\right] \tag{3.11}$$

With the proposed method, the complete modal analysis is performed using two different ANNs and the output is given by eq. (3.12). With FFNN, the mode frequency, damping ratio and *MI* are predicted according to eq. (3.13a) and the *DI* and participation factor values are determined according to eq. (3.13b). Similarly, the same outputs are predicted using another ANN architecture which is RBFNN and the results are compared.

$$\left[y_o\right]=\left[y_{o1}, y_{o2}\right] \tag{3.12}$$

where,

$$\left[y_{o1}\right]=\left[f_i, \zeta_i, MI_i\right] \tag{3.13a}$$

$$\left[y_{o2}\right]=\left[DI_i, pf_i\right] \tag{3.13b}$$

3.6 PMU-ANN Based Method for Coherent Groups Identification

In this chapter, the coherency status of generators at desired future time following a disturbance is also determined using the proposed PMU-ANN based approach. The initial few cycles post-disturbance data carries sufficient information about the future states of the system. The aim of the proposed method is to obtain this real-time coherency and oscillatory information as early as possible (in few cycles) after the disturbance. This information is required to apply emergency control actions. The optimally placed PMUs provide the bus voltages and angles in real-time which are used for ANN input and ANN provides values of damping index and coherent groups' information at the output. The proposed approach consists of data generation, feature selection and selection of neural network architecture.

3.6.1 Data Generation

A large amount of data is generated to construct the pattern vector for ANN by randomly varying the active and reactive load of the system along with N-1 contingencies (line outages) and 3-phase faults and shown by a flowchart in Fig. 3.4. The data of first four cycles after disturbance is collected from PMUs. In addition, the rotor angles at desired future instant are recorded and coherency is calculated at that instant using eq. (3.8). The generated data is normalized, shuffled and divided in two groups for training and testing. This data is dimensionally reduced using PCA as described in section 3.5.2.

3.6.2 Selection of ANN Architecture

The two ANN based architecture selected are FFNN and RBFNN to determine the coherency using the proposed approach and their results are compared. Both the ANNs

used here have the same architecture as described in previous section. The number of PMU variables used determines the size of input layer. The output of ANN gives the required real-time information of the damping index and generator coherency group number. The input vector to ANN consists of bus voltage magnitudes and angles obtained from PMUs, consisting of first four cycles of post disturbance data given by

$$\left[y_i \right] = \left[|V|, \angle V \right] \tag{3.14}$$

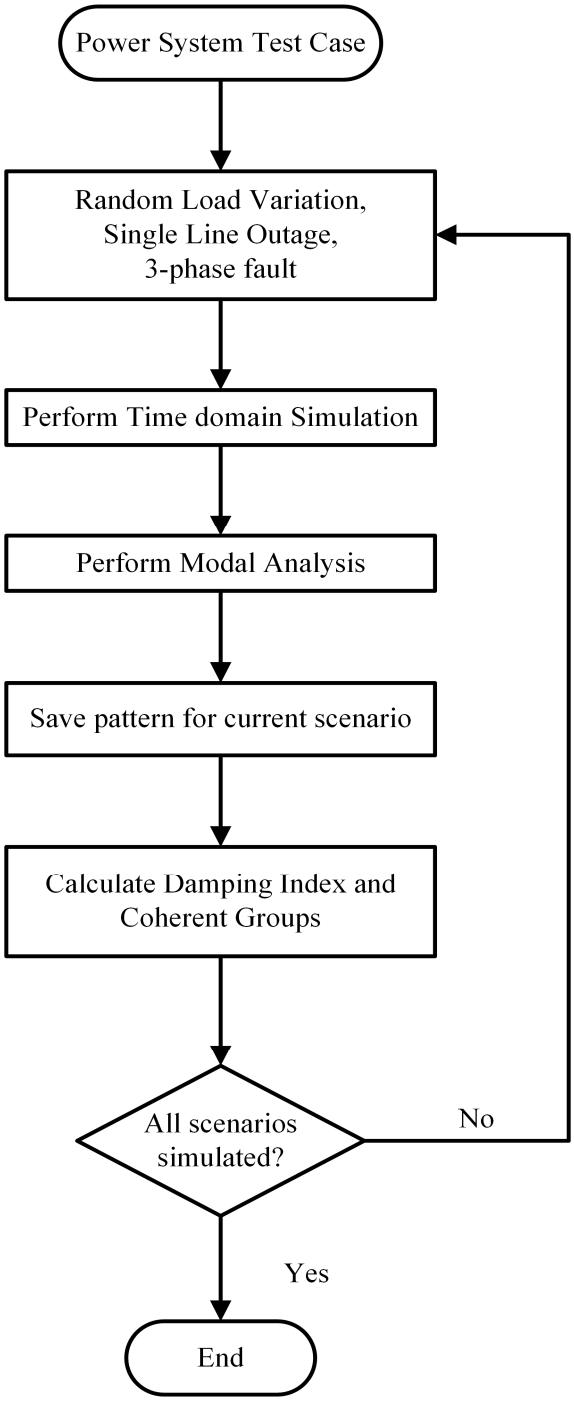

Fig. 3.4 Flowchart of data generation for Coherent Groups Identification

The output vector consists of *DI* and generator coherent groups predicted using a single ANN, given by

$$\left[y_o \right] = \left[DI_i, CG_j \right] \tag{3.15}$$

where DI_i, CG_j denotes Damping Index for each i^{th} mode and coherent group information for each j^{th} generator.

3.7 SIMULATION AND RESULTS

The effectiveness of the proposed methodology is investigated on IEEE 39-bus New England test system [116]. The system has 10 generators, 12 transformers and 46 transmission lines. Bus no. 39 is taken as slack bus. The detailed system data is given in the Appendix A and can also be referred from IEEE report [117]. The simulations are performed using MATLAB 2015b [118] and PSAT software [119] with Intel Core i5, 2.50 GHz, 4GB RAM computer.

3.7.1 Optimal PMU Placement

A multi-criteria contingency constrained methodology is proposed for OPP problem, which utilizes ILP. The methodology presented ensures complete observability under N-1 contingencies, including line outages and loss of PMUs.

A. Determination of Critical Buses

Three types of critical buses are to be identified as critical tie-line buses, critical generator buses and vulnerable buses. The results of various findings are presented below. The values of thresholds taken in different cases are system dependent and may be different for different systems. These thresholds are set based on operator experience and knowledge. The line outages are performed by opening the breaker at t=0.5 seconds for all the transmission lines.

(i) First the critical tie-lines are determined. The critical tie-lines are found from the Newton-Raphson load flow solution of the 39-bus system. The system total generation is 6138.71 MW. So, it has been decided to keep around 10% of this value as the threshold for power flow in tie-lines. So, threshold value, ε_t, is chosen as 600 MW. The critical lines having power flow more than threshold are selected using the procedure explained in section 3.2.1, and the list of critical buses T_L is formed. As shown in Table 3.2, four critical buses are selected and stored in T_L.

TABLE 3.2
RESULTS FOR CRITICAL TIE-LINE BUSES

S.No.	Line No.	From-To	Power flow (P_{ij})	T_L
1.	45	29-38	824.77 MW	
2.	19	10-32	650.00 MW	
3.	36	22-35	650.00 MW	10, 19, 22, 29
4.	31	19-33	628.95 MW	
5.	34	21-22	605.46 MW	

(ii) The next task is to find out the critical generator buses using the method discussed in section 3.2.1. The threshold value, ε_g is taken as 0.25. The generators having normalized participation factor greater than ε_g are selected as critical and the corresponding generator bus is stored in T_G. Then the buses are ordered in descending order in T_G, based on the number of times each generator bus is appearing for all the contingency cases.

In the system under study there are 46 transmission lines, so 46 N-1 contingency (line outage) cases are studied. The results are shown in Table 3.3. The result shows the top three generators appearing maximum times in critical list. Out of these three, top two participating generators buses are selected for critical list and saved in T_G as shown in Table 3.3. Fig. 3.5 shows the bar chart of generator participation in inter-area mode for a sample case when line 14-15 is opened. It shows that the generator 10 has the highest participation in the inter-area mode followed by generator 5 and 9.

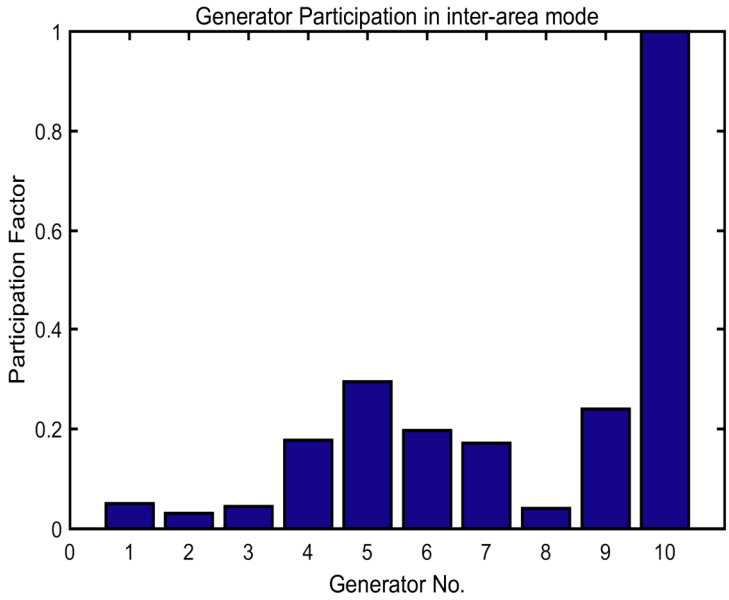

Fig. 3.5 Generator participation in LFO for outage of line 14-15

TABLE 3.3
RESULTS FOR CRITICAL GENERATOR BUSES

S.No.	Generator No.	Bus No.	No. of times bus appeared in critical list	T_G
1.	10	39	40	
2.	5	34	14	34, 39
3.	9	38	8	

(iii) The next step is to find out the vulnerable buses with large phase angle deviation. The threshold value, θ_v is taken as 10^0 [25]. The maximum angular deviations of each bus for all the 46 contingencies are computed. The buses having phase angle deviation with respect to *COI* greater than 10^0 are grouped in MV list and remaining in LV list. Then the buses are ordered in descending order in T_V, based on the number of times each bus is appearing in MV list over all the contingency cases. The results are shown in Table 3.4. The results show the top nine buses which are appearing maximum times in critical list and out of them four buses are selected and saved in T_V. The buses with maximum connecting neighbouring buses are selected. The bus no. 20, 21, 23, 33, 35 becomes observable by placing PMUs at 19, 22, 36, 19 and 22 respectively. Therefore, these buses are removed from T_V. Fig. 3.6 shows the maximum phase angle deviations for all buses for a sample case for the outage of line 16-21. It clearly shown that bus 21 has maximum angular deviation followed by bus no. 35, 22, 36, 23 and so on.

TABLE 3.4
RESULTS FOR VULNERABLE BUSES

S.No.	Bus No.	No. of times bus appeared in critical list	T_V
1.	19	19	
2.	20	19	
3.	21	19	
4.	22	19	
5.	23	19	19, 22,34, 36
6.	33	19	
7.	34	19	
8.	35	19	
9.	36	19	

The complete critical bus list is formed by summing up the critical buses obtained in above three studies and is given by C_B.

$$C_B = T_L \cup T_G \cup T_V = [10, 19, 22, 24, 29, 34, 36, 39]$$

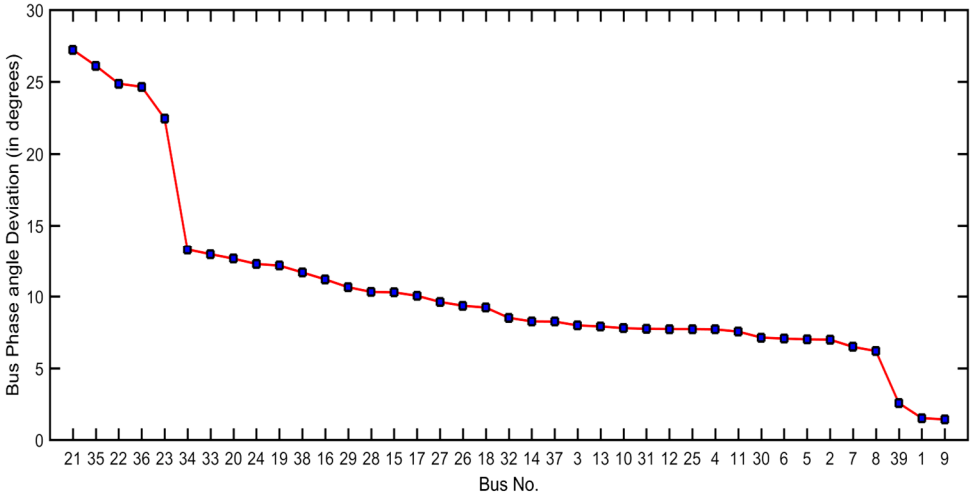

Fig. 3.6 Bus maximum phase angle deviation for the outage of line 16-21 (in descending order)

B. Optimal PMU Placement (OPP) Results

After finding the critical buses, the optimal locations of PMUs are obtained using modified ILP detailed in section 3.2. The optimal PMU placement result for IEEE 39-bus test system is shown in Table 3.5. The bus locations of PMUs are also shown in Fig. 3.7. The number of PMUs obtained using the proposed approach is 20. Thus, using the proposed method only 20 PMUs (approx. 50% of number of buses) need to be placed to monitor the low frequency oscillations in real-time considering topological variations and single PMU loss.

TABLE 3.5
RESULT OF PMU PLACEMENT

	No. of PMUs	**PMU Locations (Bus No.)**
Ref. [5]	26	2,3,6,8,10,12,13,14,16,17,19,20,22,23,25,26,29,30,31,32,33,34,35,36,37,38
Ref. [24]	22	3,6,8,9,10,16,18,20,21,22,23,25,26,29,30,31,32,33,34,35,36,37,38
Proposed Approach	**20**	3,5,6,9,10,13,16,18,19,20,22,23,25,26,29,34,36,37,38,39

The obtained results are also compared with some published results and shown in Table 3.5. In [5] and [24] also, complete system observability with single line or PMU loss with minimum number of PMUs is proposed. In [5], the authors proposed PMUs placement in stages but during end stages of deployment, a large redundancy is observed which is quite clear from the high number of PMUs to be installed. In [24] also, the no. of PMUs required are higher than the proposed approach.

The focus of this study is to have high observability of low frequency oscillations, so criteria related to oscillations are incorporated in the OPP formulation. As compared to the PMU placement results in [5] and [24], the proposed method requires only 20 PMUs for observing the low frequency oscillations on priority while maintaining

complete system observability with single PMU or line loss in the system. Thus, the proposed methodology provides a practical solution to this constrained OPP problem. The advantage of the proposed scheme is that it is a generalized approach and any other criteria can be included according to the application requirement.

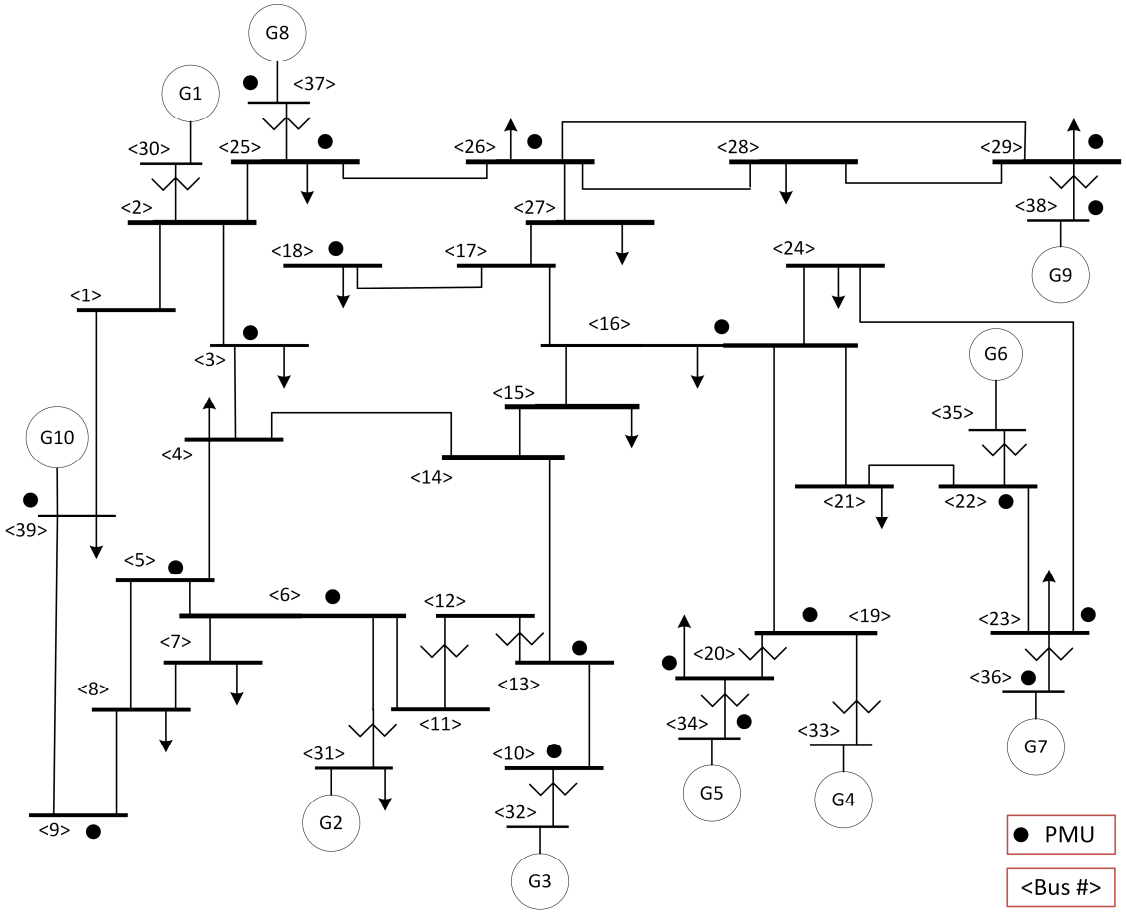

Fig. 3.7 PMU Locations for IEEE 39-bus test system

3.7.2 Low Frequency Oscillation Monitoring using PMU-ANN

The low frequency oscillation monitoring involves determination of Mode Index, frequency, damping ratio, Damping Index and participation factor of generators. This has been obtained using the proposed PMU-ANN based method. The data for ANN training is obtained from modal analysis performed offline for various operating conditions. These conditions include random load variations in the range of 100-120% of the base case values (in steps of 5%) and a number of N-1 contingencies (single line outages) to cover all possible load scenarios. Thus, a dataset of 1500 patterns is generated giving a range of operating conditions to train and test the ANN. Out of these 1500 operating conditions, 900 are used for training and 600 for testing.

The input dataset consists of bus voltage magnitudes and angles obtained from optimally placed PMUs. Thus, from 20 PMUs a total of 40 variables (20 voltages and 20 angles) are taken as initial input for features. Then, PCA is employed for selecting the most prominent and discriminatory features and the input features are reduced from 40 to 14. The approximation precision for selecting the variables calculated using (3.9) is 0.9901. This gives a dimensionality reduction of 65%. Thus total 14 variables (obtained from PMU) are fed as input to the ANN. The initial feature set and the final selected feature set is shown in Table 3.6. The features selected after dimension reduction are actually the most significant ones of the total set. It can be seen that voltage angles of important tie-line buses and generator buses are selected by PCA. It once again verifies the PMU placement methodology adopted in the previous section.

TABLE 3.6
FEATURES SELECTED USING PCA

Initial Feature Set FS_i	Final Selected Feature Set, FS_f	Dimensionality Reduction (%)
$\|V\|_3$, $\angle V_3$, $\|V\|_5$, $\angle V_5$, $\|V\|_6$, $\angle V_6$, $\|V\|_9$, $\angle V_9$, $\|V\|_{10}$, $\angle V_{10}$, $\|V\|_{13}$, $\angle V_{13}$, $\|V\|_{16}$, $\angle V_{16}$, $\|V\|_{18:20}$, $\angle V_{18:20}$, $\|V\|_{22}$, $\angle V_{22}$, $\|V\|_{23}$, $\angle V_{23}$, $\|V\|_{25}$, $\angle V_{25}$, $\|V\|_{26}$, $\angle V_{26}$, $\|V\|_{29}$, $\angle V_{29}$, $\|V\|_{34}$, $\angle V_{34}$, $\|V\|_{36:39}$, $\angle V_{36:39}$ (Total :40 features)	$\angle V_6$, $\angle V_9$, $\angle V_{10}$, $\angle V_{16}$, $\angle V_{18}$, $\angle V_{19}$, $\angle V_{22}$, $\angle V_{25}$, $\angle V_{29}$, $\angle V_{34}$, $\angle V_{36:39}$ (Total :14 features)	65.00

As discussed in section 3.5, the mode frequency, damping ratio, Mode Index, Damping Index and participation factor values are predicted using ANN. The acceptable damping limit to identify the critical modes is system dependent and typically in the range of 3-5% [120]. In this it has been assumed to be 2.5%. Two sets of ANNs have been trained for these studies. One set for prediction of Mode Index, frequency and damping ratio of modes and other for Damping Index and participation factor values prediction.

A. Prediction of Mode Index, frequency and damping ratio

In this method, single FFNN and single RBFNN is trained to predict a vector consisting of mode index, mode frequency and damping ratio values on the basis of same input set. Both ANNs have been trained for 900 operating conditions. The application results of FFNN and RBFNN are summarized in Table 3.7-3.9.

The performance evaluation of the proposed FFNN and RBFNN in predicting the outputs is given in Table 3.7. The performance function calculated is Mean Squared Error (MSE) given by eq. (3.16), where n is the number of predictions and y and y_0 are the predicted and known values of output respectively.

$$MSE = \frac{1}{n} \sum_{o=1}^{n} \left(y_o - y \right)^2 \tag{3.16}$$

It can be seen from the result that the MSE is very less for both training and testing phase for both the ANNs. Even for unforeseen conditions, the error is nearly 0.03% for FFNN and 0.04% for RBFNN which is reasonably acceptable prediction error. Also, the average prediction time for every operating state is of the order of 10^{-4} seconds which is almost real-time, which makes them suitable for online and real-time applications. It is seen from the results that the performance of both the networks is nearly same. However, FFNN performs slightly better than RBFNN as MSE is lower and the testing time per sample is also less. Thus, it can be concluded from these results that both the ANNs gives good performance and any one of these can be utilized while implementing this method for real-time applications.

TABLE 3.7
PERFORMANCE EVALUATION OF ANNS

PARAMETERS	FFNN	RBFNN
Total Operating Conditions	1500	1500
No. of Training Samples	900	900
No. of Testing Samples	600	600
No. of Features Selected	14	14
Computation Time for Training (s)	14.0968	13.1073
Computation Time for Testing/Sample (s)	2.1683×10^{-4}	5.487×10^{-4}
MSE (Training Data)	1.8473×10^{-4}	1.9867×10^{-4}
MSE (Test Data)	3.2220×10^{-4}	4.0112×10^{-4}

The sample test results of the proposed method to determine Mode Index (MI_i), and mode type for some of the sample operating conditions simulated for IEEE 39-bus system are shown in Table 3.8. Table 3.9 show the test results of the proposed method used to determine the mode frequency and damping ratio for the same sample cases. For the sake of comparison, the result obtained using modal analysis is also shown. For each sample operating condition shown, 9 modes are obtained. The modes are listed in order of their frequency from highest to lowest. The values shown in these tables are the normalized values.

The conclusions drawn from the Table 3.8 and 3.9 can be summarized as:

1. It can be seen from Table 3.8 that the values of the Mode Index predicted by both the ANNs are almost equal to the actual values. The predicted values of *MI* clearly distinguishes between the local and inter-area mode.

2. The average prediction error for FFNN for three sample cases shown for MI_i is 0.2253%, 0.5789% and 0.0398%, which is very less. Similarly, for RBFNN this error is 0.2381%, 0.6012%, and 0.0651% respectively for the three sample cases.

3. For 110% loading of base case (Case I) without any line outage, it is found that first 8 modes are local modes and the last mode is inter-area mode. Similarly, for 115% (Case II) and 105% (Case III) loading of base case with single line outages, there are two and one inter-area modes respectively. The outage of line between buses 16-17 causes triggering of an extra inter-area mode in the system.

TABLE 3.8
TEST RESULTS OF *MI* FOR SAMPLE OPERATING CONDITIONS

Operating Condition No.	Loading in % of Base Case	Mode No.	Modal Analysis		PMU-ANN based Method			
					FFNN		RBFNN	
			MI_i^*	Mode Type	MI_i^*	Mode Type	MI_i^*	Mode Type
278 (Case I)	110%	1	0.9661	Local	0.9650	Local	0.9634	Local
		2	1	Local	1	Local	1	Local
		3	0.8876	Local	0.8808	Local	0.8798	Local
		4	0.6435	Local	0.6248	Local	0.6312	Local
		5	0.9824	Local	0.9808	Local	0.9788	Local
		6	0.4620	Local	0.4531	Local	0.4511	Local
		7	0.7832	Local	0.7987	Local	0.7673	Local
		8	0.7442	Local	0.7511	Local	0.7592	Local
		9	0.1961	Interarea	0.1907	Interarea	0.2056	Interarea
860 (Case II)	115% (line outage of 16-17)	1	0.9747	Local	0.9767	Local	0.9789	Local
		2	1	Local	1	Local	1	Local
		3	0.9179	Local	0.9093	Local	0.8996	Local
		4	0.7840	Local	0.7834	Local	0.7869	Local
		5	0.9882	Local	0.9853	Local	0.9799	Local
		6	0.5240	Local	0.5170	Local	0.5187	Local
		7	0.4971	Local	0.5006	Local	0.5054	Local
		8	0.4419	Interarea	0.4834	Interarea	0.4701	Interarea
		9	0.3853	Interarea	0.3896	Interarea	0.3954	Interarea
1125 (Case III)	105% (line outage of 28-29)	1	0.9651	Local	0.9651	Local	0.9626	Local
		2	1	Local	1	Local	1	Local
		3	0.8932	Local	08948	Local	08974	Local
		4	0.6642	Local	0.6731	Local	0.6764	Local
		5	0.9747	Local	0.9733	Local	0.9791	Local
		6	0.5456	Local	0.5391	Local	0.5309	Local
		7	0.6107	Local	0.6193	Local	0.6242	Local
		8	0.8338	Local	0.8333	Local	0.8357	Local
		9	0.2315	Interarea	0.2242	Interarea	0.2169	Interarea

* Normalized Values

4. On comparing the modes frequencies and damping ratios in Table 3.9, it is found that the values obtained by the proposed method are almost same as that obtained using offline modal analysis. It has been already seen from the Table 3.7 that prediction accuracy of both the ANNs is good and same can be observed from the sample cases results. However, FFNN is performing slightly better as compared to RBFNN. Thus, the test results validate the effectiveness of the proposed method for online and real-time monitoring of the low frequency oscillation modes.

TABLE 3.9
TEST RESULTS OF FREQUENCY & DAMPING RATIO FOR SAMPLE OPERATING CONDITIONS

Operating Condition No.	Loading in % of Base Case	Mode No.	Modal Analysis		PMU-ANN based Method			
					FFNN		RBFNN	
			f_i^*	ζ_i^*	f_i^*	ζ_i^*	f_i^*	ζ_i^*
278 (Case I)	110%	1	0.2263	0.0168	0.2283	0.0207	0.2178	0.0223
		2	0.1887	0.0162	0.1929	0.0207	0.1986	0.0218
		3	0.1800	0.0149	0.1832	0.0194	0.1877	0.0201
		4	0.1721	0.0159	0.1768	0.0199	0.1792	0.0211
		5	0.1609	0.0145	0.1637	0.0179	0.1661	0.0188
		6	0.1487	0.0150	0.1514	0.0203	0.1575	0.0209
		7	0.1384	0.0146	0.1432	0.0170	0.1417	0.0198
		8	0.1246	0.0166	0.1315	0.0204	0.1337	0.0220
		9	0.0889	0.0142	0.0929	0.0187	0.0973	0.0177
860 (Case II)	115% (line outage of 16-17)	1	0.2823	0.0928	0.2813	0.0957	0.2851	0.0974
		2	0.2514	0.0919	0.2547	0.0938	0.2573	0.0963
		3	0.2410	0.0903	0.2429	0.0912	0.2445	0.0931
		4	0.2322	0.0918	0.2343	0.0938	0.2365	0.0943
		5	0.2271	0.0897	0.2258	0.0930	0.2297	0.0924
		6	0.2101	0.0901	0.2089	0.0916	0.2047	0.0930
		7	0.1997	0.0912	0.2031	0.0912	0.2083	0.0940
		8	0.1756	0.0931	0.1850	0.0913	0.1903	0.0982
		9	0.1514	0.0901	0.1513	0.0940	0.1548	0.0929
1125 (Case III)	105% (line outage of 28-29)	1	0.2350	0.0296	0.2355	0.0299	0.2375	0.0316
		2	0.1987	0.0291	0.1988	0.0292	0.1994	0.0305
		3	0.1897	0.0275	0.1902	0.0274	0.1923	0.0291
		4	0.1802	0.0287	0.1805	0.0285	0.1836	0.0298
		5	0.1718	0.0273	0.1715	0.0274	0.1731	0.0290
		6	0.1580	0.0278	0.1585	0.0277	0.1598	0.0295
		7	0.1404	0.0292	0.1416	0.0294	0.1439	0.0312
		8	0.1249	0.0289	0.1246	0.0290	0.1276	0.0310
		9	0.0996	0.0273	0.0993	0.0271	0.0971	0.0294

* Normalized Values

B. Prediction of Damping Index and participation factor

In this study, two FFNN and two RBFNN are trained to predict *DI* and participation factor values simultaneously on the basis of same input set. Both ANNs have been trained for 900 operating conditions. The application results of FFNN and RBFNN are summarized in Table 3.10-3.13.

The performance evaluation of the ANNs used for *DI* prediction is given in Table 3.10. It can be seen from the result that the MSE is very less for both the ANNs. Even for unforeseen conditions, the error is nearly 2.96% for FFNN and 1.72% for RBFNN which is reasonably acceptable prediction error. Also, the average prediction time for every operating state is of the order of 10^{-4} seconds which is almost real-time, which makes them suitable for online and real-time applications. In this case the RBFNN performs better than FFNN.

TABLE 3.10
PERFORMANCE EVALUATION OF ANNS (FOR *DI*)

PARAMETERS	FFNN	RBFNN
Total Operating Conditions	1500	1500
No. of Training Samples	900	900
No. of Testing Samples	600	600
No. of Features Selected	14	14
Computation Time for Training (s)	2.4276	0.8421
Computation Time for Testing/Sample (s)	4.1735×10^{-4}	2.5383×10^{-4}
MSE (Training Data)	0.0218	0.0155
MSE (Test Data)	0.0296	0.0172

For the base case condition, the system excites 8 local and one inter-area mode. Table 3.11 shows the value of *DI* obtained from RBFNN and FFNN for a few sample cases for the inter-area mode. These values are also compared with the actual values obtained from Modal Analysis. On the basis of the index values, system is classified as poorly damped or well damped. The values shown here are normalized values. Hence the values above 0.96 are indicating that the damping is below 2.5%. From Table 3.11, it can be seen that both FFNN and RBFNN predicts the state of all the sample conditions correctly. As value of *DI* above 0.96 is treated as poorly damped condition, it is found that all the three sample cases shown here are poorly damped and needs an increase in damping. To find the main source for this low damping situation, or the most critical generator, the participation factor values are used. The participation factor values for all modes, for every operating condition, are predicted simultaneously with *DI* prediction.

TABLE 3.11
TEST RESULTS OF *DI* FOR INTER-AREA MODE FOR SAMPLE OPERATING CONDITIONS

Operating Condition No.	Loading (in % of base case)	Damping Ratio (ζ_i)	*DI**			System Status
			Modal Analysis	FFNN	RBFNN	
286	110%	0.0197	0.9651	0.9621	0.9616	Poorly Damped
775	110% (line outage of 16-17)	0.0201	0.9668	0.9782	0.9748	Poorly Damped
1150	105% (line outage of 28-29)	0.0194	0.9694	0.9934	0.9850	Poorly Damped

* Normalized Values

Table 3.12 shows the performance evaluation of ANNs for estimating the participation factor. This time also it can be inferred that both the ANNs give accurate results with very less error and the testing time/sample for the unseen operating conditions is very small. In this case also RBFNN works better than FFNN. The result shows that the method can be suitably employed for online applications.

TABLE 3.12
PERFORMANCE EVALUATION OF ANNS (FOR *PF*)

PARAMETERS	FFNN	RBFNN
Total Operating Conditions	1500	1500
No. of Training Samples	900	900
No. of Testing Samples	600	600
No. of Features Selected	14	14
Computation Time for Training (s)	3.5243	0.8223
Computation Time for Testing/Sample (s)	3.2469×10^{-4}	2.6100×10^{-4}
MSE (Training Data)	3.8634×10^{-3}	7.5908×10^{-4}
MSE (Test Data)	5.6497×10^{-3}	8.7179×10^{-4}

Table 3.13 shows the most critical generator predicted using this method for the same three sample insecure cases. The results show that both the ANNs predict the most critical generator correctly for all conditions. The participation factor values predicted by ANNs are almost similar to the actual values for all the cases. The participation factor for G8 is nearly zero in all the cases which shows that it has negligible participation in the given interarea mode. The highest participation is of G10 and lowest of G8 which is correctly predicted by both the models of ANN. However, the close observation shows that RBFNN is slightly better than FFNN. With the main source of oscillations known, the operator can now implement the corrective actions to damp the growing oscillations.

TABLE 3.13
TEST RESULTS OF PARTICIPATION FACTOR FOR INTER-AREA MODE FOR SAMPLE OPERATING CONDITIONS

Sample Case		Participation Factor (pf_i)*										Most Critical Gen.
		G1	*G2*	*G3*	*G4*	*G5*	*G6*	*G7*	*G8*	*G9*	*G10*	
1	***Modal Analysis***	0.0159	0.0499	0.0903	0.2199	0.4798	0.2631	0.1574	~0	0.1484	1	G10
	FFNN	0.0189	0.0512	0.0978	0.2064	0.4932	0.2517	0.1756	~0	0.1579	1	G10
	RBFNN	0.0177	0.0436	0.0945	0.2253	0.4879	0.2696	0.1803	~0	0.1461	1	G10
2	***Modal Analysis***	0.0095	0.0592	0.1237	0.3495	0.6437	0.4479	0.3438	~0	0.0875	1	G10
	FFNN	0.0102	0.0645	0.1262	0.3587	0.6582	0.4598	0.3234	~0	0.0961	1	G10
	RBFNN	0.0098	0.0570	0.1203	0.3349	0.6319	0.4265	0.3301	~0	0.0869	1	G10
3	***Modal Analysis***	0.0162	0.0255	0.0699	0.1619	0.3522	0.2263	0.1564	~0	0.5108	1	G10
	FFNN	0.0142	0.0306	0.0679	0.1732	0.3678	0.2359	0.1689	~0	0.5076	1	G10
	RBFNN	0.0160	0.0273	0.0735	0.1689	0.3441	0.2179	0.1547	~0	0.5089	1	G10

* Normalized Values

These poorly damped modes may appear due to heavy power flow over the weak ties between the two areas formed or if PSSs are not well tuned in some generators and the system is highly stressed in studied scenario. Once the critical generator is known, suitable corrective control actions such as PSS retuning, reinforcing weak AC ties, generator rescheduling, etc. may be implemented. If these corrective action(s) are applied within time then the system's damping can be improved and any possible failure could be avoided.

The participation of various generators in the given inter-area mode for the three sample operating conditions is also shown by bar chart plots in Fig 3.8. It clearly shows that the participation of generator 10 is highest in the inter-area mode for all the cases. The plots also confirms that the values predicted by the ANNs are very close to the modal analysis values.

Fig. 3.9 shows mode shape plots for these three poorly damped cases for the inter-area modes. It can be seen from this figure that for all the three cases generator 10 is swinging against the remaining generators.

Thus by using the proposed method, the oscillatory dynamics and the stability of the system is obtained in real-time irrespective of system size and operating condition. For the poorly damped cases, operator can simultaneously find out the main driver of that critical mode or most critical generator, and thus can apply suitable corrective action(s). In one case, FFNN performs better while in other RBFNN performs better out of the two. However, it can be inferred from the results that both are suitable for such type of applications and any of them could be employed for real-time monitoring of low frequency oscillations in the power system.

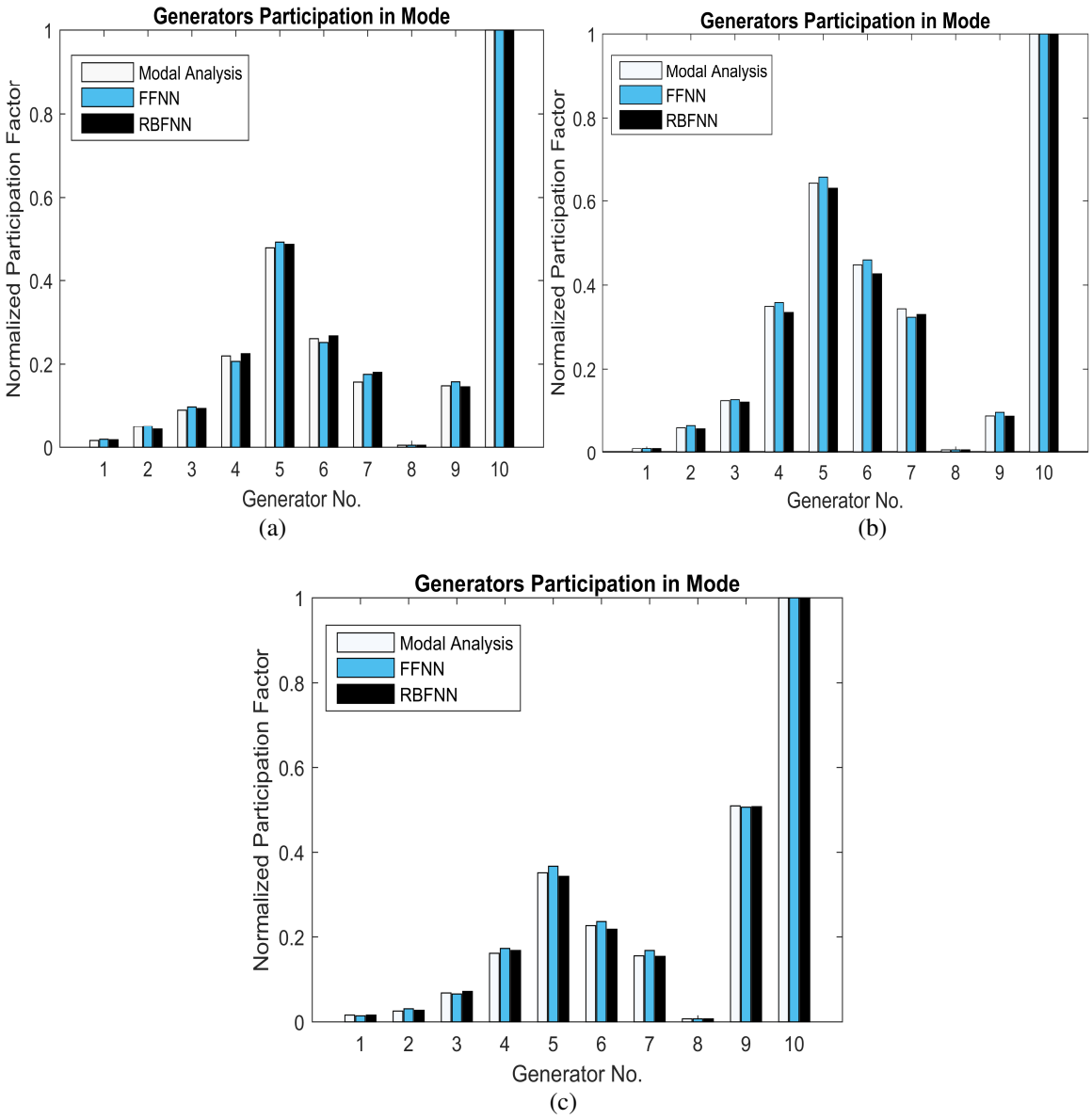

Fig. 3.8 Generators participation in inter-area mode
(a) Condition no. 286 (b) Condition no. 775 (c) Condition no. 1150

The proposed method utilizes the variable values recorded by PMUs with a very high sampling rate of around 60 samples/second. Thus, a large amount of data is available to the operator in real-time through PMUs, which validates the real-time implementation effectiveness of the proposed methodology. The ANN predicts the output accurately in very less time of the order of 10^{-4} seconds without running any simulation for all the unseen operating conditions which validates its effectiveness for online applications. Thus, the proposed method works well for the both online and real-time applications for a wide range of operating conditions.

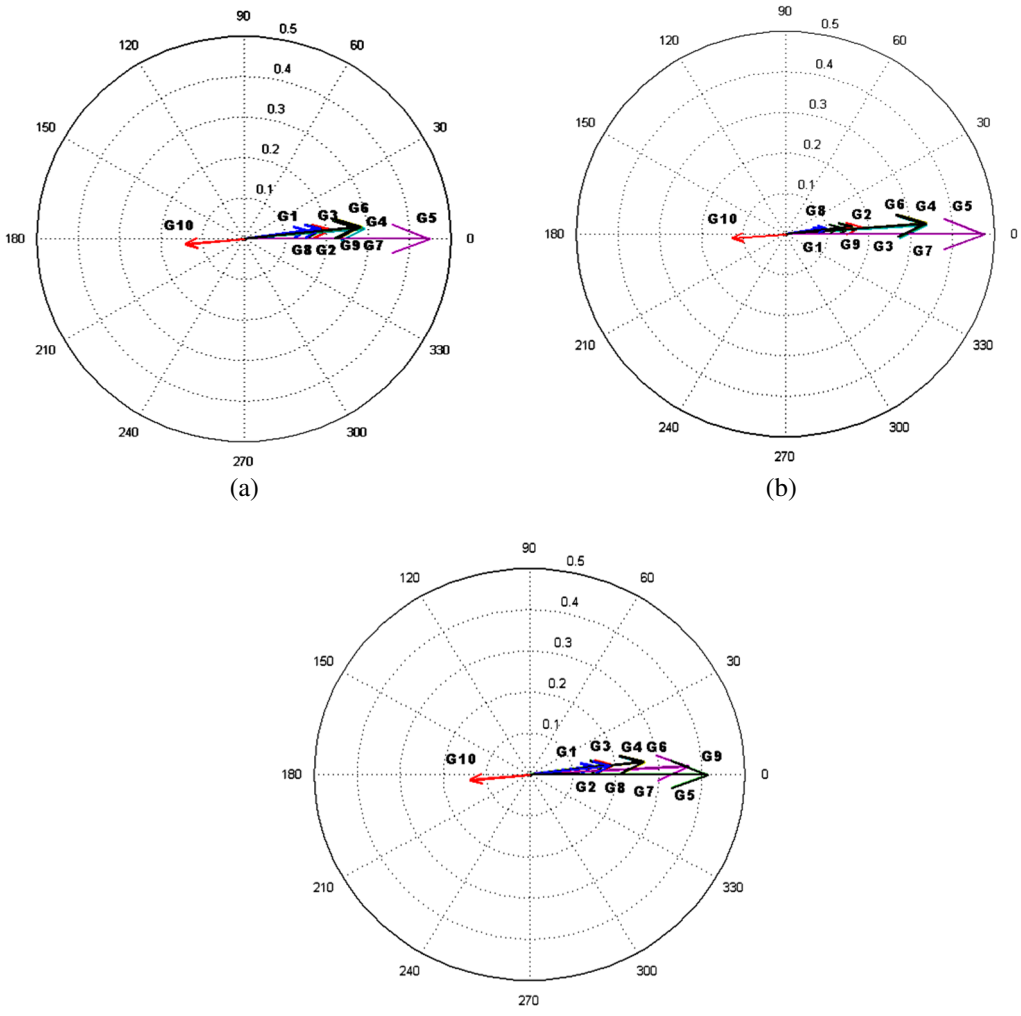

Fig. 3.9 Mode shape plots for inter-area mode
(a) Condition no. 286, (b) Condition no. 775, (c) Condition no. 1150

3.7.3 Coherent Groups Identification using PMU-ANN

The coherency identification involves identification of coherent generator groups in the system. Along with coherency, the values of *DI* are also predicted in this study. This has been obtained using the proposed PMU-ANN based method. The data for ANN training is obtained from Modal Analysis performed offline for various operating conditions. In order to cover wide operating conditions, the active and reactive loads at all buses are varied in range of 100%-110% of the base case with a step of 2.5%. Single line outages and 3-phase faults are considered as disturbances along with load change. The 3-phase faults duration is varied from six to nine cycles. Thus, a statistical, complete and comprehensive dataset of 2000 patterns is generated giving a range of operating conditions to train and test the ANN. Out of these, 1200 are used for training and 800 for testing.

For each operating condition, the line outage or fault is applied at 0.5 s and values of bus voltage magnitude, $|V|$ and angle, $\angle V$ from 20 PMUs are taken for first four cycles after the instant of disturbance. Therefore, there are 160 variables (20×4+20×4) taken as initial input for features. Then, PCA is employed for selecting the most prominent and discriminatory features out of these 160 and the input features are reduced from 160 to 8. The approximation precision for selecting the variable is 0.9995. This gives a dimensionality reduction of 95.00%. The initial feature set and the final selected feature set is shown in Table 3.14. In addition, generator rotor angles are recorded at a certain desired time (after 3 seconds in this study) to calculate generator coherency for each case. So, the values of *DI* and coherent group are predicted by both the ANNs and their results are compared using the proposed PMU-ANN based method.

TABLE 3.14
FEATURES SELECTED USING PCA

Initial Feature Set FS_i	Final Selected Feature Set, FS_f	Dimensionality Reduction (%)
$[\ \|V\|_3, \angle V_3, \|V\|_5, \angle V_5, \|V\|_6, \angle V_6, \|V\|_9, \angle V_9, \|V\|_{10}, \angle V_{10}, \|V\|_{13}, \angle V_{13}, \|V\|_{16}, \angle V_{16}, \|V\|_{18:20}, \angle V_{18:20}, \|V\|_{22}, \angle V_{22}, \|V\|_{23}, \angle V_{23}, \|V\|_{25}, \angle V_{25}, \|V\|_{26}, \angle V_{26}, \|V\|_{29}, \angle V_{29}, \|V\|_{34}, \angle V_{34}, \|V\|_{36:39}, \angle V_{36:39}\ ]_{t=1,2,3,4}$ (Total :160 features)	$[\angle V_6, \angle V_{10}, \angle V_{19}, \angle V_{29}, \angle V_{36:39}\ ]_{t=4}$ (Total :8 features)	95.00

In this method, one FFNN and one RBFNN is trained to predict a vector consisting of *DI* and coherent group values on the basis of same input set. Both ANNs have been trained for 1200 operating conditions. The application results of FFNN and RBFNN are summarized in Table 3.15-3.17.

The performance evaluation of the proposed FFNN and RBFNN in predicting the outputs is given in Table 3.15. It can be seen from the result that the MSE is very less for both training and testing phase for both the ANNs. Even for unforeseen conditions, the error is nearly 0.4% for FFNN and 0.6% for RBFNN which is reasonably acceptable prediction error. Also, the testing time per sample is very small of the order of 10^{-5} seconds which is almost real-time, which makes them suitable for real-time applications. It is seen from the results that the performance of both the networks is nearly same. However, FFNN performs slightly better than RBFNN as MSE is lower and the testing time per sample is also less. Thus, it can be concluded from these results that both the ANNs gives good performance in predicting *DI* values and Generator Coherent Groups' information and any one of these can be utilized while implementing this method for real-time applications.

TABLE 3.15
PERFORMANCE EVALUATION OF ANNS

PARAMETERS	FFNN	RBFNN
Total Operating Conditions	2000	2000
No. of Training Samples	1200	1200
No. of Testing Samples	800	800
No. of Features Selected	8	8
Computation Time for Training (s)	72.5715	57.1073
Computation Time for Testing/Sample (s)	8.800×10^{-5}	11.487×10^{-5}
MSE (Training Data)	0.0037	0.0052
MSE (Test Data)	0.0044	0.0064

The mode damping and thus the oscillatory stability status of the system is monitored and reported using the *DI* which is obtained from the output of ANN. For the base case condition of IEEE 39-bus system, the system excites 8 local and one inter-area mode. The modes are extracted using modal analysis. Both the ANNs are tested for various unseen operating conditions. The three sample conditions are shown in Table 3.16. The results obtained from ANNs are compared with the offline modal analysis values. The index values shown in table are normalized values. Hence, the *DI* values above 0.96 are indicating that the damping is below 2.5%. For each of the sample operating condition shown here system excites eight local and one interarea mode.

It can be observed from the results that the values of the *DI* predicted by both the FFNN and RBFNN are almost equal to the actual values. For Case I, the interarea mode is the poorly damped mode as indicated by the *DI* value. Both FFNN and RBFNN correctly identifies it as a poorly damped mode as clear from *DI* values predicted by these ANNs. Thus, the ANNs correctly classify the system as in insecure state. For Case II, two local modes are having damping below 2.5%. In this case also ANNs correctly identifies the critical modes. Similarly, in Case III, where the interarea mode is poorly damped, ANNs correctly identifies the poorly damped mode. In Table 3.16, all the three cases shown have poorly damped critical modes. Due to these critical modes, the system is small signal insecure. Therefore, some control actions must be applied before the system becomes unstable. For applying the emergency control actions the generator coherency information might be required which is also predicted by the ANNs.

TABLE 3.16
TEST RESULTS OF DI_i FOR SAMPLE OPERATING CONDITIONS

Operating Condition No.	Loading in % of Base Case	Mode Type	Modal Analysis	PMU-ANN Based Method		
				Damping Index(DI_i)*		System Status
			Damping Index(DI_i)*	FFNN	RBFNN	
1987 (Case I)	105% (3-phase fault at bus 16 of 9 cycle)	Local	0.5162	0.5166	0.5182	**Insecure**
		Local	0.3193	0.3336	0.3100	
		Local	0.4404	0.4377	0.4622	
		Local	0.7194	0.7155	0.7025	
		Local	0.8456	0.8446	0.8552	
		Local	0.6968	0.7043	0.6950	
		Local	0.8273	0.8246	0.8134	
		Local	0.6178	0.5941	0.6337	
		Interarea	**1.0000**	**1.0048**	**0.9998**	
747 (Case II)	102.5% (line outage of 13-14)	Local	0.5908	0.5852	0.5065	**Insecure**
		Local	0.3373	0.3421	0.4348	
		Local	0.4159	0.4181	0.4182	
		Local	0.7851	0.7818	0.7914	
		Local	**1.0000**	**0.9943**	**0.9719**	
		Local	0.5710	0.5669	0.5927	
		Local	0.6015	0.5753	0.6277	
		Local	**1.0000**	**0.9914**	**0.9712**	
		Interarea	0.7972	0.7593	0.8111	
1561 (Case III)	110% (line outage of 5-6)	Local	0.5897	0.4931	0.4272	**Insecure**
		Local	0.3324	0.4093	0.4818	
		Local	0.4188	0.4172	0.4188	
		Local	0.7682	0.7543	0.7565	
		Local	0.8169	0.8205	0.7968	
		Local	0.6016	0.6131	0.6057	
		Local	0.8805	0.8651	0.8541	
		Local	0.6206	0.6282	0.6164	
		Interarea	**1.0000**	**0.9936**	**1.0020**	

* Normalized Values

The coherent groups information at some desired future instant (3 second in this study) is obtained using this method in real-time. For all the three insecure cases, coherency information available early in real-time might be useful in applying suitable control actions. The coherency results for above shown sample cases are shown in Table 3.17. The results shows that the proposed method predicts correct grouping information for all the sample cases using both the ANNs. Different number of coherent groups are formed in all the cases and the generators in coherent group also changes with change in operating scenario. The results show that when the system condition changes or the network topology varies, the classification of generators in a coherent group may change and thus the coherency information may also change with varying condition. Thus, it is required to evaluate this information in real-time after the disturbance for properly applying the required control action for insecure cases.

TABLE 3.17
TEST RESULTS OF COHERENT GROUPS FOR SAMPLE OPERATING CONDITIONS

Sample Case No.	Actual Coherent Groups (Generator No.)	Predicted Coherent Groups (Generator No.)	
		FFNN	RBFNN
Case I	Group 1: (1,2,3,4,5,6,7,8,9), Group 2: (10)	Group 1: (1,2,3,4,5,6,7,8,9), Group 2: (10)	Group 1: (1,2,3,4,5,6,7,8,9), Group 2: (10)
Case II	Group 1:(4,8,9), Group 2:(3,6), Group 3:(5,7), Group 4:(1,10), Group 5:(2)	Group 1:(4,8,9), Group 2:(3,6), Group 3:(5,7), Group 4:(1,10), Group 5:(2)	Group 1:(4,8,9), Group 2:(3,6), Group 3:(5,7), Group 4:(1,10), Group 5:(2)
Case III	Group 1:(2,3,4,5,6), Group 2:(7,8,9), Group 3:(1), Group 4:(10)	Group 1:(2,3,4,5,6), Group 2:(7,8,9), Group 3:(1), Group 4:(10)	Group 1:(2,3,4,5,6), Group 2:(7,8,9), Group 3:(1), Group 4:(10)

The coherency results are verified with time-domain simulation results. Fig. 3.10 shows the plots of relative rotor angle variation with time of various groups of coherent generators formed. The plots for each sample case are shown for 10 s duration. Also, a zoomed view of 3 s duration is shown for each case.

For Case I, it can be seen from Fig. 3.10(a) that there are two coherent groups formed. Generator 10 forms one group and remaining other generators forms one separate group. The rotor angle values are very high showing that the fault is pretty severe. The rotor angle values are increasing rapidly after the fault indicating that the system is going out of synchronism and is moving rapidly towards oscillatory instability.

Similarly, relative rotor angle variation plots are shown for Case II and III in Fig. 3.10(b) and Fig. 3.10(c). In Case II five coherent groups are formed and in Case III four groups are formed as predicted by ANNs. The rotor angle values are increasing continuously with time in these cases and thus these are oscillatory unstable cases and require application of control actions in real-time. All these plots validate the results obtained with the proposed method using ANN and proves the effectiveness of the method used. It proves that the ANNs correctly identify the insecure cases and the coherent group of generators in the system.

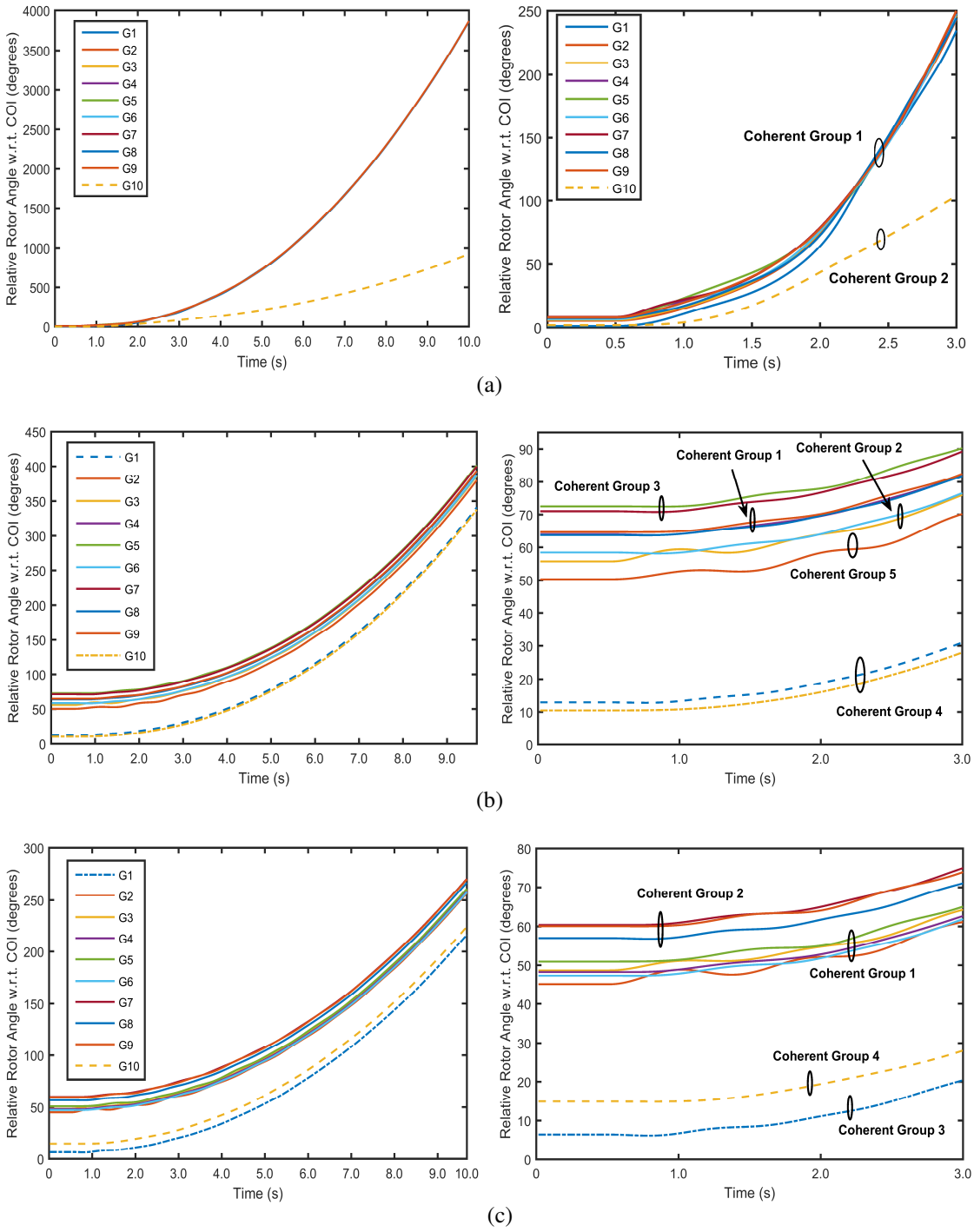

Fig. 3.10 Rotor angles variation with time (a) for Case I (b) for Case II (c) for Case III

In the proposed method, the oscillatory stability status and coherency information is obtained in real-time by using only first four cycle data after the instant of disturbance. It is utilizing the variable values recorded by PMUs with a very high sampling rate of around 60 samples/second. Thus, a large amount of data is available to the operator in real-time through PMUs, which validates the real-time implementation effectiveness of the proposed methodology. The testing time per

sample is in the order of 10^{-5} seconds without requiring any time taking mathematical computations, for all the unseen operating conditions, which also validates the method's effectiveness for online applications. As the coherency information is available within a few cycles of disturbance, the required emergency control measures can be put into operation accordingly in real-time.

3.8 SUMMARY

The information about oscillatory instability and their source should be known to the operator in real-time to initiate appropriate control actions. The determination of system oscillatory status using conventional methods is time consuming and at the same time not possible in real-time. Therefore, a PMU-ANN based monitoring is proposed in this chapter to identify the poorly damped modes and their source (most critical generator) in real-time under varying system conditions. In addition, the generator coherency status is predicted in advance which can assist in implementing emergency control strategies in real-time. Prior to that, a multi-criteria contingency constrained optimal PMU placement approach is also proposed. The analysis is carried on the IEEE 39-bus system to study the effectiveness of the proposed method in changing system conditions.

Following conclusions drawn from this chapter:

1. The proposed multi-criteria constrained optimal PMU placement approach for wide area low frequency oscillation monitoring effectively identifies the PMU locations for monitoring requirements. The advantage of the proposed scheme is that it is a generalized approach and any number of criteria can be included in problem formulation according to application requirement.
2. The proposed PMU-ANN based method employing FFNN and RBFNN performs well in predicting the Mode Index, frequency, damping ratio and critical generators of low frequency modes in real-time giving very small MSE and testing time/sample values.
3. The proposed PMU-ANN method provides a comprehensive tool for predicting the Mode Index, frequency, damping ratio and key drivers of low frequency modes in real-time which works very well even under varying system topology. Thus, it relieves the burden of designing a separate tool for each possible system operating topology. Moreover, it minimizes the need to keep abreast with every possible change in system topology which is a difficult task, specially, in the context of modern power systems.

4. Both the ANNs show excellent results in predicting the damping index and coherent groups in real-time giving very small MSE and testing time/sample values. The FFNN performs slightly better than RBFNN, and any one of them can be used for implementing this method.
5. The generator coherency information is predicted accurately in real-time utilizing only first four cycle data after the instant of disturbance for all unseen operating conditions independent of topological variation and most probable contingencies. The proposed scheme thus can be utilized while designing and implementing control actions requiring coherent generators information in real-time.
6. The proposed method is very fast and may serve as a promising tool for the both online and real-time applications for a wide range of operating conditions.

CHAPTER 4

DYNAMIC IMPACT ANALYSIS OF DFIG INTEGRATION ON LOW FREQUENCY OSCILLATIONS

4.1 INTRODUCTION

Due to rising global electricity demand, depleting fossil fuels and increasing environmental concerns, world is turning towards clean energy for electricity generation [78]. The wind energy is emerging as one of the most prominent renewable energy resources to augment present generation and in some cases replace the fossil based generation. Amongst the existing technologies, Variable Speed Wind Turbine (VSWT) equipped with Doubly Fed Induction Generator (DFIG) [79] is the most popular and widely used Wind Turbine Generator (WTG). This machine has noticeable advantages like improved efficiency, smooth grid connection, better control of active as well as reactive power and economy when compared with other WTGs. However, the WTG technology differs considerably from that of conventional Synchronous Generators (SGs). The increasing penetration of WTGs affects many aspects of the dynamic and operational characteristics of SG dominated power system. Thus, it is imperative to analyse their impact on system stability, reliability and security. One of the main concerns is their impact on the Low Frequency Oscillations (LFOs).

The WTGs are usually located in remote areas resulting in long distance power transmission which may significantly change the network power flow that affects system damping [74]. The change in the eigenvalue or the mode damping is caused by the change in load flow and system configuration and due to addition of dynamic interaction between conventional SGs and DFIG [75]. Wind power has characteristics of randomness, volatility and intermittence which affect the small signal stability of the system. The rotating mass of DFIG is decoupled from the grid frequency and does not inherently exhibit an inertial response unless controlled for that specific purpose. Being asynchronous machines, DFIGs do not inherently participate in LFO but the interaction of their dynamics with LFO modes of nearby SGs may change the characteristics of oscillations [76], [77]. The wind integration impacts oscillatory stability in two ways- (a) by changing the damping of the already present low frequency critical modes in the system, and (b) by addition of new modes of low damping in the system. If the damping

of critical mode improves and no new low damping mode shows up by wind integration, then it is beneficial for oscillatory stability of the system, otherwise not.

Literature survey shows both favorable and adverse effects of DFIG integration on LFO modes. It is necessary to systematically analyse the influence of wind power integration on power system oscillation modes and their damping characteristics. It is noted that in almost all of the studies the impact is studied by randomly integrating DFIG at any bus of the system or by randomly replacing some SGs partially or fully. However, the location of wind integration is crucial and affects the oscillatory stability. The effect of DFIG integration on system damping can be either positive or negative depending upon the location of penetration as found out in this study. Therefore, in this thesis, the location of DFIG is presented as an important factor influencing the damping of LFOs.

There are mainly two ways to integrate DFIG in the system:

a) By fully or partially replacing some existing SGs, or
b) By adding it directly to non-generator buses.

When the focus of integration is to serve the increasing load demand the DFIGs may be directly added and when the focus is on replacing the old conventional generation, the DFIGs may be added replacing existing SGs partially or fully. Most of the WTGs integrated in existing power systems in the recent times are serving to meet the new load growth. Therefore, practically they do not replace existing SGs. In this chapter, DFIGs are integrated by both the ways and their dynamic impact on LFOs damping is studied.

In the first case when DFIGs are integrated replacing the SGs in the system, the dynamic impact analysis of DFIG integration on the LFO based on the damping ratio sensitivity is carried out. The results obtained with sensitivity analysis are validated with detailed eigenvalue analysis of all the study cases. The results are tested with different operating conditions and disturbance scenarios. The analysis is further extended to examine the individual impacts of SG removal and wind addition in the system. Also, the increased penetration of DFIG and its impact on LFOs are analysed.

In the second case when DFIGs are integrated on non-generator buses, the impact of locations of DFIG integration on damping is carried out using eigenvalue analysis and dynamic sensitivity analysis. The former is a well-established conventional technique while latter is based on the values obtained from PMUs. These methods

provide information about the suitable location of DFIG integration and their impact on small signal stability of system.

4.2 DFIG MODELLING

The DFIG based wind power generation mainly composed of a wind turbine, gear box, generator, power electronic based Grid Side Converter (GSC) and Rotor Side Converter (RSC) and the supplementary controllers [79]. The wind farm is represented as a single equivalent unit at a bus having MVA rating equal to the sum ratings of all the wind turbines. Fig. 4.1 shows the basic block diagram representation of the DFIG wind turbine [101]. A number of components that are essential for modelling the dynamics of DFIG based wind generation are included in the study. These are: turbine aerodynamics, turbine mechanical control, shaft dynamics, generator electrical characteristics, three controllers for controlling frequency/active power, voltage/reactive power, and pitch angle/mechanical power.

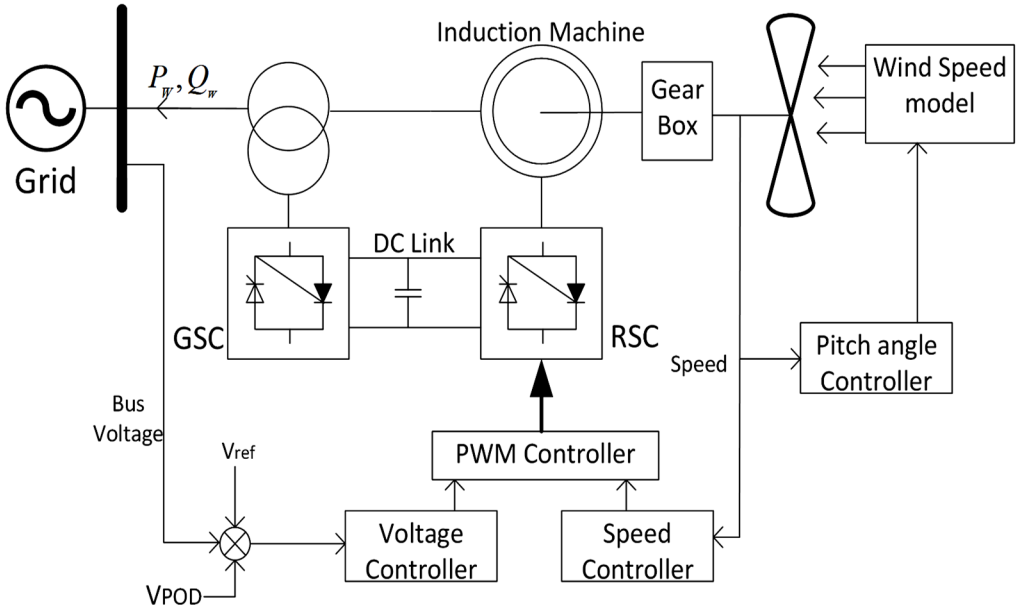

Fig. 4.1 Basic block diagram of DFIG wind turbine

The rotor and stator flux dynamics of the DFIG are fast as compared to the grid dynamics, so the steady state model is assumed. The electrical dynamics of DFIG is shown in eq. (4.1)-(4.4). The stator and rotor voltages are a function of stator and rotor currents and the rotor speed. The equations are formulated in terms of real (*d*-) and imaginary (*q*-) axes, with respect to the network reference angle [122-123].

$$v_{sd} = -r_s i_{sd} + ((x_s + x_m) i_{sq} + x_m i_{rq}) \tag{4.1}$$

$$v_{sq} = -r_s i_{sq} - ((x_s + x_m) i_{sd} + x_m i_{rd}) \tag{4.2}$$

$$v_{rd} = -r_r i_{rd} + (1 - \omega_m)((x_s + x_m) i_{rq} + x_m i_{sq}) \tag{4.3}$$

$$v_{rq} = -r_r i_{rq} - (1 - \omega_m)((x_s + x_m) i_{rd} + x_m i_{sd}) \tag{4.4}$$

where v_{sd} and v_{sq} are *d*- and *q*-axis stator voltages, respectively, v_{rd} and v_{rq} are *d*- and *q*-axis rotor voltages, respectively, i_{sd} and i_{sq} are *d*- and *q*-axis stator currents, respectively, i_{rd} and i_{rq} are *d*- and *q*-axis rotor currents respectively, r_s is stator resistance, r_r is rotor resistance, x_s is stator reactance, x_m is magnetization reactance, x_r is rotor reactance and ω_m is rotor speed.

The power injected in the grid depends on the operating mode of the converter and are given by [97]

$$p_i = \frac{x_m}{x_s + x_m} v_i i_{rq} \tag{4.5}$$

$$q_i = -\frac{x_m v_i i_{rd}}{x_s + x_m} - \frac{v_i^2}{x_m} \tag{4.6}$$

where p_i and q_i are real and reactive powers respectively injected in the grid and v_i is the bus voltage. As converter controls are assumed to filter shaft dynamics, the generator motion equation is modelled as a single shaft and given by:

$$\dot{\omega}_m = (T_m - T_e)/2H_m \tag{4.7}$$

$$T_e = -\frac{x_m v_i i_{rq}}{\omega_b (x_s + x_m)} \tag{4.8}$$

where T_e is electromagnetic torque, ω_b is the system frequency rate in rad/s, & H_m is inertia constant in kWs/kVA. The mechanical torque is

$$T_m = \frac{P_w}{\omega_m} \tag{4.9}$$

where P_w is the mechanical power extracted from the wind. It is given by

$$P_w = \frac{n_g \rho}{2S_n} c_p(\kappa, \theta_p) A_r v_w^3 \tag{4.10}$$

where n_g is the number of machines that compose the wind park, S_n is the total power in MVA of the single or aggregated wind turbine, ρ is the air density, v_w is the wind speed, c_p is the performance coefficient, κ is the tip speed ratio and A_r is the area swept by the rotor. The additional details can be found in [123].

Converter dynamics are fast with respect to the electromechanical transients and thus highly simplified. Thus, the converter is modelled as an ideal current source, where i_{rq} and i_{rd} are state variables and are used for the rotor speed control and the voltage control respectively, which are depicted in Figures 4.2 and 4.3.

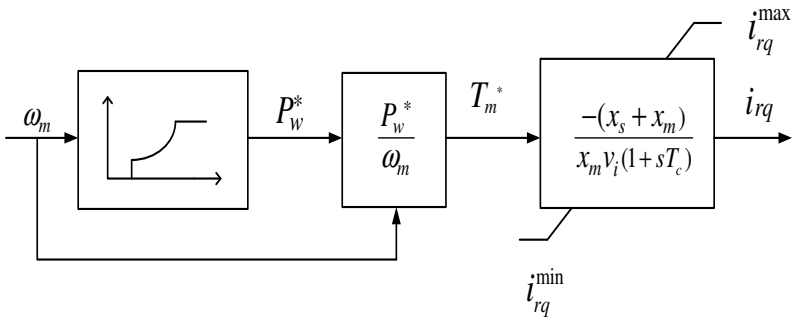

Fig. 4.2 Basic block diagram of rotor speed control scheme

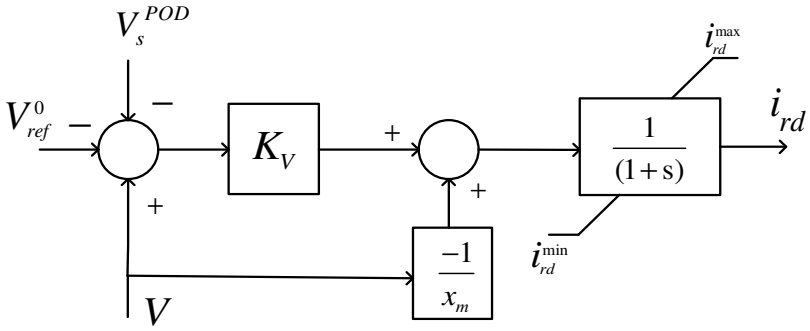

Fig. 4.3 Basic block diagram of voltage control scheme

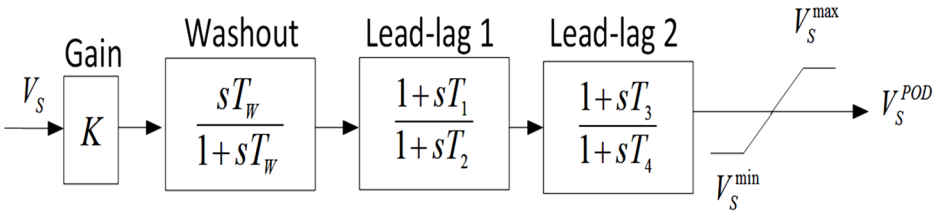

Fig. 4.4 PSS or POD structure

Differential and algebraic equations for the converter currents are as follows:

$$\dot{i}_{rq} = -\left(\frac{x_s + x_m}{x_m v_i} P_w^*(\omega_m) \Big/ \omega_m - i_{rq} \right) \frac{1}{T_e} \tag{4.11}$$

$$\dot{i}_{rd} = K_V (V - V_{ref}) - V / x_m - i_{rd} \tag{4.12}$$

$$0 = V_{ref}^0 - V_{ref} + V_s^{POD} \tag{4.13}$$

where V_{ref}^{0} is the initial reference voltage; V_s^{POD} the additional signal of the POD shown in Fig 4.4 ; and $P_w^*(\omega_m)$ the power-speed characteristic which roughly optimizes the wind energy capture and is calculated using the current rotor speed value, as follows:

$$P_w^*(\omega_m) = \begin{cases} 0 & \text{if } \omega_m < 0.5 \\ (2\omega_m - 1) & \text{if } 0.5 \le \omega_m \le 1 \\ 1 & \text{if } \omega_m > 1 \end{cases} \tag{4.14}$$

In this analysis, it is assumed that the power electronic converter consists of lossless components, and the switching dynamics are not taken into account. This study is done for open loop, where the rotor voltage remains constant at its initial value. The uncertainties associated with the wind speed are modelled using Weibull distribution function. Ref. [82], [123] provide complete details of the DFIG modelling and its controls employed in this study.

4.3 INTEGRATING DFIG BY REPLACING CONVENTIONAL SG

In this section, the dynamic impact analysis of DFIG-based wind turbine generators on low frequency oscillations in power system is carried out when DFIGs are integrated by replacing the conventional SGs in the system.

4.3.1 Proposed Methodology for Impact Analysis of DFIG Integration

The proposed study aims to find out the impact of wind integration on the oscillatory stability of the transmission system. First, the sensitivity analysis is performed. The magnitude of impact of the dynamic interaction of DFIG and conventional generators is calculated separately, and then the impact of increase in penetration of DFIG is investigated.

A. Sensitivity Analysis

The proposed analysis determines the beneficial or detrimental impact of adding DFIG based WTGs replacing the SGs on damping of LFOs. The replacement of conventional sources by DFIGs leads to a reduction in system inertia that influences the dynamic stability of the system.

The DFIG based WTGs integration impact on the oscillatory stability of the system can be obtained by calculating the sensitivity of damping ratio of critical modes with respect to the changes in system inertia. For i^{th} mode, it is given by

$$\frac{\partial \zeta_i}{\partial H_j} = -\frac{\omega_i^2}{(\sigma_i^2+\omega_i^2)^{3/2}}\frac{\partial \sigma_i}{\partial H_j} + \frac{\sigma_i \omega_i}{(\sigma_i^2+\omega_i^2)^{3/2}}\frac{\partial \omega_i}{\partial H_j} \tag{4.15}$$

where ζ_i is damping ratio of i^{th} critical mode and H_j is inertia constant of j^{th} conventional generator. In this study, a new index named Damping Ratio Sensitivity Index (*DRSI*) is proposed to identify the impact of DFIG penetration on LFOs. For a system having *n* critical modes, for j^{th} generator, it is defined as

$$DRSI_j = \sum_{i=1}^{n}\frac{\partial \zeta_i}{\partial H_j} = \begin{cases} +\ , if\ \sum_{i=1}^{n}\frac{\partial \zeta_i}{\partial H_j} > 0 \\ -\ , if\ \sum_{i=1}^{n}\frac{\partial \zeta_i}{\partial H_j} < 0 \end{cases} \tag{4.16}$$

The negative value of *DRSI* indicates the increase in the damping ratio (ζ_i) of critical modes with wind integration and positive values indicates decrease in ζ_i values. Since ζ_i is directly proportional to the real part of eigenvalue (σ_i), so *DRSI* also indicates the sensitivity of $\sigma_i$with respect to inertia. The *DRSI* values (− or +) directly indicates whether the critical eigenvalues are shifting left towards negative half or right towards positive half making the system stable or unstable respectively. The algorithm steps for the proposed method are as follows:

(i) Perform detailed eigenvalue analysis for the base case without DFIG and identify the critical modes.

(ii) Replace each SG one at a time by DFIG of the same MVA rating and calculate *DRSI* for each case.

(iii) Perform detailed eigenvalue analysis for each case with DFIG to compare and verify results obtained from *DRSI*.

(iv) Perform time domain simulations by applying a 3-phase fault for each case with DFIG.

B. Dynamic impact of DFIG and SG interaction on system damping

When the wind turbine replaces SGs of same MVA rating, the system configuration and load flow remains unchanged. Thus, the impact on small signal stability is only due to dynamic interaction between DFIG and SGs. However, this change is again caused by two factors: (a) removal of dynamic interaction between replaced generator and remaining SGs; (b) addition of dynamic interaction between the added DFIG and remaining SGs [75]. Only determining the effect on system damping by wind addition

do not show the actual impact of these factors on dynamic performance of the system. Thus, in this study, the effect on damping due to both the factors is obtained separately to get more details about dynamic impact of wind integration.

The dynamic interaction between the DFIG and the SGs is due to the variation in power exchange $\Delta P_{SG} + j\Delta Q_{SG}$ or $\Delta P_W + j\Delta Q_W$. When displaced SG is modelled as constant power source, the variation in power exchange becomes zero, and thus dynamic interaction between the displaced SG and remaining system do not exist. In this way, both the factors can be studied independently. The steps to perform the study are as:

(i) Perform eigenvalue analysis of the system for the base case. Calculate the damping ratio of the critical modes (ζ_i, i =1, 2,…).

(ii) Model the displaced SG as constant power source and perform the eigenvalue analysis. Then calculate the damping ratio of critical modes (ζ_{gi}).

(iii) Replace that SG by DFIG and again perform the eigenvalue analysis. Calculate the damping ratio of critical modes (ζ_{wi}).

(iv) Perform these steps for all the SGs replaced by DFIG.

The effect of interaction between replaced generator and remaining SGs and the effect of interaction between the added DFIG and remaining SGs can be determined using eq. (4.17) and (4.18) respectively as

$$\Delta\zeta_{gi} = \zeta_{gi} - \zeta_i \tag{4.17}$$

$$\Delta\zeta_{wi} = \zeta_{wi} - \zeta_{gi} \tag{4.18}$$

The total impact of DFIG replacing SG can be calculated as

$$\Delta\zeta_i = \Delta\zeta_{gi} + \Delta\zeta_{wi} = \zeta_{wi} - \zeta_i, \quad i = 1, 2, ... \tag{4.19}$$

C. Impact of Increased Penetration of DFIG

To study the impact of increased penetration of wind on the small signal stability, the DFIG integration is increased in steps. Randomly increasing DFIG penetration is not a practical approach, therefore in this study, the increase in DFIG penetration is carried out on the basis of participation of SGs in critical modes and the results of sensitivity analysis. The generators having the highest participation in the critical modes are the first to be replaced by DFIG. The highest participating generator is replaced by a DFIG of same capacity and the effect on system damping is observed. In this way, generators are removed one by one based on their participation to increase the

penetration of DFIG. For this study the maximum penetration of DFIG is taken around 42%. The detailed eigenvalue analysis is carried for all the cases to examine the effect of increased wind penetration on small signal stability of system.

4.3.2 Simulation and Results

The proposed methodology has been thoroughly investigated on IEEE 39-bus New England test system detailed in Appendix A. It consists of 10 synchronous generators, 19 loads and 46 transmission lines. All SGs are of fourth order and equipped with AVR Type II and PSS Type II. The IEEE New England is actually a prototype of existing power system in New England region of USA (ISO NE). The New England region has abundant wind power generation potential up to 12000 MW, according to [124] and thus suitable for this study. In this study, PMUs are placed on the same locations obtained in Chapter 3.

A. Sensitivity Analysis Results

The eigenvalue analysis is performed for the base case scenario and all the wind integration cases. The *DRSI* is calculated for all the wind cases in order to analyse the impact of wind integration on oscillatory stability.

- ***Base case Scenario without DFIG***

In the base case, there is no wind integration and the system consists of 10 conventional SGs. In this case, system excites nine electromechanical modes, with eight local modes and one interarea mode. It is found that only interarea mode has damping below threshold limit of 2.5% and thus it is a critical mode. The details of the critical mode are shown in Table 4.1. The eigenvalue plot is shown in Fig. 4.5 with different damping ratio lines. All the eigenvalues lie on the left of 2.5% damping line except the 0.6299 Hz mode. Although the real part of all the eigenvalues obtained is negative, the interarea mode has damping ratio less than 2.5%. The generators participation plot is shown in Fig. 4.6 with SG10 having the highest participation in this mode. In Chapter 3 also, SG10 was found to be the most critical and highest participating generator in the interarea mode.

TABLE 4.1
CRITICAL MODE IN BASE CASE

f (Hz)	Damping Ratio (%)	Real part of Eigenvalue	Dominant Generator
0.6299	2.40	-0.1066	SG10 (Bus 39)

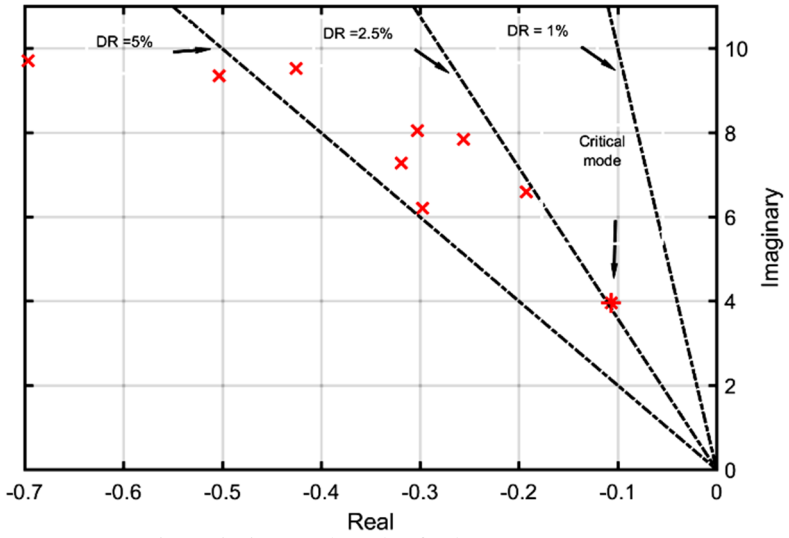

Fig. 4.5 Eigen-value plot for base case

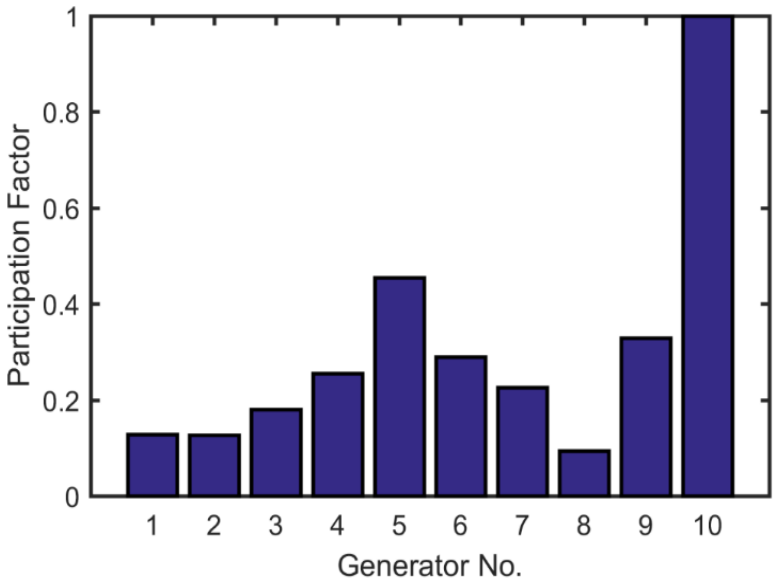

Fig. 4.6 Generators Participation in Critical mode in base case

- ***Case Scenarios with DFIG***

To observe the effect of wind integration and reduced inertia on oscillatory stability of the system, 10 cases are studied. In each case, the conventional generator is replaced one at a time by a DFIG of same capacity. For Case 1, SG1 is replaced by a DFIG and so on till Case 10 where the SG10 is replaced by a DFIG. The sensitivity analysis with respect to inertia is performed and *DRSI* is calculated for each case. The *DRSI* obtained in each case for the critical interarea mode are shown in Table 4.2. The generator inertia is shown on 100 MVA base and the DFIG inertia is also converted to be on the same base.

TABLE 4.2
RESULTS OF SENSITIVITY ANALYSIS

Case No.	Generator Bus No.	Base Generator Inertia (kWs/kVA)	*DRSI*
1	30	42.00	–
2	31	30.30	+
3	32	35.30	+
4	33	28.60	+
5	34	26.00	+
6	35	34.80	+
7	36	26.40	+
8	37	24.30	+
9	38	34.50	+
10	39	500	–

The information of *DRSI* can be used to identify the location for DFIG integration in the system without detrimental impact on the oscillatory stability. The *DRSI* value for two cases in Table 4.2 is found to be '–' which shows that even the decrease in inertia turns out to be beneficial in Case 1 and 10. Thus, replacing SG1 or SG10 by DFIG has positive impact on the system damping and oscillatory stability is improved for these cases. For all other cases, DFIG integration has adverse effect on the damping of critical mode. Thus, the proposed sensitivity analysis suggests the SG1 and SG10 are the suitable locations for replacing the conventional SGs by DFIG.

B. Eigenvalue Analysis with DFIG

A complete eigenvalue analysis is performed for wind integration Cases 1 to 10 to identify the critical modes in the low frequency range of 0.1-2 Hz and to verify the results obtained with sensitivity analysis. Table 4.3 shows the results of eigenvalue analysis performed for the critical mode listed in Table 4.1.

TABLE 4.3
RESULTS OF EIGENVALUE ANALYSIS OF CRITICAL MODE WITH WIND INTEGRATION

Case No.	Real Part	*f* (Hz)	Damping Ratio (%)	Dominant Generators
1	-0.1130	0.6481	2.77	10,5,9,6,4,7,3,2,8
2	-0.0961	0.6548	2.33	10,5,9,6,4,7,3,1,8
3	-0.0943	0.6628	2.26	10,5,9,6,4,7,1,2,8
4	-0.0887	0.6827	2.07	10,9,5,6,7,3,2,1,8
5	-0.0750	0.6871	1.74	10,9,6,7,3,4,2,1,8
6	-0.0980	0.6879	2.27	10,5,9,4,3,7,2,1,8
7	-0.0906	0.6769	2.13	10,6,9,5,4,3,2,1,8
8	-0.0942	0.6534	2.29	10,5,9,6,4,7,3,2,1
9	-0.0821	0.6825	1.91	10,5,6,4,7,3,2,1,8
10	-0.1095	0.5993	2.91	5,9,6,4,7,3,1,2,8

The critical mode is obtained in all the 10 cases. It is clearly seen that the damping ratio of the critical interarea mode increases in only two cases (Case 1, 10) and in all the other cases (Case 2 to 9) the damping ratio of critical mode decreases from the base case value. In Case 1 and Case 10, the damping ratio improves and becomes more than damping threshold limit of 2.5. The dominant generators in decreasing order of participation in critical mode are also shown. Although the inertia reduces in all the cases, still in some cases damping of critical mode improves. In Case 10, when the dominant generator SG10 is replaced by a DFIG, damping improves to reduce the impact of decreased system inertia. The same result is obtained by proposed *DRSI* method. This verifies the effectiveness of proposed sensitivity analysis results shown in Table 4.2. Moreover, this validates the effectiveness of the proposed index in evaluating the sensitivity of the damping ratio with change in system inertia. On comparing the real part of eigenvalues shown in Tables 4.1 and 4.3, it is found that the eigenvalue is shifting left towards negative half for '−' *DRSI* cases and making the system more stable with respect to the base case. Table 4.3 shows that in Cases 1 to 9, SG10 is the dominant machine and in Case 10, when SG10 is replaced by a DFIG dominant machine is SG5 as shown in Fig. 4.7(a). However, in this case the participation of most of the generators have improved. This also suggests that mode damping improves when all the generators have comparable participation in that mode.

When DFIG is integrated, new critical LFO mode(s) may get excited in the system due to interaction between DFIG and remaining SGs. Table 4.4 shows the eigenvalue analysis results for the new critical mode excited (if any) for all the cases.

TABLE 4.4
RESULTS OF EIGENVALUE ANALYSIS OF NEW INTERAREA MODE WITH WIND INTEGRATION

Case No.	Real Part	f (Hz)	Damping Ratio (%)	Dominant Generators
2	0.0033	0.1360	-0.39	10,1,9,3,6,4,5,7,8
3	0.0076	0.1437	-0.84	10,1,9,6,4,2,7,5,8
4	0.0096	0.1330	-1.15	10,1,3,9,2,6,7,8,5
5	0.0058	0.1260	-0.73	10,1,3,9,2,6,7,8,5
6	0.0161	0.1450	-1.77	10,1,3,9,2,4,8,5,7
7	0.0138	0.1230	-1.79	10,1,3,9,2,6,4,8,5
8	0.0052	0.1148	-0.72	10,1,3,9,6,2,4,5,7
9	0.0544	0.1330	-6.50	10,1,3,6,2,7,4,5,8

It is seen that only one new critical mode is excited in all the wind cases, except Case 1 and 10. In Case 1 and 10, no new mode is introduced in the system. The new mode is an interarea mode of around 0.13 Hz and has negative damping in all the cases.

It means that the mode is very critical as its amplitude increase with time. Fig. 4.7(b) shows the eigenvalue plot for Case 9. It clearly shows that one eigenvalue lies in right half plane making the system unstable. This also proves that Case 2 to 9 are oscillatory unstable cases. The dominant machine in all the cases is G10 in this mode. The generators participation in new mode for Case 9 is shown in Fig. 4.7(c).

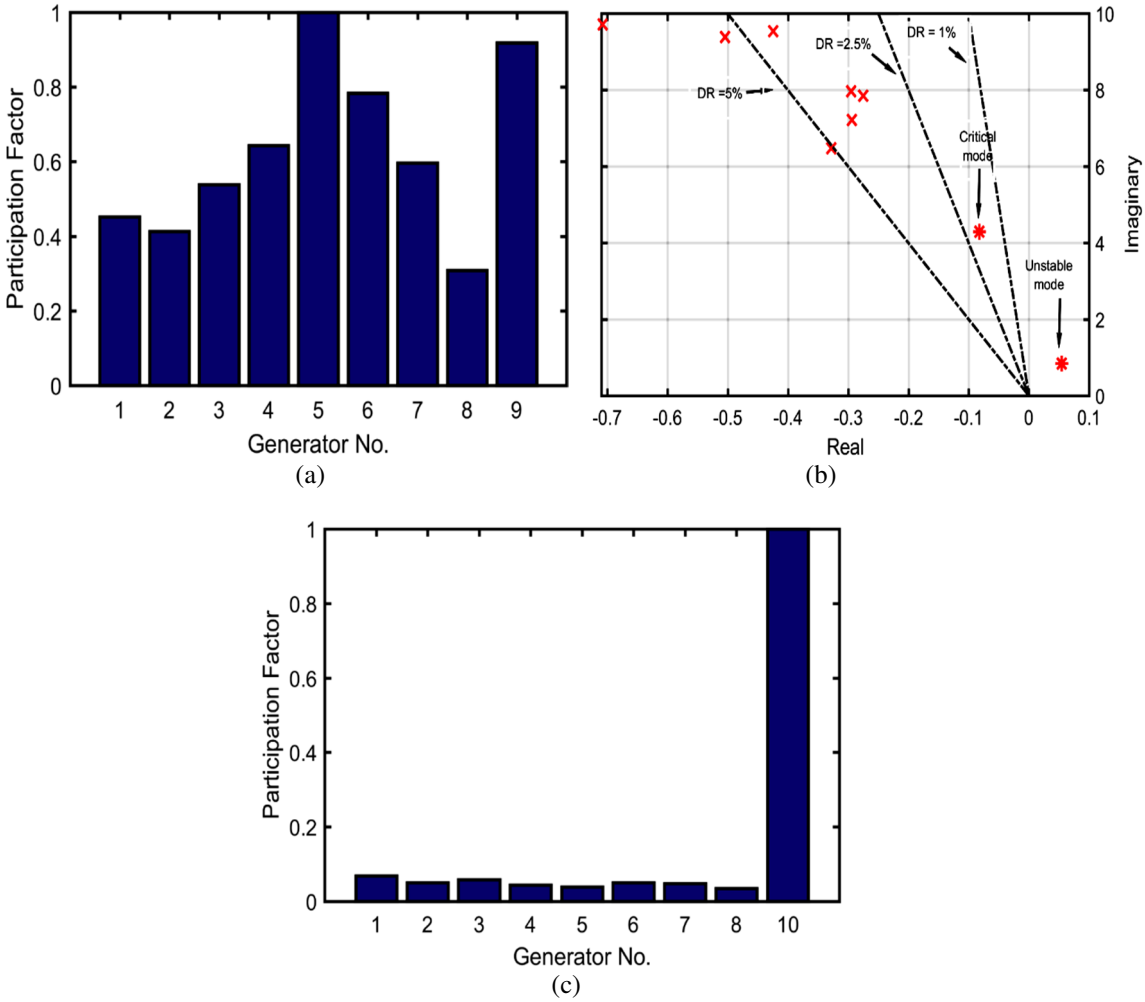

Fig. 4.7 Eigenvalue analysis results for wind integration cases
(a) Generators participation in critical mode in Case 10, (b)Eigen-value plot for wind Case 9, (c) Generators participation in new mode in wind Case 9

In Case 1, as the size of integrated DFIG is small as compared to other cases, so it does not introduce any new mode in the system. But in Case 10, a large sized DFIG is integrated which may affect the oscillatory stability of the system negatively. However, in this case, the dominant generator in new critical interarea mode is G10 itself and it is replaced by DFIG of same size, therefore, in this case this mode is not excited and there is no negative impact. Thus, it is clear from the results that DFIG can be integrated by replacing the most dominant generator in the critical mode which also improves the oscillatory stability of the system. For Cases 2 to 9, wind integration leads to

deterioration of oscillatory stability as the damping of critical mode reduces and a new mode of very low damping is also introduced in the system. It is clear from these findings that only Case 1 and Case 10 of wind integration are beneficial for small signal stability of the system.

From the coherency analysis results of Chapter 3 also, it is found out that for many cases SG1 and SG10 forms a separate coherent group with remaining SGs in other groups. These two SGs are moving differently as compared to other generators in the system similar to the results obtained in this study.

C. Wind integration scenario under disturbance

To investigate the dynamic performance of the wind-integrated system under disturbance, time domain simulations are carried out. A 3-phase fault of 5-cycle duration is applied at bus 16 at t=0.5 s. As interarea oscillations are highly observable in active power output of participating generators, so active power outputs of the few highest participating generating units are compared in base case and wind integration Case 1.

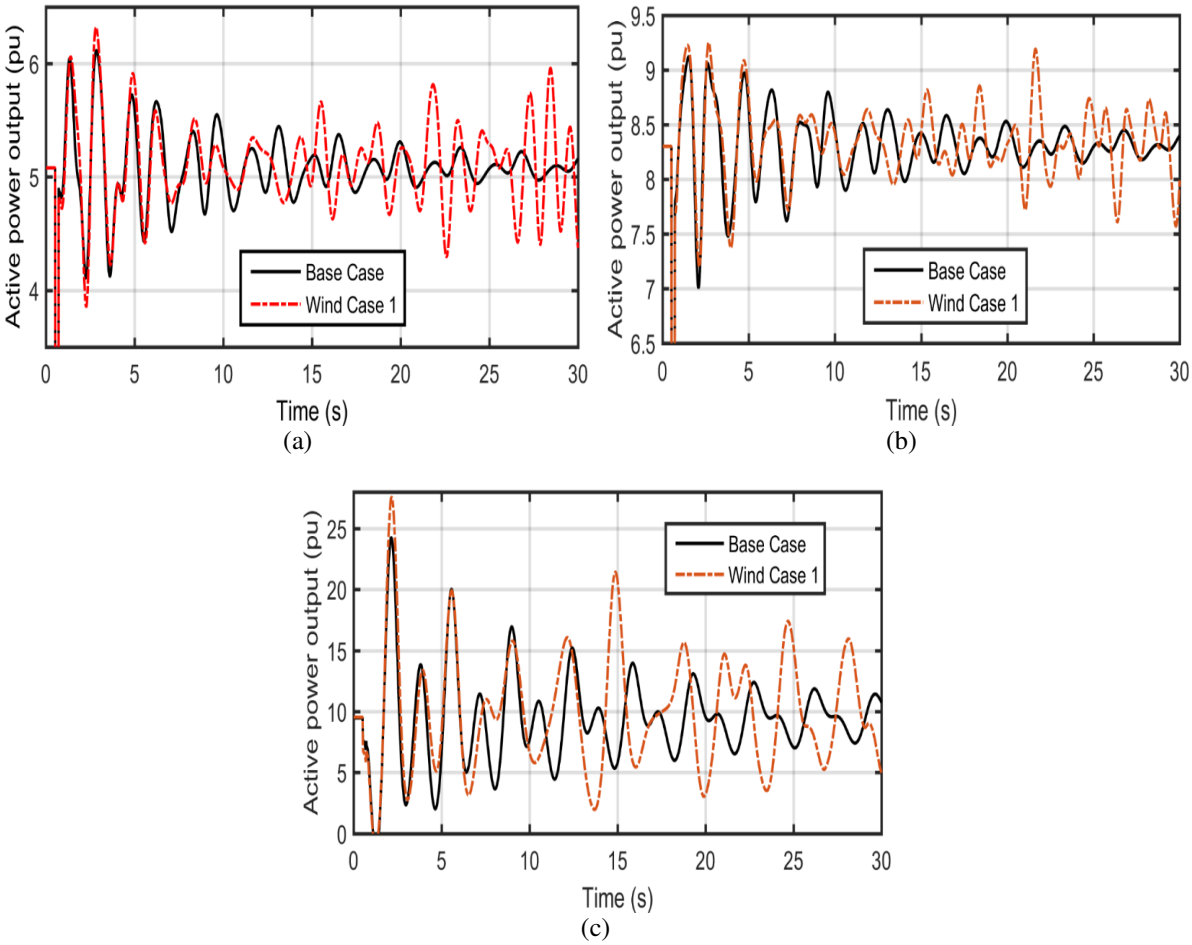

Fig. 4.8 Active power outputs compared in base case and wind Case 1 (a) SG5, (b) SG9, (c) SG10

Fig. 4.8 shows the comparison of active power outputs of SG5, SG9 and SG10. The wind case 1 is oscillatory stable in steady state but becomes less stable on application of 3-phase fault. In all the three generators SG5, SG9 and SG10, damping in active power outputs is more in base case as compared to wind Case 1. The system is oscillatory unstable in wind Cases 2 to 9 as found in Table 4.4. This may be due to reasons such as improper tuning of PSSs or the poor damping of the system. Thus, it can be emphasized here that there is a need to re-tune the PSSs or to add some additional device to increase the damping of critical modes in the wind cases and bring the system to oscillatory stable state.

D. Impact Analysis of DFIG and SG interaction

The separate analysis of dynamic interaction as explained in section 4.2 is performed in this study to find out their individual effect on critical modes damping in the system. The critical mode in base case is the interarea mode, so the damping of that mode is studied in different cases. For each case, the SG to be removed is modelled as a constant power source. Then wind integration is performed by replacing each SG by DFIG one at a time.

The effect of interaction between replaced generator and remaining SGs ($\Delta\zeta_{gi}$), effect of interaction between the added DFIG and remaining SGs ($\Delta\zeta_{wi}$), and the total impact ($\Delta\zeta_i$), are computed using eq. (4.17), (4.18), (4.19) and results are shown in Table 4.5.

TABLE 4.5
RESULTS OF SEPARATE ANALYSIS OF DYNAMIC INTERACTION FOR CRITICAL MODE

Case No.	ζ_{gi} (%)	ζ_{wi} (%)	$\Delta\zeta_{gi}$ (%)	$\Delta\zeta_{wi}$ (%)	$\Delta\zeta_i$ (%)
1	2.89	2.77	0.49	-0.12	0.37
2	2.02	2.33	-0.38	0.31	-0.07
3	1.80	2.26	-0.60	0.46	-0.14
4	2.48	2.07	0.08	-0.41	-0.33
5	1.84	1.74	-0.56	-0.10	-0.66
6	2.69	2.27	0.29	-0.42	-0.13
7	2.44	2.13	0.04	-0.31	-0.27
8	2.40	2.29	0	-0.11	-0.11
9	2.88	1.91	0.48	-0.97	-0.49
10	2.91	2.91	0.51	0	0.51

It is found from the results that the effect of dynamic interaction between the replaced generator and remaining SGs is positive for some cases and negative for other

cases and depends on the location of SG. An increase of around 0.5% damping ratio is obtained in Case 1, 9 & 10, which is a significant improvement. On the other hand, addition of wind farm is detrimental in almost all the cases. However, for Case 1 and 10, the negative impact of wind addition is very less and thus the overall combined impact of DFIG integration is positive for these cases. In Case 2 & 3, with the SG withdrawal, there is reduction in damping while wind addition causes increment in damping, but the negative impact is more, so overall impact is negative in these cases. In Case 5, both SG removal and wind addition causes negative impact. In all other cases, wind addition cancels any positive impact caused by SG removal and the overall damping of critical mode reduces. From these results, it is found that no set pattern of individual effects can be drawn. The results thus obtained depend entirely on the location of DFIG. However, these studies may be useful at planning stage in selecting the suitable preventive control measures for wind integration.

E. Impact of Increased DFIG Penetration

The impact of increased penetration of wind on LFO is studied as explained in section 4.3.1. The penetration is increased by replacing SGs according to their participation factors in critical modes and sensitivity analysis results. There are two critical modes; one present in base case, and other introduced due to wind addition. The dominant generators on the basis of participation factor values are shown in Tables 4.3 and 4.4. The four most dominant generators in both modes are SG10, SG1, SG9 and SG5. Also the sensitivity analysis results suggest that removal of SG1 & SG10 is beneficial for oscillatory stability. Considering both these factors, SG1, SG5, SG9 & SG10 are found to suitable locations for DFIG penetration and these SGs are replaced by DFIGs stepwise to increase penetration to around 42%. Four different cases are studied and their eigenvalue analysis results are presented in Table 4.6. These are:

Case 1: SG1 & SG10 are replaced by DFIGs of same capacity (20.3 % penetration).

Case 2: SG1, SG5 & SG10 are replaced by DFIGs of same capacity (28.6 % penetration).

Case 3: SG1, SG9 & SG10 are replaced by DFIGs of same capacity (33.88 % penetration).

Case 4: SG1, SG5, SG9 & SG10 are replaced by DFIGs of same capacity (42.4 % penetration).

It is clear from the results of Table 4.6 that there is no mode in any case which has damping below the threshold limit. Fig. 4.9 shows the eigenvalue plots for these four

cases. Increasing penetration according to proposed approach has a positive impact on damping and damping ratio of all the modes increases in each case. All the eigenvalues lie on the left side of 2.5% damping line as seen from the eigenvalue plots. In Case 1, there are 8 modes, 7 local and 1 interarea mode. The base case critical mode does not exist in this case. Similarly, there are 6 modes in Case 2, 7 modes in Case 3 and 6 modes in Case 4.

TABLE 4.6
RESULTS FOR INCREASED PENETRATION OF DFIG

Case No.	Mode No.	Real part of Eigenvalue	f (Hz)	Damping Ratio (%)
Case 1 (20.3 % Penetration)	1	-0.88213	1.7459	08.0154
	2	-0.62294	1.5248	06.4880
	3	-0.61508	1.2471	07.8253
	4	-0.43363	1.1709	05.8838
	5	-0.30054	1.0162	04.7015
	6	-0.20450	1.0308	03.1556
	7	-0.19605	0.8541	03.6505
	8	-0.12420	0.1841	10.6747
Case 2 (28.6 % Penetration)	1	-0.75196	1.5737	07.5827
	2	-0.47793	1.4791	05.1358
	3	-0.61706	1.3923	07.0362
	4	-0.26069	1.2752	03.2518
	5	-0.25028	1.1505	03.4602
	6	-0.23728	1.0316	03.6583
Case 3 (33.88 % Penetration)	1	-0.62308	1.4954	06.6170
	2	-0.53256	1.4308	05.9135
	3	-0.45246	1.3137	05.4731
	4	-0.26913	1.2170	03.5175
	5	-0.30145	1.1043	04.3406
	6	-0.31310	0.9776	03.6583
	7	-0.33364	0.4188	12.5790
Case 4 (42.4 % Penetration)	1	-0.64112	1.5005	06.7847
	2	-0.47956	1.4085	05.4108
	3	-0.46036	1.3128	05.5725
	4	-0.26079	1.2249	03.3866
	5	-0.21947	1.0831	03.2232
	6	-0.28803	0.5220	08.7489

Thus, the proposed analysis shows that the number of low frequency modes in the system decreases with increase in DFIG penetration and the system is oscillatory stable in all the cases. Increasing penetration of DFIG based on generators participation in critical modes and sensitivity results proves to be beneficial for system's oscillatory stability and can be utilised as one of the methods to increase wind penetration aiding small signal stability. It is interesting to note that replacement of SG5 alone by DFIG

have negative impact on oscillatory stability and similarly replacement of SG9 alone by DFIG have negative impact on oscillatory stability. However, when they are replaced by DFIG along with SG1 and SG10, the impact on oscillatory stability is positive.

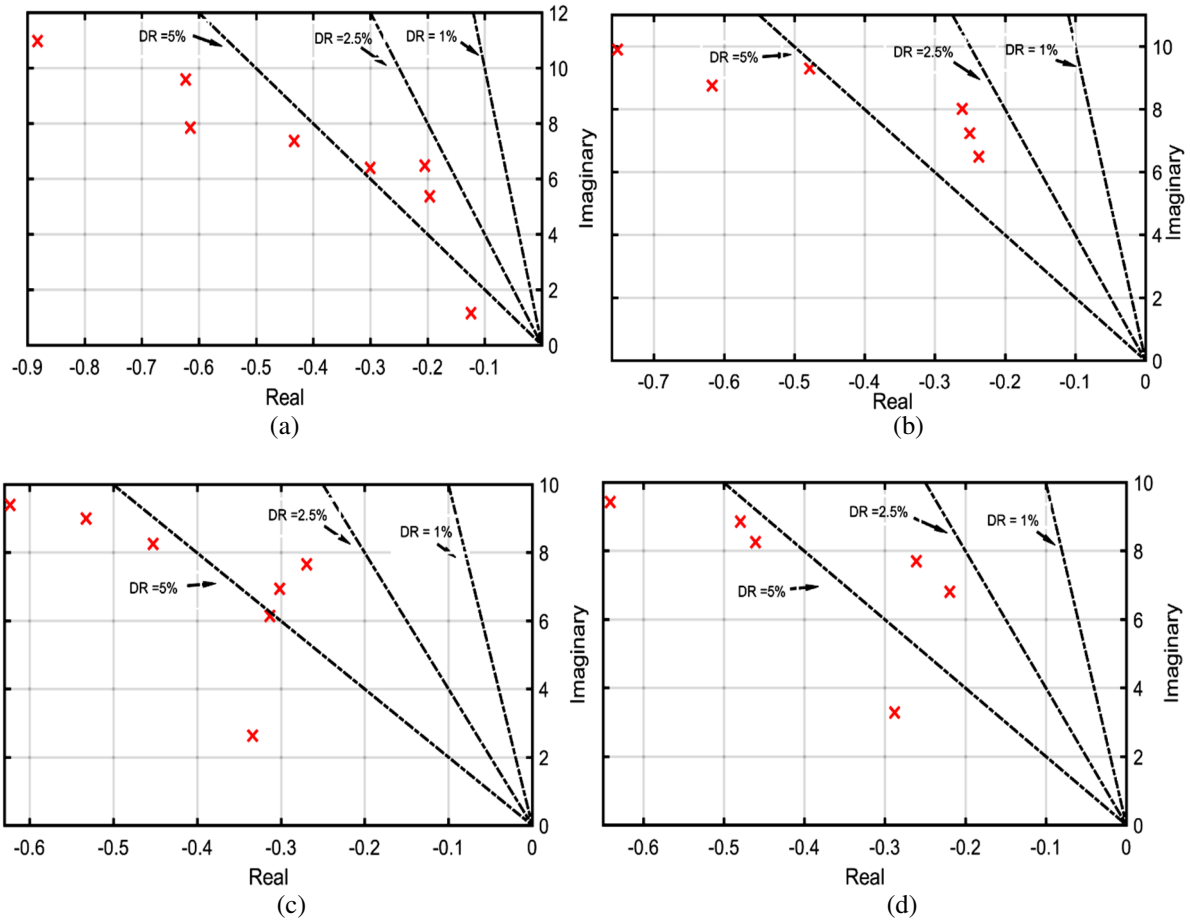

Fig. 4.9 Eigenvalue plots for different wind penetration scenarios
(a) Case 1, (b) Case 2, (c) Case 3, (d) Case 4

4.4 INTEGRATING DFIG WITHOUT REPLACING CONVENTIONAL SG

Practically, WTGs are integrated without replacing the existing SGs. So, in this section the impact of DFIG integration location on low frequency oscillations is carried out when DFIGs are integrated at non-generator buses of the system. As found out in previous section that removal of some SGs is beneficial for system oscillatory stability while replacing other causes negative impact. Similarly, DFIG location is one of the crucial factors that drives the positive or negative impact of wind integration in the power system. In this study the location of DFIG is presented as an important factor that influences the damping of LFOs.

4.4.1 Proposed Methodology for Impact Analysis

This study uses eigenvalue analysis and dynamic trajectory sensitivity analysis techniques. The eigenvalue analysis has already been discussed in Chapter 3.

A. Dynamic Trajectory Sensitivity Analysis

Dynamic trajectory sensitivity analysis computes the sensitivity of the dynamics with respect to the parameters. It calculates the sensitivity along the system's evolving trajectory and thus differs from static sensitivity [125, 126]. From differential-algebraic equation, the flows of *x* and *y* is given as

$$x(t) = \phi_x(x_0, t, \kappa) \tag{4.20}$$

$$y(t) = \phi_y(y_0, t, \kappa) \tag{4.21}$$

The sensitivities can now be calculated using Taylor's series expansion as

$$\Delta x(t) = \frac{\partial x(t)}{\partial \kappa}\Delta\kappa = x_\kappa \Delta\kappa \tag{4.22}$$

$$\Delta y(t) = \frac{\partial y(t)}{\partial \kappa}\Delta\kappa = y_\kappa \Delta\kappa \tag{4.23}$$

In this study, a simple numerical procedure has been used to evaluate the sensitivities x_κ and y_κ using the values obtained from PMUs.

$$x_\kappa = \frac{\partial x}{\partial \kappa} \approx \frac{\phi_x(x_0, t, \kappa+\Delta\kappa) - \phi_x(x_0, t, \kappa)}{\Delta\kappa} \tag{4.24}$$

$$y_\kappa = \frac{\partial y}{\partial \kappa} \approx \frac{\phi_y(y_0, t, \kappa+\Delta\kappa) - \phi_y(y_0, t, \kappa)}{\Delta\kappa} \tag{4.25}$$

Eq. (4.24) is used in this study to find out the rotor angle sensitivity with respect to real power injection, P_w, by WTG. The dynamic sensitivity is used to find out the angular separation among SGs due to increasing wind penetration. The relative rotor angle is calculated by using Center of Inertia (*COI*) angle, δ_{COI}, as a reference.

$$\delta_{i,COI} = \left|\delta_i - \delta_{COI}\right| \tag{4.26}$$

Thus, the relative rotor angle dynamic sensitivity (*RAS*) of i^{th} SG at any time instant *t* can be defined as

$$RAS_i(t) = \frac{\partial \delta_{i,COI}(t)}{\partial P_w} \tag{4.27}$$

Using the values of *RAS* obtained above, the rotor angle sensitivity index (*RSI*) is calculated for time *t=1 to T*.

$$RSI_i = \left| \sum_{t=1}^{T} w_t \left[\frac{\partial \delta_{i,COI}(t)}{\partial P_w} \right]_{t=t_n} \right| \tag{4.28}$$

where, w_t has values 0 or 1 for different time instants based on time for which oscillations persists in the system. Here, value '1' is assigned to time instants just after the fault. The value of *RSI* indicates the effect of DFIG penetration at different locations.

4.4.2 Simulation and Results

The proposed methodology is investigated on IEEE 39-bus New England test system keeping all the parameters and components same as in previous study. The total generation in the system is P_G=6138.71 MW. The study is performed for different wind penetrations and for each penetration different WTG locations and their impact on LFO damping are investigated. The maximum penetration of DFIG studied is 25%. A total of four different scenarios are studied. For first three cases, two wind farms are added and all the possible placement combination cases are studied for each penetration. In the fourth case, three wind farms are added to the system and rest of the procedure remains same. The load of the system is increased by the same amount as DFIG penetration to study the impact of DFIG location on damping. In this study, PMUs are assumed to be placed on the same locations which were found out in Chapter 3, such that system is completely observable in normal and N-1 contingency cases.

The wind penetration is defined based on the existing generation in base case and given by

$$Wind\ Penetration\ (\%) = \frac{P_w}{P} \times 100 \tag{4.29}$$

where P is total generation in MW in base case.

A. Eigenvalue Analysis Results

The eigenvalue analysis has been performed for the base case and several different DFIG penetrations. Results are shown for four different penetration cases of DFIG - 15%, 20%, 25% (two wind farms) and 25% (three wind farms). In the base case (no wind penetration) system excites 8 LFO modes (7 local, 1 inter-area) as shown in Table 4.7. The interarea mode has damping of 8.73%. The high values of damping ratio are obtained as all SGs have PSSs installed. Only one local mode has damping below 5%.

TABLE 4.7
LFO MODES IN BASE CASE

S.No.	f (Hz)	DR (%)
1	1.8160	04.38
2	1.5517	05.12
3	1.4912	05.33
4	1.3126	06.05
5	1.2523	06.37
6	1.1327	07.01
7	0.9984	07.95
8	**0.6797**	**08.73**

A comparative analysis is done to show the impact of location of DFIG on modes damping at different penetration levels. The top two beneficial and detrimental locations for modes damping (in terms of inter-area modes) are shown for all penetration cases.

Case 1: 15% DFIG Penetration

The wind penetration is taken 920 MW in this case using two wind farms of 460 MW each placed at any two buses and all such possible placement combinations of buses are investigated. The results are shown in Table 4.8 for the two locations (bus no. 3, 18 & 12, 26) which are most beneficial for modes damping. The damping of all the modes increases, particularly the damping of inter-area mode increases from the base case value of 8.73% to become more than 16%. Thus, DFIG integration at these locations proves to be beneficial for system's oscillatory stability.

TABLE 4.8
BENEFICIAL LOCATIONS RESULTS IN CASE 1 (15% PENETRATION)

S.No.	Bus No. 3 & 18		Bus No. 12 & 26	
	f (Hz)	DR (%)	f (Hz)	DR (%)
1	1.7274	09.27	1.7650	07.23
2	1.5639	06.68	1.5464	06.62
3	1.4005	08.37	1.3163	07.01
4	1.2679	06.57	1.2745	07.86
5	1.2213	08.82	1.1930	08.46
6	1.0830	07.05	1.0234	06.27
7	0.9847	07.47	0.9140	07.83
8	**0.4950**	**16.79**	**0.4850**	**16.43**

Similarly, Table 4.9 shows the two locations (bus no. 26, 27 & 9, 28) which are most detrimental for system damping. When DFIGs are located at bus 26 and 27, there exists two inter-area modes in system and damping is below threshold value for both of them. One inter-area mode has negative damping and thus makes the system oscillatory

unstable. For the second location also damping is very low for inter-area mode. In this scenario, system excites only 7 LFO modes. So, these results clearly indicate that DFIG penetration proved to be adverse for system damping at these locations.

TABLE 4.9
DETRIMENTAL LOCATIONS RESULTS IN CASE 1 (15% PENETRATION)

S.No.	Bus No. 26 & 27		Bus No. 9 & 28	
	f (Hz)	DR (%)	f (Hz)	DR (%)
1	1.7500	08.10	1.7891	05.84
2	1.5502	06.46	1.5499	06.41
3	1.4501	07.11	1.4448	07.42
4	1.2499	07.94	1.2852	07.76
5	1.2481	06.38	1.2263	06.38
6	1.0170	06.33	1.0077	07.27
7	**0.7927**	**03.38**	**0.7091**	**02.89**
8	**0.3368**	**−11.80**	-	-

Case 2: 20% DFIG Penetration

The wind penetration is taken 1228 MW in this case using two wind farms of 614 MW each. Tables 4.10 and 4.11 shows the eigenvalue analysis results for beneficial and detrimental locations respectively in this case. It can be seen from Table 4.10 that for both the locations damping of inter-area mode improves to 20% and above. The damping all other modes is also above the threshold value. Conversely, damping becomes poor with wind integration at the locations shown in Table 4.11. The damping of inter-area mode becomes negative for both the locations shown in Table 4.11 and thus system is unstable for these integration scenarios.

TABLE 4.10
BENEFICIAL LOCATIONS RESULTS IN CASE 2 (20% PENETRATION)

S.No.	Bus No. 9 & 27		Bus No. 1 & 27	
	f (Hz)	DR (%)	f (Hz)	DR (%)
1	1.7595	07.60	1.7620	07.42
2	1.5448	06.38	1.5448	06.46
3	1.4166	08.30	1.4551	06.97
4	1.2819	07.32	1.2593	07.22
5	1.2194	07.65	1.2474	06.88
6	1.0148	06.49	1.0063	06.32
7	0.9585	08.88	0.9427	09.05
8	**0.6001**	**21.33**	**0.6158**	**19.97**

TABLE 4.11
DETRIMENTAL LOCATIONS RESULTS IN CASE 2 (20% PENETRATION)

S.No.	Bus No. 1 & 9		Bus No. 1 & 12	
	f (Hz)	DR (%)	f (Hz)	DR (%)
1	1.7955	05.46	1.7827	06.03
2	1.5456	06.51	1.5353	06.82
3	1.4417	07.57	1.3129	07.29
4	1.2934	07.15	1.2813	08.42
5	1.2306	07.31	1.1840	11.57
6	1.0997	07.11	1.0968	06.08
7	0.9823	07.78	0.9743	07.42
8	**0.5630**	**−01.62**	**0.6485**	**−01.19**

Case 3: 25% DFIG Penetration

The wind penetration is taken 1536 MW in this case using two wind farms of 768 MW each. Tables 4.12 and 4.13 shows the eigenvalue analysis results for beneficial and detrimental locations respectively. It is clear from Table 4.12 that the locations shown are highly beneficial as the damping of interarea mode improves to become greater than 23% in both the scenarios. Contrarily, damping becomes negative for locations shown in Table 4.13 and thus system is oscillatory unstable in these integration scenarios.

TABLE 4.12
BENEFICIAL LOCATIONS RESULTS IN CASE 3 (25% PENETRATION)

S.No.	Bus No. 9 & 27		Bus No. 3 & 26	
	f (Hz)	DR (%)	f (Hz)	DR (%)
1	1.7544	07.77	1.7308	09.00
2	1.5354	06.52	1.5570	06.38
3	1.4068	08.53	1.3970	08.39
4	1.2762	07.83	1.2352	08.58
5	1.2060	07.11	1.2164	05.97
6	0.9912	06.39	1.0210	06.41
7	0.8738	08.84	0.8503	05.88
8	**0.7493**	**27.19**	**0.5900**	**23.87**

TABLE 4.13
DETRIMENTAL LOCATIONS RESULTS IN CASE 3 (25% PENETRATION)

S.No.	Bus No. 1 & 9		Bus No. 1 & 26	
	f (Hz)	DR (%)	f (Hz)	DR (%)
1	1.7678	06.01	1.7974	05.23
2	1.5342	05.71	1.5651	07.02
3	1.4124	07.31	1.3784	06.99
4	1.3323	06.98	1.2780	08.81
5	1.2357	06.84	1.1980	09.76
6	1.0987	07.19	1.0900	07.20
7	0.9769	07.66	0.9567	07.81
8	**0.5934**	**−00.51**	**0.6280**	**−00.02**

Case 4: 25% DFIG Penetration (three wind farms)

The wind penetration is taken 1536 MW in this case using three wind farms of 512 MW each. This case illustrates the possible impact of number of wind farms on system damping for the same penetration. With integration of three wind farms in the system the number of LFO modes in the system increases to nine. There are eight local modes and one interarea mode present in the system. Tables 4.14 and 4.15 shows the eigenvalue analysis results for beneficial and detrimental locations respectively. It is clear from Table 4.14 that the locations shown are beneficial for system damping as the damping of inter-area mode improves and becomes greater than base case in both the scenarios. However, the improvement in damping ratio is not very significant as compared to results of other three cases. Contrarily, interarea mode damping decreases to very low value for locations shown in Table 4.15 and thus these locations proves to be adverse for system damping and system becomes less stable as compared to base case with no wind integration.

TABLE 4.14
BENEFICIAL LOCATIONS RESULTS IN CASE 4 (25% PENETRATION)

S.No.	Bus No. 4, 19 & 21		Bus No. 4, 19 & 24	
	f (Hz)	DR (%)	f (Hz)	DR (%)
1	1.6425	24.81	1.6414	24.77
2	1.6360	18.78	1.6358	18.76
3	1.3735	10.10	1.3719	10.16
4	1.4192	30.30	1.4198	30.27
5	1.3590	16.90	1.3625	16.47
6	1.1237	18.59	1.1211	18.42
7	1.0237	30.91	1.0233	31.08
8	0.9825	24.23	0.9814	23.86
9	**0.5450**	**08.78**	**0.5432**	**08.76**

TABLE 4.15
DETRIMENTAL LOCATIONS RESULTS IN CASE 4 (25% PENETRATION)

S.No.	Bus No. 1, 9 & 12		Bus No. 1, 6, & 9	
	f (Hz)	DR (%)	f (Hz)	DR (%)
1	1.6412	24.82	1.6414	24.82
2	1.6233	16.34	1.6224	16.39
3	1.3652	09.78	1.3661	09.79
4	1.4522	28.37	1.4440	28.83
5	1.3640	16.56	1.3636	16.60
6	1.1141	17.92	1.1166	18.07
7	1.0032	30.51	1.0051	30.67
8	0.9986	21.85	0.9975	21.76
9	**0.5167**	**01.71**	**0.5162**	**01.79**

The eigenvalue plot of one of the beneficial location (bus no. 9, 27) for Case 3 is shown in Fig. 4.10. It is clear from the figure that all the modes have damping ratio greater than 5% as all modes lie on left of 5% damping line. The inter-area mode has damping more than 20% as shown in figure and thus system is small signal stable. Similarly, Fig. 4.11 shows eigenvalue plot for one of the detrimental locations (Bus No. 1, 9) for this case. Here, it can be seen that one mode has negative damping and lies on the right half plane making the system oscillatory unstable.

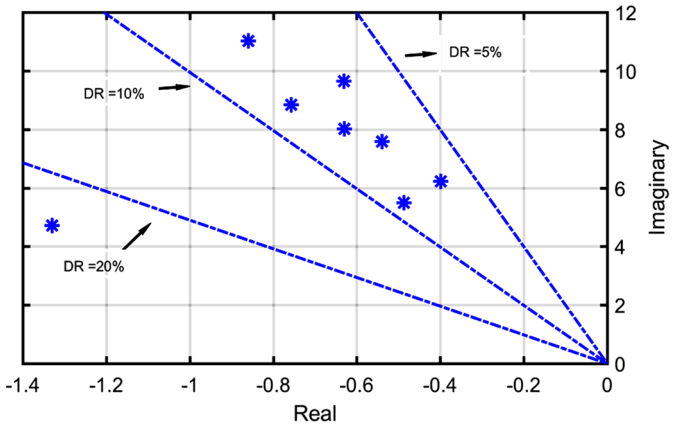

Fig. 4.10 Eigenvalue plot for Case 3 (Bus No. 9, 27)

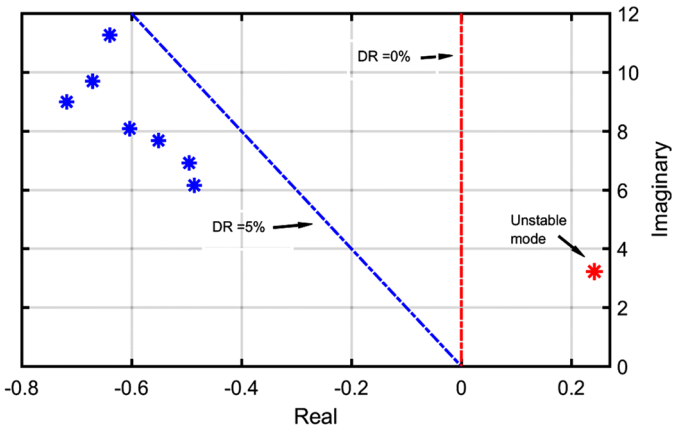

Fig. 4.11 Eigenvalue plot for Case 3 (Bus No. 1, 9)

The above study provides a complete analysis in terms of impact of different penetrations and number of wind farms on system damping. From tables 4.8 to 4.15, it may be observed that for modes damping, favourable locations of DFIGs varies with the level of penetration and coordinated locations of DFIG. For example, location 26 with 3 provides most favourable location for 25% wind penetration (Case 3). However, location 26 with 1 provides most detrimental location for the same level of wind penetration. Similarly, location 26 with 12 provides most favourable location for 15% wind penetration. However, location 26 with 27 provides most detrimental location for

the same level of wind penetration. Similarly, when number of DFIGs increased from two to three for same level of penetration, the beneficial locations again changes to 4, 19 and 21. From this study it may be concluded that modes damping should not be the criteria to find optimal location of DFIGs. It is neither feasible nor technically correct to find optimal location of DFIG on the basis of modes damping or small signal stability. Above study is needed to determine whether DFIG penetration at certain location proves to be detrimental to system small signal stability. In such cases, proper counter preventive measures should be employed to neutralize the detrimental effect of wind penetration.

B. Dynamic Sensitivity Results

To gain more insight on the impact of DFIG location on small signal stability of system, dynamic or trajectory sensitivity analysis is carried out in this study. The *RSI* is calculated for each generator in all the scenarios. The rotor angle values are obtained using PMUs placed in the system at the sampling rate of 60 samples/second. To observe the system's evolving trajectory, a 3-phase fault of 6 cycles is applied at bus 12 at 1.0 second in all the cases. In calculating the indices using Eq. (4.28), the value of w_t is taken as 1 for all the time instant starting from 1 to 2 sec, i.e., for 60 time instances w_t =1 and zero for all other instants. As initial time instants after the fault are important, higher value are given to them.

For 15% wind penetration case (Case 1), the *RSI* values obtained is compared for most beneficial (Bus No. 3, 18) and adverse (Bus No. 9, 28) locations and shown in Fig. 4.12. The result clearly indicates that the relative rotor angle deviation of existing SGs with respect to active power injection is higher in case of detrimental location (Bus No. 9, 28) as compared to beneficial location (Bus No. 3, 18). It indicates that wind penetration at Bus No. 9 and 28 in the system creates higher angular separation among SGs resulting in more oscillations and less damping.

Similarly, the *RSI* values comparison results for Cases 2, 3 and 4 are shown in Figures 4.13, 4.14 and 4.15 respectively. The observation in these cases is also the same as that for Case 1. The relative rotor angle deviation is much higher in detrimental locations as compare to locations which are beneficial for oscillatory stability. This observation becomes clearer as the penetration of wind is increased in the system. It is seen in Fig. 4.14 that the relative rotor angle variation difference is very high for two

different locations. This also explains why system has very low damping for one location and high in another.

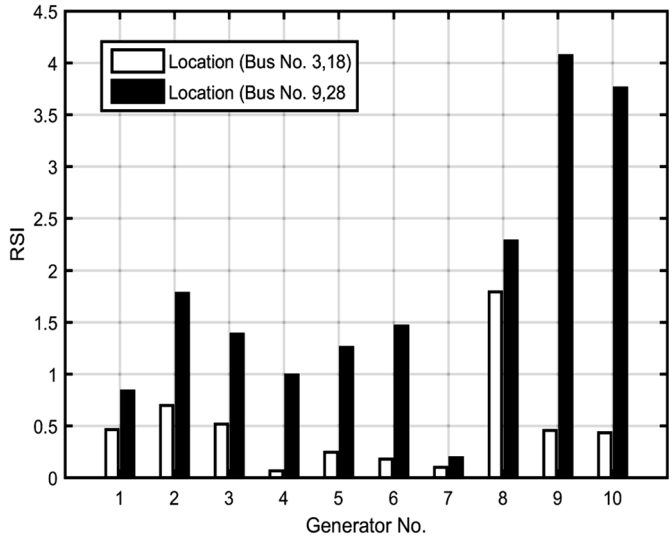

Fig. 4.12 *RSI* values comparison (Case 1)

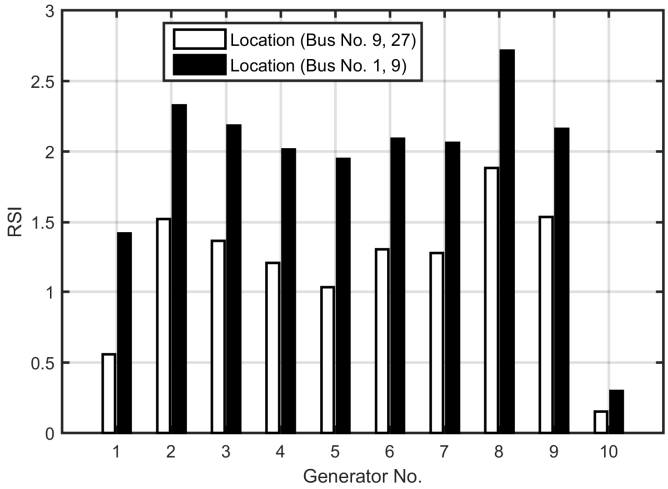

Fig. 4.13 *RSI* values comparison (Case 2)

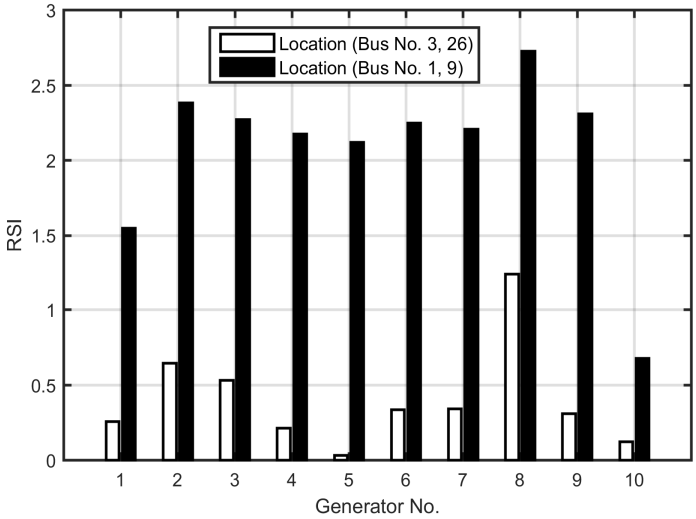

Fig. 4.14 *RSI* values comparison (Case 3)

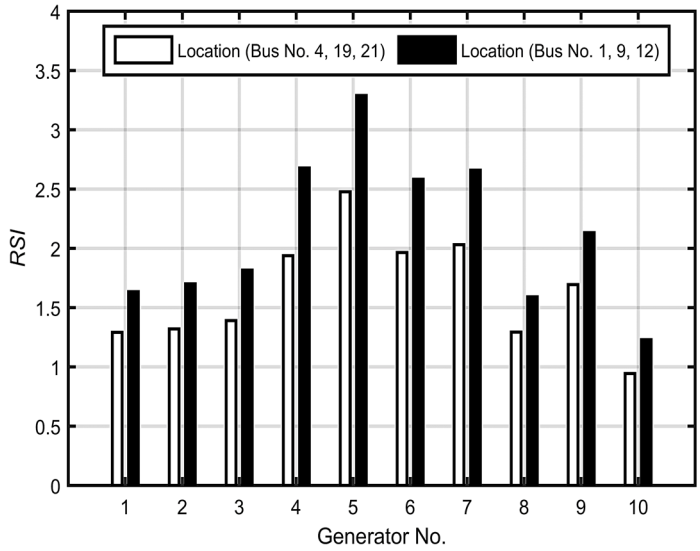

Fig. 4.15 *RSI* values comparison (Case 4)

The results obtained using the dynamic trajectory sensitivity verifies the results obtained from the eigenvalue analysis and signify the importance of wind integration location and its impact on system's small signal stability. This analysis is useful to take counter preventive measures to neutralize the detrimental effect of wind penetration at certain locations.

The dynamic sensitivity result indicates how DFIG interacts with the system at different locations. There is a major difference between conventional SGs and DFIGs due to their inertial contribution to the system. Due to this, there is a significant variation of active power flow with wind integration in system which affects the rotor angles of the SGs of the system. For different locations, this angular separation varies which may result in oscillations problem. The locations with smaller angular deviation, leads to higher damping and thus an oscillatory stable system. On the contrary, DFIG placement at some locations causes higher angular separation resulting in less damping torque and oscillatory problem in the system. Thus, the investigations performed in this section emphasizes the fact that for understanding the proper impact analysis of DFIG on LFO, analysis should be done on the basis of DFIG insertion point as system damping changes with the location of DFIG instead of randomly adding them to any bus as this do not provide correct impact.

The two methods are employed in this chapter to integrate the WTGs in the power system. First one involves replacing some existing SGs and the second suggests DFIG integration at non-generator buses. Both the studies emphasizes the fact that location of DFIG is a very crucial factor which affects the damping of LFOs. In the first study, it

has been seen that replacing SG10 by DFIG is found to be the beneficial case and improves system damping. However, this result is not applicable in practical scenarios. The reason being that SG10 is the slack generator and it is not practical to replace it by an intermittent source like wind. Also, if the present scenario is taken into consideration, the energy need is growing every day and these new technologies are still in development phase. So, replacing well established high inertia synchronous generation by wind generation is not practical in current scenario. Most of the WTGs which are integrated in recent times are to meet the load growth. So, in practical scenarios they do not replace existing SGs. So, the second option of integrating DFIGs without replacing SGs is more practical and expedient one.

4.5 SUMMARY

The WTGs proliferation in the system affects many aspects of the dynamic and operational characteristics of SG dominated power system. Thus, it is imperative to analyse their impact on damping of LFOs in the system. In this chapter, a comprehensive analysis to show the impact of DFIG integration on power system oscillations is carried out for a practical test system. The DFIGs are integrated by two ways – by replacing existing SGs and by adding them directly to non-generator buses without replacing existing SGs. In both the studies, the location of DFIG is shown to be one of the key factors that impact the oscillatory stability of the system.

Following are the major contributions and highlights of this chapter:

1. A Damping Ratio Sensitivity Index (*DRSI*) based method is proposed for impact analysis of DFIG integration on small signal stability while replacing SGs. The detailed eigenvalue analysis verify the effectiveness of the proposed *DRSI* based method.
2. The integration of DFIG penetration may cause positive or negative impact on system's damping depending on its location. The decrease in inertia due to WTG reduces damping of critical interarea modes in the system, except when DFIG is integrated replacing the most participating generator in critical mode.
3. The eigenvalue analysis and dynamic trajectory sensitivity analysis used here proved to be sufficient and adequate techniques for studying DFIG integration without replacing SGs and provide effective results.
4. It is found that for the same DFIG penetration, the change in location of WTG alter the damping of LFO modes in the system and thus affect the system's small signal stability.

5. The DFIGs integration without replacing SGs is far more practical case considering present scenario where WTGs are deployed to meet the load growth.
6. The small signal stability should not be the sole criteria to find optimal location of DFIGs. It is neither feasible nor technically correct to find optimal location of DFIG on the basis of modes damping or small signal stability. Above study is needed to take counter preventive measures to neutralize the detrimental effect of wind penetration if they are not optimally placed at certain locations. The investigations carried out in this work can be employed for planning studies of power system integrated with DFIG.

CHAPTER 5

ROBUST COORDINATED CONTROL FOR DAMPING LOW FREQUENCY OSCILLATIONS

5.1 INTRODUCTION

The preeminence of wind power as a source of clean power generation is growing very fast. The increasing wind penetration however escalates the problem of LFOs in the modern grid. The DFIG is the most prevalent and widely accepted WTG due to its superior control, smooth grid connection, reactive power support and lower cost. But, this rapid proliferation of WTGs in the system may adversely impact the damping of LFOs. The oscillations limit the power transfer capacity of tie-lines and in severe cases the system may collapse leading to blackout [31]. With high penetration of DFIGs in the system, the rotating mass of DFIG is decoupled from the grid frequency and does not inherently exhibit an inertial response unless controlled for that specific purpose and this escalates the LFOs problem in the system. In order to improve the system damping, conventional Power System Stabilizers (PSSs) are employed but they are not effective under these conditions. They need to be supported using some supplementary controllers to have acceptable system damping under widely varying operating conditions. Recently many researchers have proposed methods to improve damping in wind integrated systems using the Power Oscillation Dampers (PODs) employed with DFIGs [91-97]. The PODs when designed in coordination with PSSs are found to be more effective in damping the LFOs.

The investigations carried out in Chapter 4 suggests that the location of DFIGs is one of the crucial factors that affects system damping. The impact of DFIG integration can be beneficial or detrimental depending on its location. However, it has also been concluded that it is neither feasible nor technically correct to find location of DFIG on the basis of modes damping or small signal stability. Practically, wind locations depend on the wind power resource and cannot be optimized. Thus, those locations could be either beneficial or detrimental to system damping which can be found out using impact analysis study carried out in previous chapter. The next step would be to implement a robust control methodology to neutralize the detrimental effect of wind penetration if they are negatively affecting system damping at certain locations and improve the damping of LFOs with high wind penetration in the system.

Also, as identified in many papers that the actual impact of DFIGs on the system damping can only be realized for higher penetration (>15-20%) of wind in the system [76, 87, 107]. However, most of the coordinated control strategies are designed and verified for small penetration of DFIGs in the system which do not guarantee the effective damping for higher wind penetration [101, 103]. The realization of the coordinated tuning of multiple controllers simultaneously for high penetration of wind in the system for damping improvement is a challenging task. Thus, there is need to achieve a better coordinated control strategy for higher penetration of wind in the system where abundant wind potential is available. This will help in resolving the LFO problem effectively in order to integrate more renewables in the system.

The objective of this chapter is to develop a suitable methodology to improve the system damping with a sufficient margin so as to keep system oscillatory stable for wide range of operating scenarios when wind is present in the system. A robust coordinated tuning strategy of PSSs and PODs has been proposed in this chapter to improve the damping performance of a high wind penetrated system. A systematic and complete approach is presented to effectively manage the LFO problem with increasing wind integration in the system. The geometric measure of modal observability is used to select the suitable wide-area based input signal for the PODs. These signal are obtained using optimally placed PMUs in the system. An improved eigenvalue based multi-objective function is used to design the proposed coordinated control strategy for PSSs and PODs. A new optimization algorithm called Grey Wolf Optimizer (GWO) is explored for the proposed work and its application and effectiveness is investigated for this complex coordinated control problem. Eigenvalue analysis, time-domain simulations and robustness analysis are carried out to validate the oscillatory stability improvement and robustness of the proposed control by checking damping performance of the system against faults, line outages and different loading conditions. A new index called Robustness Index (*RI*) is also proposed to assess the robustness of proposed control approach.

5.2 DFIG AND CONTROLLERS MODELLING

The modelling of DFIG has already been detailed in previous chapter. As explained in [105], the damping effect of RSC reactive power controller is much higher as compared to GSC. Hence, in this study RSC controls are used and reactive power is regulated to suppress the oscillations.

The second order lead-lag compensator structure of POD and PSS is used in this study as shown in Fig. 5.1. Using the same structure as PSSs makes it easy to implement PODs in practical power system. They have a stabilizer gain K (K_{PSS} or K_{POD}), wash-out time constant T_W (=10 s), and two phase compensators with time constants T_1, T_2, T_3 and T_4 [101]. The wash-out stage make sure that the controller steady state output is zero. The maximum and minimum limits of controllers output is limited by anti-windup limiter between ±0.2 pu. The input signal of PSS is the generator active power output and of POD is a wide area signal obtained from optimally placed PMU. The stabilizer gain regulates the damping provided by the controllers while the phase compensator blocks deliver the suitable lead-lag compensation of the output signal. The parameters of POD are tuned optimally along with PSS parameters using the proposed approach. The output of PSS is fed to AVR loop while the output of POD is fed to the voltage controller of DFIG which then helps in reactive power modulations and improves the system damping performance. As only the reactive power output of DFIG is varied to control the oscillations, it does not disturb its active power generation.

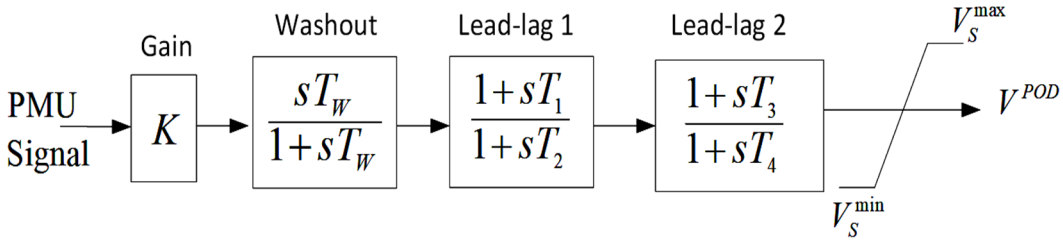

Fig. 5.1 PSS or POD structure

5.3 PROPOSED METHODOLOGY FOR DAMPING IMPROVEMENT

The objective of the proposed work is to improve damping of power systems with high wind penetration by designing robust coordinated control strategy for damping controllers.

5.3.1 DFIG Location

The New England wind integration report [124] suggests that this region has abundant wind potential of up to 12000 MW. The proposed study is implemented on IEEE 39-bus benchmark system which is an adaptation of this practical New England region and thus possesses very high wind potential. Thus, there are multiple potential locations for DFIG placement. As pointed out in Chapter 4, the wind farm location is a significant factor that impacts the LFO damping. The LFO damping may increase or

decrease depending on the location of penetration. However, the small signal stability should not be the sole criteria to find optimal location of DFIGs. Moreover, the DFIG locations are practically governed by the abundance of wind resource available at a location. As the New England region has multiple possible placement locations, so instead of randomly placing the DFIGs again for this analysis, the locations obtained in previous analysis are used. The penetration is kept at 25%. The most detrimental locations obtained for the Case 4 in Chapter 4, when DFIGs are placed at non-generator buses, are chosen as wind farm locations in this study. This is performed to test the effectiveness of proposed control approach. If proposed control improves the system damping for most detrimental case, it could be concluded that it will be equally effective for any other probable locations of DFIGs in the system.

The suggested detrimental locations have the worst damping as compared to other locations and thus they are chosen to be DFIG placement buses for the remaining part of study.

5.3.2 Wide-area feedback signal selection

The interarea oscillations involve many machines swinging against each other in different areas. These machine are more observable with wide-area signals as compared to local signals. The feedback signal should be chosen such that it has very high modal observability of the critical mode(s), as this simplifies the designing of controller and enables a robust damping performance over a wide range of operating conditions [115]. In this study, the geometric measure of modal observability is used to select the input signals for the PODs. The modal observability corresponding to the i^{th} oscillation mode is defined as

$$O_h = \frac{\left|C_h \phi_i\right|}{\left\|C_h\right\| \left\|\phi_i\right\|} \tag{5.1}$$

where C_h is the h^{th} row of C matrix. The transmission line active power which has the maximum observability of critical mode is used as an input signal to POD for the coordinated control. The wide area signal is obtained with the help of optimally placed PMUs in the system. These PMUs enables real-time monitoring of critical buses for oscillation monitoring and complete system observability even under N-1 contingency and single PMU loss with minimum number of PMUs as suggested in Chapter 3.

5.3.3 Proposed Optimization Formulation

The goal of the proposed coordinated control strategy of supplementary controllers is to improve the system oscillatory stability and to obtain a robust damping performance. The aim is to obtain this goal without increasing much complexity of the system and to keep the approach as simple as possible. This optimal coordination of controllers is accomplished by converting it into an optimization problem that looks for optimal parameters of PSSs and PODs.

An improved eigenvalue based multi-objective function is considered to simultaneously maximise the system damping ratio and shift the eigenvalues to a more stable region. The dual objective is combined to form a single objective to be minimized and given as

$$f = \sum_{k=1}^{oc} \sum_{\xi_{i,k} \le \xi_{spec}} \left(\frac{\xi_{spec} - \xi_{i,k}}{\xi_{spec}}\right)^2 + \sum_{k=1}^{oc} \sum_{\sigma_{i,k} \ge \sigma_{spec}} \left(\frac{\sigma_{spec} - \sigma_{i,k}}{\sigma_{spec}}\right)^2 \tag{5.2}$$

where oc is the number of operating conditions for which parameters are simultaneously tuned, $\sigma_{i,k}$ and $\xi_{i,k}$ are the real part and the damping ratio of the i^{th} eigenvalue corresponding to the k^{th} operating condition. In this work, the values of specified real part of eigenvalue and damping ratio, σ_{spec} and ξ_{spec} are set at -1.0 and 0.1(10%) respectively. The targeted damping ratio is deliberately kept 10% so as to have a sufficient damping margin available for a wide range of operating scenarios. It also test the effectiveness of proposed control to achieve such improved damping ratios for all the LFO modes in the system against faults, line outages and different loading conditions.

The objective function consists of two terms. It is improved from previous works by normalizing these two terms. The first term is the sum of the difference between the required and actual damping ratio of all the modes having damping ratio less than specified value. The second term is the sum of the difference between the specified and actual real part of eigenvalues. The values of these two terms are of different order and thus cannot be added together directly. So, both the terms are normalized with respect to specified values to achieve more practical and accurate results. The proposed objective function will move the unstable or critical eigenvalues of all operating conditions to a D-shape region in the left-half of s-plane where $\sigma_{i,k} \le \sigma_{spec}$ and $\xi_{i,k} \ge \xi_{spec}$ as shown in Fig. 5.2.

The proposed objective formulation with constraints is given as

$$\begin{aligned} &\textit{Minimize } f \\ &\text{Subject to:} \\ &K^{\min} \le K \le K^{\max} \\ &T_{1,3}^{\min} \le T_{1,3} \le T_{1,3}^{\max} \\ &T_{2,4}^{\min} \le T_{2,4} \le T_{2,4}^{\max} \end{aligned} \tag{5.3}$$

where the gain K includes both K_{PSS} and K_{POD}, and time constants $T_{1,2,3,4}$ includes the time constants of both PSS and POD ($T_1 = T_3$, $T_2 = T_4$). The values of $K^{\min}$, $K^{\max}$ are set as 0.1 and 50 respectively, $T_{1,3}^{\min}$, $T_{1,3}^{\max}$ are set as 0.1 and 1 respectively, and $T_{2,4}^{\min}$, $T_{2,4}^{\max}$ are set as 0.01 and 0.1 respectively.

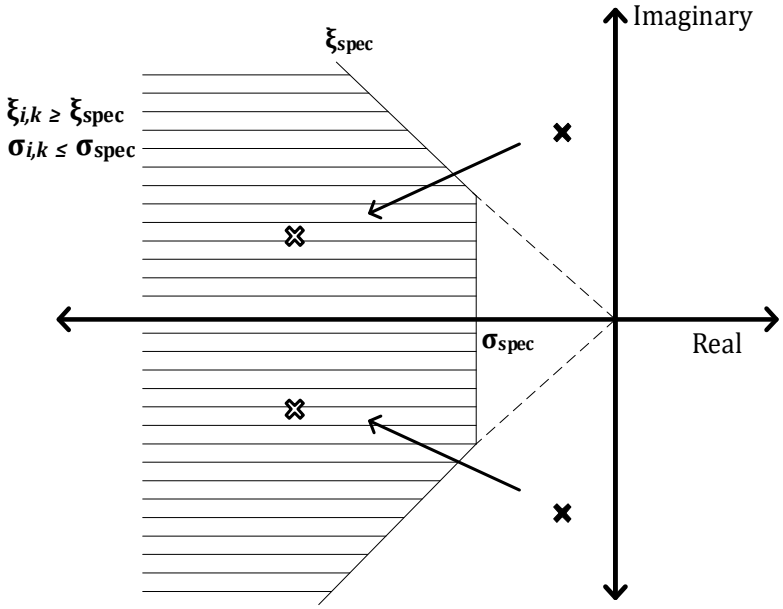

Fig. 5.2 D-shape region in left-half of s-plane

For the optimal tuning of controllers, three optimization techniques – Particle Swarm Optimization (PSO) [127], Grey Wolf Optimization (GWO) [128] and Whale Optimization Algorithm (WOA) [129] have been tested and compared. Out of them GWO has been selected to tune the controllers and discussed in next subsection.

5.3.4 Grey Wolf Optimization Algorithm

For coordinated control of damping controllers metaheuristic techniques are very suitable as they do not require past knowledge of the problem. They are independent of system complexity, number of devices to be tuned and gives a faster solution. The GWO [128] has been explored in this study to obtain the parameters of multiple damping controllers. This algorithm is used because of its simplicity, flexibility, derivation-free mechanism, and local optima avoidance ability. GWO is used in this here as it has very

few parameters, and strikes good balance between exploration and exploitation. Thus, it is suitable to employ for a large number of problems without any specific modification in algorithm [130].

A. Overview of GWO

GWO is inspired by the hunting behaviour of grey wolves (Canis Lupus) and works on their social hierarchy and group hunting mechanism. The Grey wolves are apex predators and prefers to live in a pack of 5-12 wolves. There exists a well-established societal hierarchy according to which they can be categorised as Alpha (α), Beta (β), Delta (δ) and Omega (ω). Alpha is the leader and decision maker and act as fittest solution. The beta wolf and delta wolf represent second and third best, respectively and omega wolves are the candidate solutions influenced by α, β, and δ. The other main characteristic is their hunting mechanism which involves:

- Tracking, chasing, and approaching the prey.
- Pursuing, encircling, and harassing the prey until it stops moving.
- Attacking the prey.

B. Mathematical Modelling of GWO

In the GWO algorithm the hunting (optimization) is guided by α, β, and δ. The ω wolves follow these three wolves. The mathematical model of encircling behaviour to update their positions around the prey randomly is expressed by using eq. (5.4)-(5.7).

$$\vec{D} = \left| \vec{C} \cdot \vec{X}^{*}(t) - \vec{X}(t) \right| \tag{5.4}$$

$$\vec{X}(t+1) = \vec{X}^{*}(t) - \vec{A} \cdot \vec{D} \tag{5.5}$$

where t represents the current iteration, $\vec{A}$ and $\vec{C}$ are coefficient vectors, $\vec{X}^{*}$ is the position of prey and $\vec{X}$ gives the position vector of grey wolf. The values of $\vec{A}$ and $\vec{C}$ are given by

$$\vec{A} = 2\vec{a} \cdot \vec{r}_1 - \vec{a} \tag{5.6}$$

$$\vec{C} = 2 \cdot \vec{r}_2 \tag{5.7}$$

where components of $\vec{a}$ are linearly decreased from 2 to 0 over the course of iterations and $\vec{r}_1$, $\vec{r}_2$ are random vectors in [0, 1].

Next, the hunting behaviour of grey wolves is modelled. It is assumed that α, β, and δ have better knowledge of probable position of prey. So, three best solutions are saved as α, β, and δ and following them ω wolves update their position. The corresponding equations are given by (5.8)-(5.14). The flowchart of GWO is shown in Fig. 5.3.

$$\vec{D}_\alpha = \left| \vec{C}_1 \cdot \vec{X}^*_\alpha - \vec{X} \right| \tag{5.8}$$

$$\vec{D}_\beta = \left| \vec{C}_2 \cdot \vec{X}^*_\beta - \vec{X} \right| \tag{5.9}$$

$$\vec{D}_\delta = \left| \vec{C}_3 \cdot \vec{X}^*_\delta - \vec{X} \right| \tag{5.10}$$

$$\vec{X}_1 = \vec{X}^*_\alpha - \vec{A}_1 \cdot \vec{D}_\alpha \tag{5.11}$$

$$\vec{X}_2 = \vec{X}^*_\beta - \vec{A}_2 \cdot \vec{D}_\beta \tag{5.12}$$

$$\vec{X}_3 = \vec{X}^*_\delta - \vec{A}_3 \cdot \vec{D}_\delta \tag{5.13}$$

$$\vec{X}(t+1) = \frac{\vec{X}_1 + \vec{X}_2 + \vec{X}_3}{3} \tag{5.14}$$

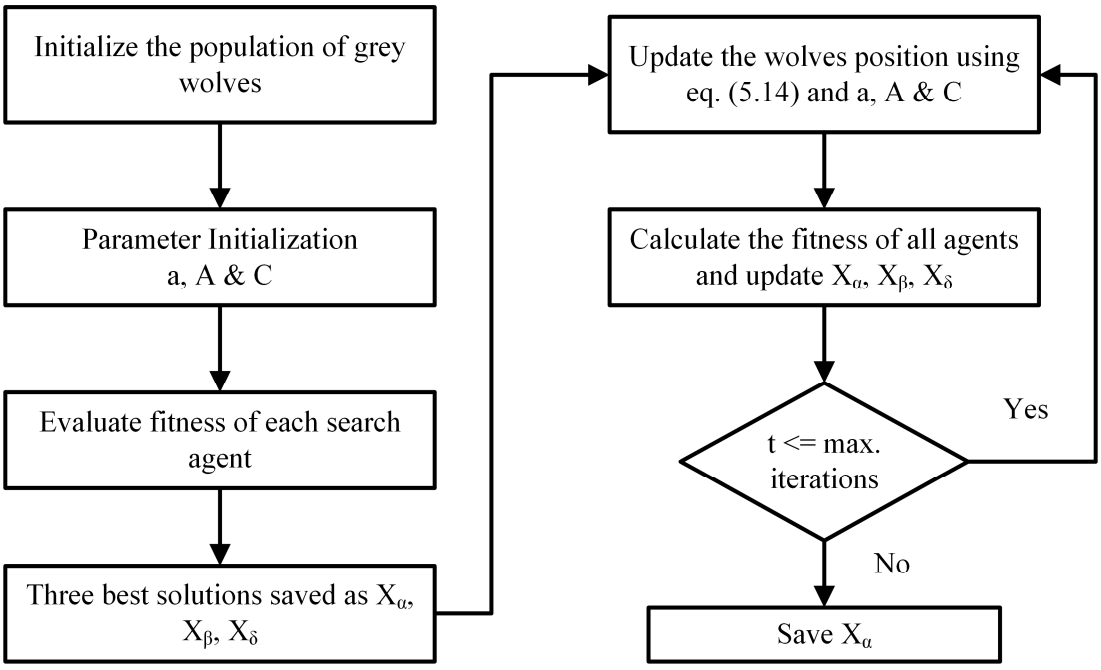

Fig. 5.3 Flowchart of GWO

The optimization process for parameters search starts by creating a random population of grey wolves. With iterations, the positions of α, β, and δ wolves gives the

probable position of the solution and accordingly the omega wolves update their position. The parameter a is decreased from 2 to 0 in order to emphasize exploration and exploitation, respectively. Candidate solutions tend to diverge from the prey when $\left|\vec{A}\right| > 1$ and converge towards the prey when $\left|\vec{A}\right| < 1$. The adaptive values of a and A helps in smooth transition between exploration and exploitation. The main advantage of this algorithm is that there are only two main parameters to be adjusted (a and C). Finally, the algorithm terminates according to some end criterion satisfaction and position of Alpha wolf gives the final optimized solution. The more detailed explanation about the algorithm can be found in [128].

5.4 SIMULATION AND RESULTS

The robustness and efficiency of the proposed coordinated control of multiple damping controllers is studied and tested on IEEE New England benchmark system. It comprises of 10 SGs, 19 loads and 46 transmission lines. All SGs are of fourth order equipped with static AVRs. All SGs except slack are installed with Type II PSSs.

The maximum DFIG penetration, for wind integration without replacing SGs, tested in previous chapter is 25%. In this chapter also the maximum penetration is kept same and the case of three wind farms integration is chosen to make such high penetration of DFIG more practical. The system total generation is $P_G = 6138.71$ MW. Thus each wind farm is of 512 MW. The system load is increased by the same amount as wind penetration to keep the balance between load and generation. The system is modified to place three DFIG based wind farms at most detrimental locations determined in Chapter 4 (Section 4.4.2). The locations are bus no. 1, 9 and 12.

In the base case, with no wind farm installed and with untuned PSSs, the system excites 9 LFO modes. There are 8 local modes and one interarea mode as given in Table 5.1. The high damping ratio of local modes show that, although untuned, the PSSs are fairly effective in damping local modes. It can be seen that the damping ratio of interarea mode is less than 10%. As PSSs are not tuned one local mode also has damping below 10%. So these two modes are the critical modes in the base case (without wind). The eigenvalue plot is shown in Fig. 5.4(a). All the modes are on the left side of 10% damping line except the two critical modes. Although, the real parts of all modes are negative but the interarea mode has damping less than 10%. The generator participation plot in interarea mode is shown in Fig. 5.4(b). It can be seen that SG10

has the highest participation in this mode. Now, three wind farms are introduced in the system at the given locations.

TABLE 5.1
LFO MODES IN BASE CASE (WITHOUT WIND)

S.No.	*f*, Hz	Damping ratio, %	Mode	Dominant Generator
1	1.6625	24.92	Local	SG 8
2	1.6362	19.18	Local	SG 4
3	1.3746	09.85	Local	SG 1
4	1.4081	30.85	Local	SG 7
5	1.3741	19.31	Local	SG 3
6	1.1281	18.92	Local	SG 2
7	1.0369	30.30	Local	SG 8
8	0.9723	24.20	Local	SG 4
9	**0.5334**	**04.98**	**Interarea**	**SG 10**

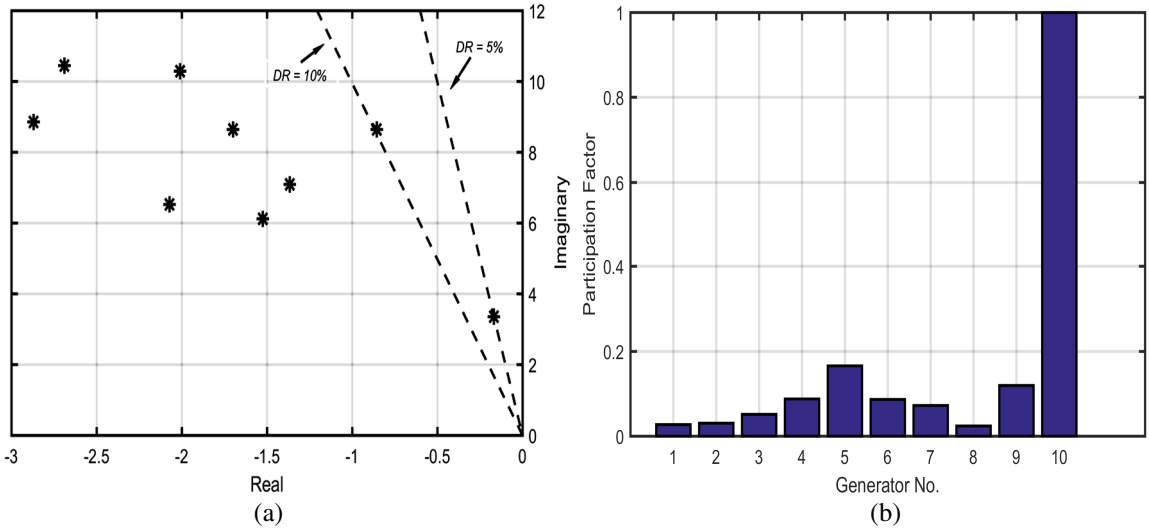

(a) (b)

Fig. 5.4 Base case modal analysis results (a) Eigenvalue plot, (b) Generators participation in interarea mode

5.4.1 Selection of PODs input signal

It is clear from the Table 4.15 that in the wind integrated system, there is one critical mode which is the interarea mode with damping less than 10% in the system. So, supplementary damping controllers can be employed along with PSS to increase the damping. Before employing POD, a suitable wide-area input signal should be selected first. The modal observability for the critical mode is calculated using eq. (5.1) in the active power flow of all the lines. The results are shown in Fig. 5.5. It can be seen from the figure that line 16 (between bus 9 and 39) has the greatest value of modal observability of the critical interarea mode. Thus, the active power flow in line 16 is chosen as the input signal for the DFIG PODs. The feedback signal is measured by the help of PMUs placed in the system.

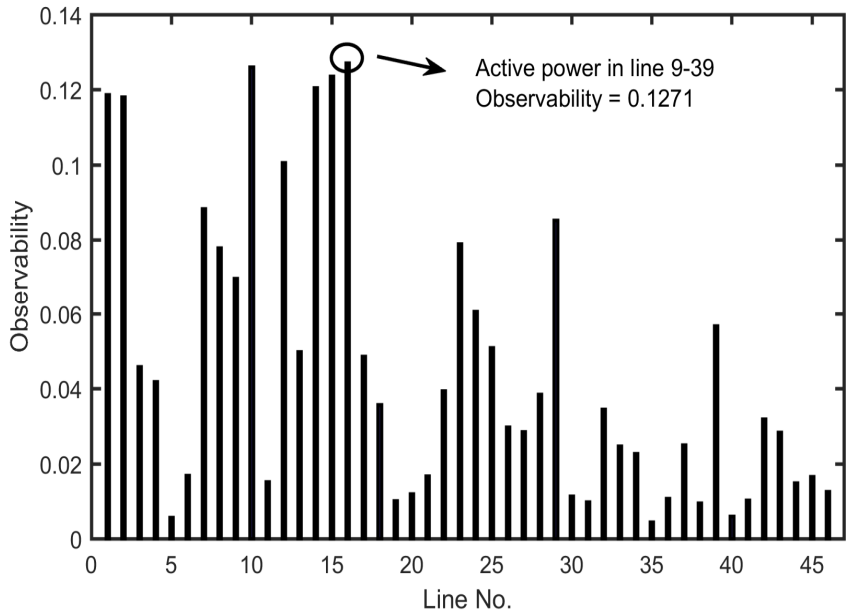

Fig. 5.5 Observability of critical interarea mode in line active power flow

5.4.2 Robust Tuning of Controllers

The robust tuning of the PSSs and PODs is done using different optimization techniques. The performance of three optimization techniques – PSO, GWO and WOA are compared to choose the best optimization technique suitable for this study. The comparison is done on the basis of convergence characteristics. Same search parameters (population = 50, maximum iterations = 100) are taken for all the three techniques.

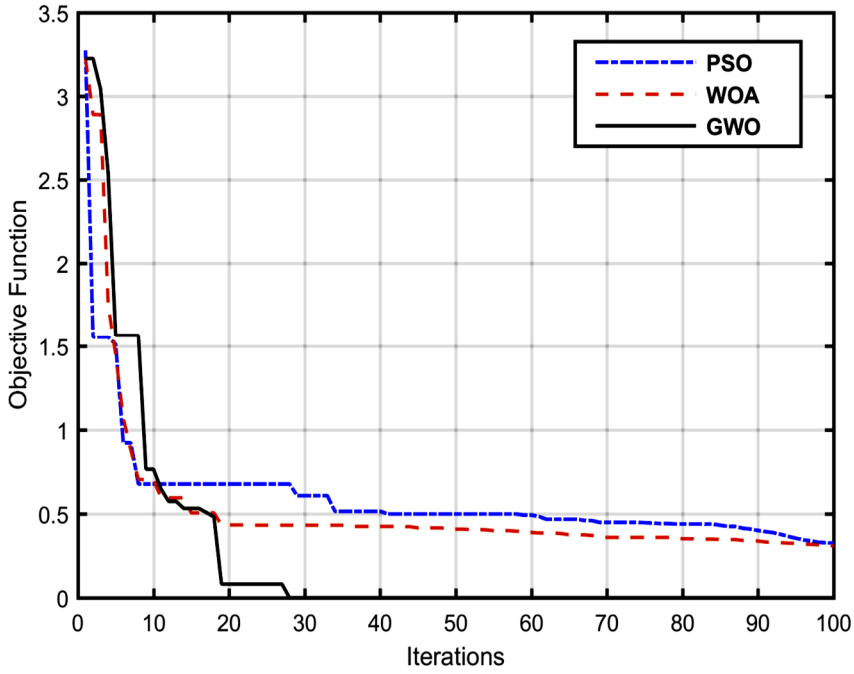

Fig. 5.6 Convergence Characteristics Comparison

The comparison has been done for the highest problem dimension, i.e., when there are 9 PSSs and 3 PODs in the system which gives a dimension of 36 (each contributing three variables). The convergence rate of all three optimization techniques is shown in Fig. 5.6. The result shows that GWO performs better than other two as it converges faster than other two techniques. The other two techniques do not converge even at the end of 100 iterations. Therefore, GWO technique is employed in this work for parameters optimization.

The DFIGs are placed at bus no. 1, 9 and 12 of 512 MW each as shown in Fig. 5.7.

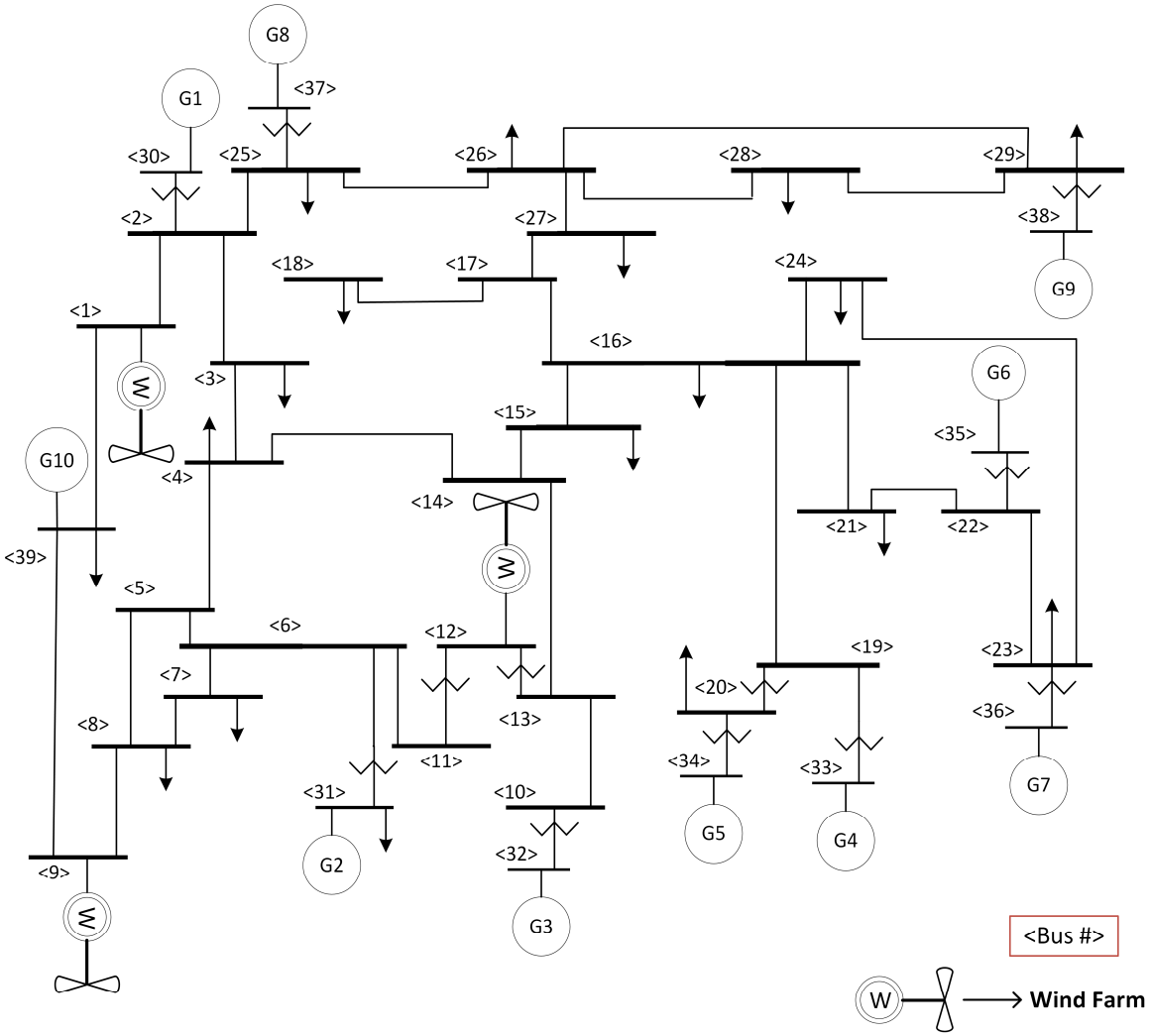

Fig. 5.7 Modified IEEE New England 39-bus benchmark system

The GWO algorithm is used to obtain the parameters of the PSSs and PODs of this system having high wind penetration. The search parameters of the GWO are set as: population = 50, maximum iterations = 100, and the problem dimension depends on the number of controllers involved (each controller contributing three parameters). The parameters are tuned simultaneously for multiple operating conditions to obtain a robust

damping performance. The operating conditions considered here are: base case (with wind), 20% underload, 20% overload and outage of tie-line between buses 14-15. The effectiveness of the proposed coordinated control design is verified by comparing the results of following three cases:

Case 1: Wind integrated system with untuned PSSs, no POD;

Case 2: Wind integrated system with tuned PSSs, no POD;

Case 3: Wind integrated system with coordinately tuned PSSs and PODs.

Case 1 is the base case scenario of the wind integrated system. In this case, there are 9 PSSs installed in the system which are untuned and there are no PODs in the system. In Case 2, the parameters of these PSSs are tuned using GWO to improve the system damping. The PODs are introduced in the system in Case 3, where the 9 PSSs and 3 PODs are coordinately tuned using GWO. The optimized parameters of controllers obtained are given in Appendix B.

To assess the robustness of the proposed coordinated control and to compare different cases, a new index called Robustness Index (*RI*) is proposed in this study, given as

$$RI = \sum_{j=1}^{N_g} \left| \frac{1}{T} \sum_{n=1}^{N} \left(\omega_{jn} - \omega_{COI,n} \right) \right| \tag{5.15}$$

where N_g is the total number of SGs in the system, T is the total simulation time, N represents the total number of data samples recorded, ω_{jn} and $\omega_{COI,n}$ are the SGs rotor speed and rotor COI speed at the n^{th} instant respectively. The controller giving the lowest value of *RI* will be the most robust to the changing operating conditions and will improve the oscillatory stability most effectively.

A. Eigenvalue Analysis Results

The eigenvalue analysis results for the three cases are shown in Table 5.2. In Case 1, there are 9 modes and out of these, interarea mode is critical (mode 9) having damping less than the desired threshold. One local mode also has damping less than 10%. To damp the interarea mode and to improve the damping of other modes, two control strategies are employed – one is to tune the PSSs alone and other is to employ PODs and coordinate the PSSs and PODs to improve the system damping. The GWO algorithm is used for both the strategies (Case 2 and Case 3) with same search parameters. From Table 5.2, it can be seen that both the methods increase the DR of the critical mode beyond the threshold value and also improve the damping of other modes.

In both the cases there are 7 local and one interarea mode, as one local mode vanishes by use of tuned controllers. The real part of eigenvalues is also smaller than the desired σ_{spec} for both the cases. The damping is better in Case 3 as compare to the Case 2 which shows the effectiveness of proposed coordinated control strategy.

TABLE 5.2
RESULTS OF EIGENVALUE ANALYSIS FOR DIFFERENT CASES

Mode	Case 1			Case 2			Case 3		
	Real part	*f*, Hz	*DR*, %	Real part	*f*, Hz	*DR*, %	Real part	*f*, Hz	*DR*, %
1	-2.64	1.6412	24.82	-1.81	1.7886	15.96	-4.24	1.7664	35.71
2	-1.70	1.6233	16.34	-2.30	1.5066	23.65	-2.55	1.6048	24.53
3	-0.81	1.3652	09.78	-1.36	1.2774	16.82	-2.68	1.4350	28.51
4	-2.73	1.4522	28.37	-1.55	1.2435	19.46	-2.31	1.1804	29.75
5	-1.46	1.3640	16.56	-1.25	1.1031	17.75	-2.83	1.1162	37.45
6	-1.33	1.1141	17.92	-2.54	1.0273	36.66	-2.22	1.0088	33.14
7	-2.03	1.0032	30.51	-1.68	0.9944	26.05	-2.96	0.8287	49.47
8	-1.40	0.9986	21.85	**-1.33**	**0.6546**	**30.85**	**-2.39**	**0.7042**	**47.55**
9	**-0.10**	**0.5162**	**01.73**	-	-	-	-	-	-

The eigenvalue plot for Case 1 is shown in Fig. 5.8(a), which shows that except the critical interarea mode all modes lie to the left of 10% damping line or are very close to it. The eigenvalue plots for Case 2 and 3 are shown in Fig. 5.8(b) and 5.8(c). It can be seen from these plots that all the modes including the critical one have been shifted to the desired D-shaped region. These plots also shows that damping of modes is higher in Case 3 as all modes lie to the left of 20% damping line, whereas some modes lie between 10% and 20% damping line in Case 2.

It is seen that in both the cases 2 and 3 the required damping target is achieved. However, as the system is highly dynamic the operating conditions vary widely; the controller should be able to provide the sufficient damping in all the scenarios. Thus, the coordinated control becomes important because the control strategy employing only PSSs may fail to improve stability for some critical contingency cases. The robustness analysis performed in the next sections highlights the importance of coordinated control effectiveness over the PSS working alone.

B. Time-domain Analysis Results

To investigate the effectiveness of the proposed control strategies and to verify the results of the eigenvalue analysis, time domain simulations are carried out for this high wind penetrated system. A 6 cycles 3-phase fault is simulated at bus 16 at t=1.0 s. The dynamic performance of all the three cases is compared for this fault scenario. The active power outputs of SG1 and SG10 are shown in Fig. 5.9(a) & (b). It can be clearly

seen from these figures that the oscillations in the system are damped in a very short time by both the methods, whereas in the base case with no designed controllers the system is moving toward instability with growing oscillations. For this fault scenario both the control strategies fares equally well in improving the system's oscillatory stability.

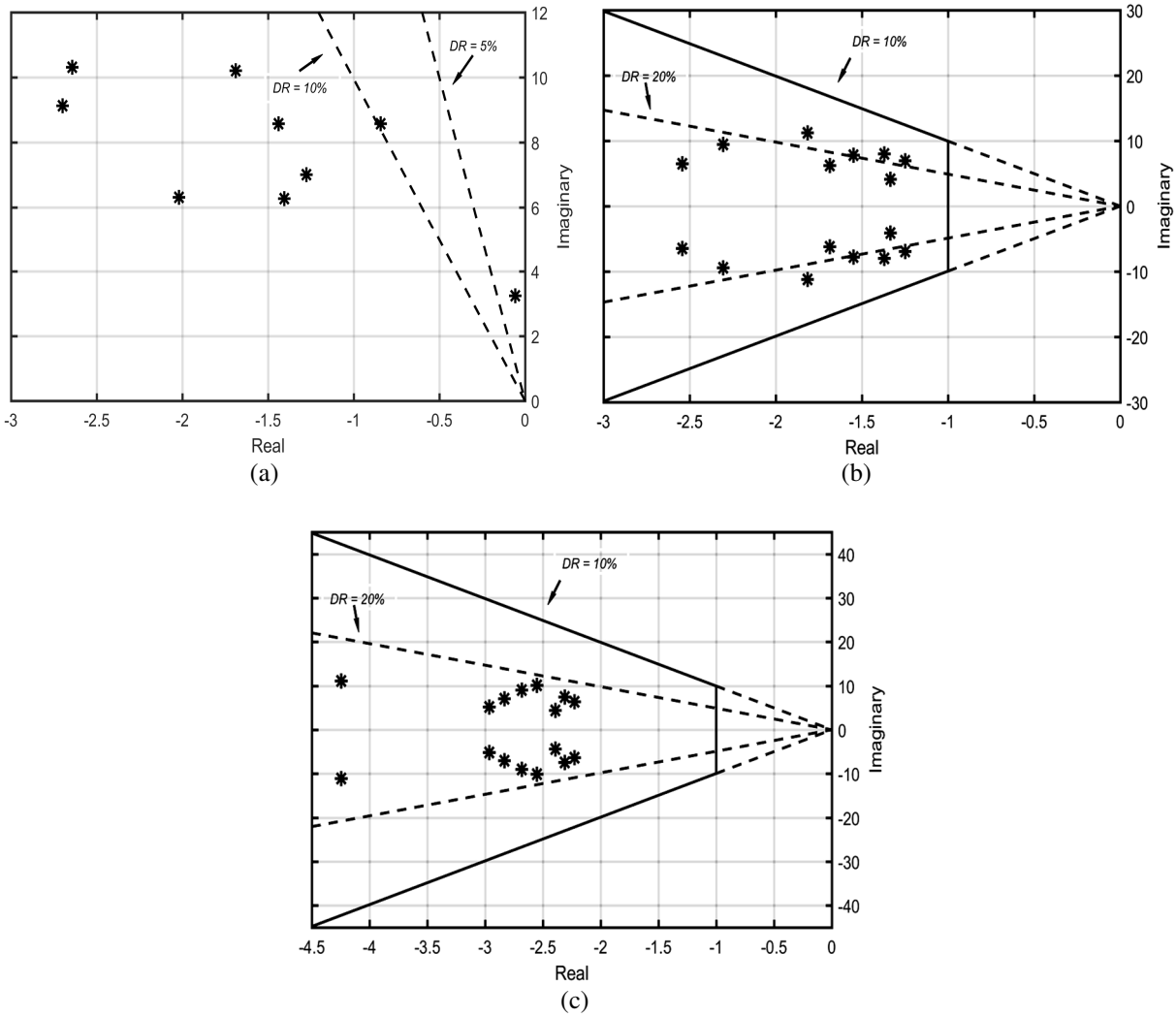

Fig. 5.8 Eigenvalue plots results for proposed control strategy (a) Case 1, (b) Case 2, (c) Case 3

The LFOs limits the power transfer capability of the tie-lines and may trigger cascaded events leading to tie-lines outages and system blackouts. So the power flow on the important tie-lines of the system is also studied for this fault scenario for all the cases. The power flow in line between bus 1 & 39 and between bus 3 & 4 are shown in Fig. 5.9(c) & (d). These power flow plots clearly show the difference between the three cases. The oscillations in the power flow are very high in the base case for both the lines, and leading the system to instability. However, the oscillations are damped out using both the proposed control strategies within 5-6 seconds. Out of the two, the

proposed coordinated control of PSSs and PODs is performing better as it brings the power flow in the lines to the same pre-fault values. In case of only PSSs, the power flow stabilizes to a value slightly lower than pre-fault power flows.

So, the time domain analysis results prove the effectiveness of the proposed control strategies as the results are consistent with the eigenvalue analysis findings.

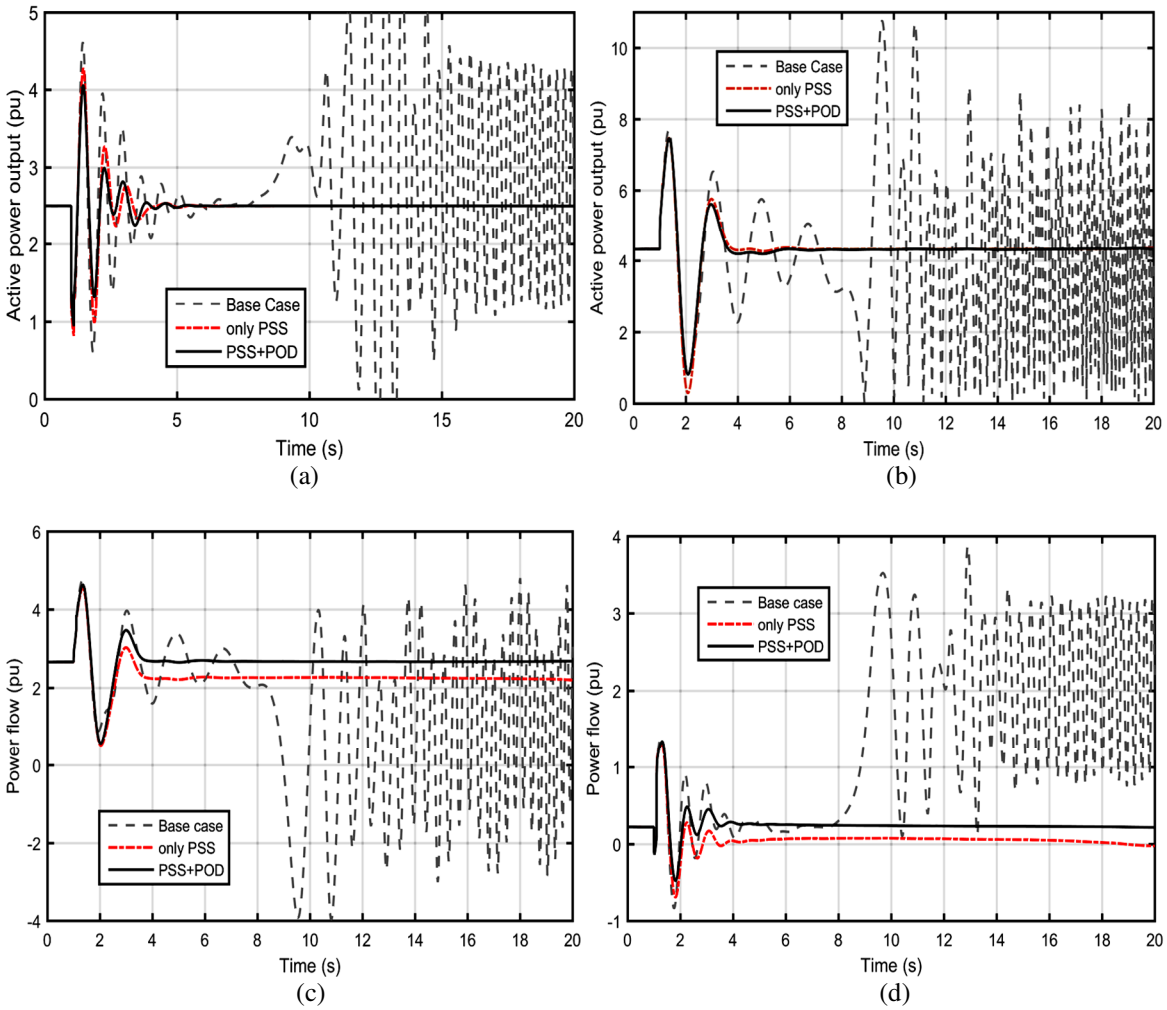

Fig. 5.9 Time-domain analysis results (a) Active power output of SG1, (b) Active power output of SG10, (c) Power flow in tie-line between bus 1 & 39, (d) Power flow in tie-line between bus 3 & 4

C. Robustness Analysis Results

The method employing only PSS tuning to damp the modes might fail in case of some critical contingencies. The coordinated control proposed in this chapter is effective in sufficiently damping the system for all such contingencies. To investigate the robustness of the proposed control strategy, a number of critical scenarios are simulated. Five of them are discussed here:

1) Simultaneous line outages of tie-lines between buses 3-4 and 21-22 and a 3-phase fault at bus 29 of 6 cycles at 1.0 s.

2) The power outputs of all SGs are decreased by 40%, with same line outages and fault condition as mentioned in scenario 1.
3) The system load is increased by 40%, with same line outages and fault condition.
4) The system load is decreased by 40%, with same line outages and fault condition.
5) The power output of all three DFIGs is decreased by 100 MW, with same line outages and fault condition.

The active power output of SG1 is shown in Fig. 5.10 for the above five critical scenarios, comparing the results of the two control strategies employed. For the critical scenario 1, undamped oscillations occurs in base case which makes the system unstable as the generator goes out of step around 11.5 seconds as depicted in Fig. 5.10(a). When controllers are employed, the oscillations die out quickly with both the control strategies. Similarly, in critical scenario 2 as shown in Fig. 5.10(b), the system goes out of step in base case, whereas the oscillations settles within 6 seconds with proposed controllers.

It is found from the results of critical scenario 1 & 2, the performance of both the control strategies is similar. However, when the system is subjected to critical scenario 3 & 4, it is found that the system robustness for such operating conditions improves only with the coordinated control. As seen from critical scenario 3, base case has large undamped oscillation shown in Fig 5.10(c). With only tuned PSSs, the oscillations remain and die out slowly in the end. But, when the proposed coordinated PSSs and PODs are introduced the oscillations damped out within no time. Similarly, in scenario 4 shown in Fig. 5.10(d), the oscillations are damped very quickly by the coordinated controllers, whereas there are sustained undying oscillations with the tuned PSSs alone. In scenario 5 also, oscillations damped out in very less time using the coordinated control approach while there are undamped oscillations when only PSS is employed as shown in Fig. 5.10(e).

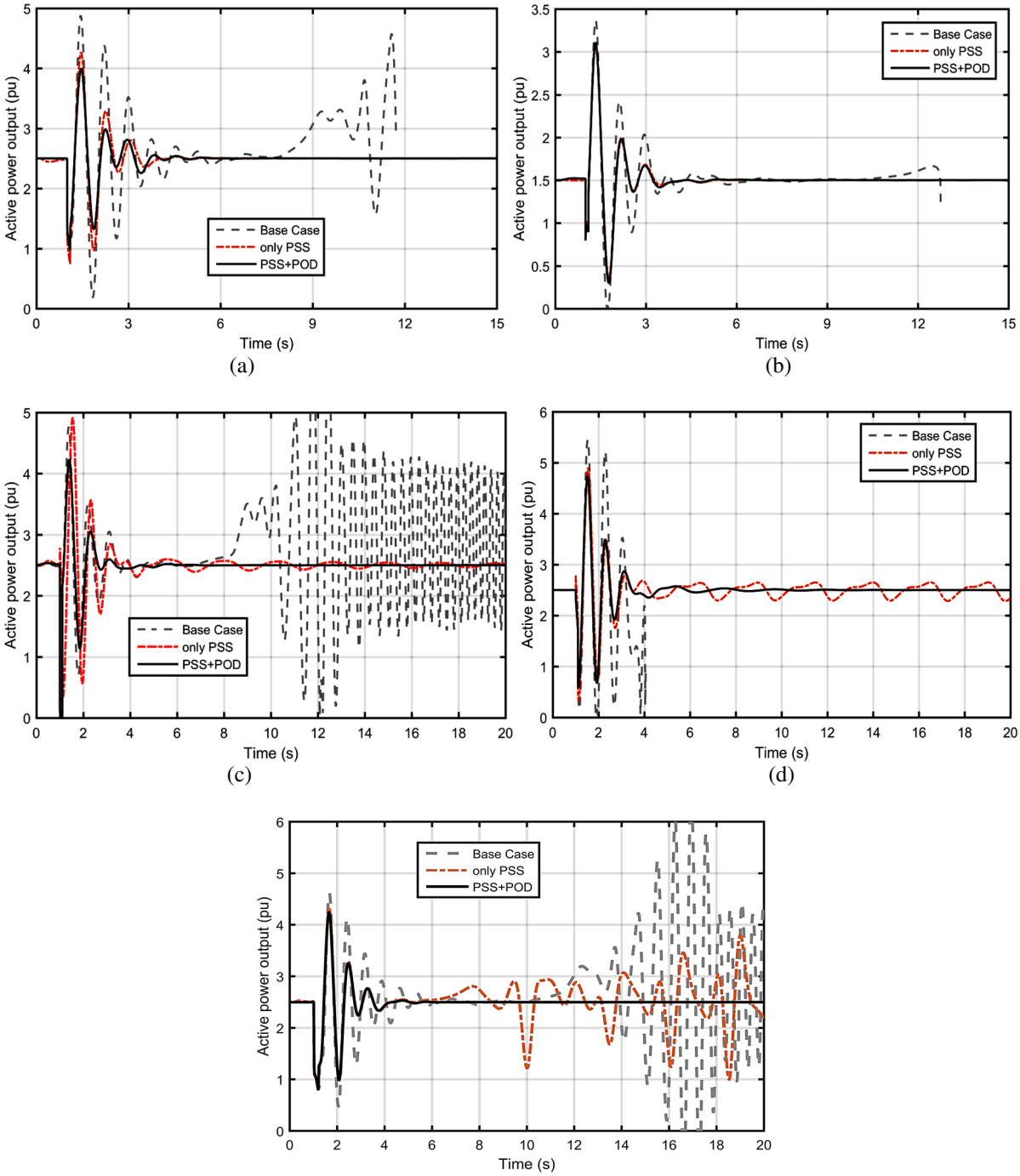

Fig. 5.10 Robustness Analysis results for different critical scenarios (a) Critical scenario 1, (b) Critical scenario 2, (c) Critical scenario 3, (d) Critical scenario 4, (e) Critical scenario 5

The values of *RI* are compared in Table 5.3, to further highlight the robustness of the proposed coordinated approach. The values of rotor speeds are recorded for 30 seconds with a rate of 60 samples/second to calculate *RI* using eq. (5.15). It can be seen from the Table 5.3 that the value of index is lowest with the proposed coordinated control for all the five scenarios considered which proves its robustness to changing

operating conditions. The robustness analysis results further substantiate the results of eigenvalue analysis and time domain analysis.

TABLE 5.3
RESULTS OF ROBUSTNESS ANALYSIS (*RI* VALUES)

Critical Scenario	Base Case	Only PSS	Coordinated PSS+POD
1	0.0495	0.0051	0.0037
2	0.0217	0.0050	0.0043
3	0.0308	0.0058	0.0047
4	0.7936	0.0093	0.0032
5	0.0876	0.0157	0.0039

The results show that PODs coordinated very well with PSSs using the proposed technique and effectively contributes to improve system damping. The robustness of the proposed coordinated control improves the damping performance of the system against faults, line outages and different loading conditions. Thus, proposed control strategy successfully damped the LFOs in presence of high wind penetration in the system and paves the way for further increase in renewables integration in the system while maintaining the system oscillatory stability.

5.5 SUMMARY

In this chapter, a coordinated control of PSSs and PODs for robust damping performance of a multi-machine high wind integrated system is proposed. The main conclusions and highlights of this study are:

1. The PSSs and PODs are coordinated simultaneously for multiple operating conditions, using an improved eigenvalue based multi-objective function to enhance system damping and stability.
2. The modal observability is used to obtain the suitable wide-area based signals for the PODs, which provide global observability of the interarea modes.
3. Optimization algorithm called GWO has been investigated for coordinated tuning of controllers. It is found that GWO algorithm is very effective in the proposed coordinated tuning of controllers and provide robust results.
4. The eigenvalue analysis and time domain simulations proves the controllers coordination and verifies the ability of designed controllers to augment system damping under faults, line outages and different loading conditions.
5. A comparison of dynamic performance of PSS alone and coordinated PSSs and PODs is carried out. Investigation results show that the proposed coordinated control of PSSs and PODs performs much better.

6. The proposed coordinated control of PSSs and PODs has been tested under diverse operating conditions including critical operating conditions such as line outage, loss of load, loss of generation etc. It is found that the proposed coordinated control of PSSs and PODs improves the system damping even for most detrimental case in terms of interarea mode damping.
7. A new Robustness Index (*RI*) is employed to measure the controller robustness to varying system conditions. The robustness analysis results proves that the proposed coordinated control provide remarkable stabilizing effect and robustness as compared to tuned PSS working alone. It stabilizes the system in a very small time even for severe contingencies, when other controllers fail to damp the oscillations.
8. The proposed coordinated control strategy is found to be effective even for most detrimental DFIG locations and therefore may be equally effective for other probable locations of DFIGs.

A general and systematic procedure is proposed in this chapter which can be suitably applied to any large realistic system where abundant wind potential is available. The proposed method can be used for planning studies in modern power grids to augment LFO damping with high renewable integration.

CHAPTER 6

CONCLUSIONS

The monitoring and control of Low Frequency Oscillation (LFO) has assumed significant importance in the context of modern power systems. With rising electricity demand the modern power systems are working in stressed condition closer to their stability limits and are getting highly interconnected day by day giving rise to small signal stability problem. The increasing concerns to reduce carbon emission leads to increase in wind integration in the modern grids. This causes reduction in overall system inertia and further complicates the system's small signal stability problem. Therefore, impact of wind penetration on small signal stability needs to be analysed. The electric power utilities around the globe are undergoing a huge transformation from current Supervisory Control and Data Acquisition (SCADA) systems to synchrophasor-based Wide Area Monitoring and Control Systems (WAMCS). The WAMCS has become an effective tool in analysing the small signal stability problem of power systems.

In modern power systems, which are characterised by complexity and stressed operating conditions, small disturbances are frequently occurring. These small disturbance may excite poorly damped low frequency oscillations in power systems. LFOs can persist for longer durations and can cause cascading tripping events and may lead to a system blackout. Therefore, quick and accurate approaches to detect approaching oscillatory instability in real-time are required so as to initiate proper corrective action within the safe time limit. Also, there is an urgent need to analyse the impact of high wind penetration on low frequency oscillations and to develop a control strategy to improve system damping in such scenarios for a wide range of operating conditions.

This thesis addresses the problem of monitoring and control of low frequency oscillations in power systems. The thesis proposes suitable methods for online and real-time monitoring of low frequency oscillations in power system. It also proposes methods to investigate the dynamic impact of wind penetration Doubly Fed Induction Generator (DFIG) on LFOs and a control strategy to improve LFOs damping in high wind integration scenarios.

The thesis work is organised in six chapters. In chapter-1 a brief introduction of the proposed research work is presented. Chapter 2 presents a comprehensive literature survey of significant works in the areas of Optimal PMU placement, LFOs monitoring, coherency determination, impact analysis of wind integration and control of LFOs as inferred from textbooks, technical reports and research publications. On the basis of literature survey, the research objectives formed are also presented. In this chapter, the main findings and contributions of the research work are encapsulated and some possible future research directions in this work are suggested.

Chapter 3 of this thesis discusses a PMU-ANN based method for online and real-time monitoring of LFOs in the system. In this chapter, first the optimal placement of PMUs is performed taking different criteria like critical tie-line oscillations monitoring, critical generators monitoring, and vulnerable bus monitoring into consideration. The optimal placement also ensures complete observability under N-1 contingencies (PMU or line loss) with minimum number of PMUs. Two ANN-based architectures namely, FFNN and RBFNN have been investigated for online and real-time oscillation monitoring and coherency identification purpose using synchronously sampled data from PMUs. Feature selection is an important step towards the success of trained ANN and thus PCA has been employed for dimensionality reduction. The oscillatory stability status is predicted with the help of two indices – Mode Index and Damping Index. Also, other mode related information like frequency, damping ratio and participation factor values are predicted at the same time. The analysis is carried on the IEEE 39-bus system to study the efficiency of the proposed method in changing system conditions. Simulation results and performance evaluation of the proposed methodology are presented. The effectiveness of developed method is thoroughly investigated and presented. Following conclusions are drawn from this chapter:

1. The proposed multi-criteria constrained optimal PMU placement approach for wide area low frequency oscillation monitoring effectively identifies the PMU locations for monitoring requirements. The advantage of the proposed scheme is that it is a generalized approach and any number of objectives can be included in problem formulation according to application requirement.
2. The proposed PMU-ANN method provides a comprehensive tool for predicting the Mode Index, frequency, damping ratio and key drivers of low frequency modes in real-time which works very well even under varying system topology. Thus, it relieves the burden of designing a separate tool for each possible system operating

topology. Moreover, it minimizes the need to keep abreast with every possible change in system topology which is a difficult task, specially, in the context of modern power systems.

3. With the proposed method the generator coherency information is predicted accurately in real-time utilizing only first four cycle data after the instant of disturbance for all unseen operating conditions independent of topological variation and most probable contingencies. The proposed scheme thus can be utilized while designing and implementing control actions requiring coherent generators information in real-time.
4. The proposed method is very fast and may serve as a promising tool for the both online and real-time applications for a wide range of operating conditions.

In Chapter 4 of this thesis, a dynamic impact analysis of DFIG-based wind generators integration on LFOs has been presented. There are mainly two ways to integrate DFIG in the system; either by adding it directly to non-generator buses or by fully or partially replacing some existing SGs. In this chapter, DFIGs are integrated by both the ways and their dynamic impact on LFOs damping is studied. In the first case when DFIGs are integrated replacing the SGs in the system, the damping ratio sensitivity to inertia is used to evaluate the impact of DFIG integration on the critical modes. This study identifies that the impact could be positive or negative based on the location of DFIG. The results obtained are verified by detailed eigenvalue analysis and time domain simulations for different operating conditions with three phase fault. The analysis is further extended to examine the individual impacts of SG removal and wind addition in the system. Further, increased penetration of DFIG and its impact on LFO are analysed. In the second case when DFIGs are integrated on non-generator buses, the impact of locations of DFIG integration on damping is carried out using eigenvalue analysis and dynamic sensitivity analysis. These methods provide information about the impact of DFIG integration on small signal stability of system. The analysis is performed on IEEE 39-bus test system. The effectiveness of developed methods are thoroughly investigated and presented. Following conclusions are drawn from this chapter:

1. The proposed Damping Ratio Sensitivity Index (*DRSI*) is an effective tool for impact analysis of DFIG integration on small signal stability while replacing SGs.

The detailed eigenvalue analysis verify the effectiveness of the proposed *DRSI* based method.

2. The integration of DFIG penetration may cause positive or negative impact on system's damping depending on its location. The decrease in inertia due to WTG reduces damping of critical interarea modes in the system, except when DFIG is integrated replacing the most participating generator in critical mode.
3. The eigenvalue analysis and dynamic trajectory sensitivity analysis proved to be sufficient and adequate techniques for studying DFIG integration without replacing SGs and provide effective results.
4. It is found that for the same DFIG penetration, the change in location of WTG alter the damping of LFO modes in the system and thus affect the system's small signal stability.
5. The small signal stability should not be the sole criteria to find optimal location of DFIGs. It is neither feasible nor technically correct to find optimal location of DFIG on the basis of modes damping or small signal stability. Above study is needed to take counter preventive measures to neutralize the detrimental effect of wind penetration if they are not optimally placed at certain locations. The investigations carried out in this chapter can be employed for planning studies of power system integrated with DFIGs.

In Chapter 5, LFOs damping improvement is presented by a robust coordinated control strategy of the Power System Stabilizer (PSS) and Power Oscillation Damper (POD) of DFIG. This control strategy is achieved using an improved eigenvalue based objective function, optimized using Grey Wolf Optimizer (GWO). The wide-area based PMU signals are used as PODs input selected using modal observability criterion. The eigenvalue analysis, time-domain simulations and robustness analysis are performed to verify the efficacy of the proposed control strategy on a modified IEEE New England system. A new Robustness Index (*RI*) is employed to measure the controller robustness to varying system conditions. The simulation results shows the improvement in LFO damping with the proposed control strategy for a wide range of operating scenarios including faults and line outages at different loading conditions. Following conclusions are drawn from this chapter:

1. The PSSs and PODs are coordinated simultaneously for multiple operating conditions, using an improved eigenvalue based multi-objective function to enhance system damping and stability.
2. Optimization algorithm called GWO has been investigated for coordinated tuning of controllers. It is found that GWO algorithm is very effective in the proposed coordinated tuning of controllers and provide robust results.
3. The eigenvalue analysis and time domain simulations proves the controllers coordination and verifies the ability of designed controllers to augment system damping under faults, line outages and different loading conditions.
4. The proposed coordinated control of PSSs and PODs has been tested under diverse operating conditions including critical operating conditions such as line outage, loss of load, loss of generation etc. It is found that the proposed coordinated control of PSSs and PODs improves the system damping even for most detrimental case in terms of interarea mode damping.
5. *RI* is employed to measure the controller robustness to varying system conditions. The robustness analysis results proves that the proposed coordinated control provide remarkable stabilizing effect and robustness as compared to tuned PSS working alone. It stabilizes the system in a very small time even for severe contingencies, when other controllers fail to damp the oscillations.

FUTURE RESEARCH SCOPE

The future smart grids require active inclusion of vast amount of information acquired from monitoring devices like PMUs in real-time operation of power system. This will drastically improve the power system functionality and greatly reduce the time taken in applying the control actions in the event of any disturbance. Power system low frequency oscillations is a major power system stability problem. Thus, operators requires efficient methodologies for real-time monitoring of these low frequency modes. At the same time robust control methodologies are required to damp these modes and maintain system stability. This thesis attempts to address the key issue of monitoring and control of low frequency oscillations in power system. The following are the possible future extensions of the present work:

1. In the proposed work, only wind generators are considered for renewable energy generation. However, other clean energy sources with much lower inertia like photovoltaic etc. can also be incorporated in this study.

2. The proposed analysis has been performed only for DFIG-based WTGs. However, it can be extended to evaluate impact of other type of WTGs and a comparative analysis can be performed.
3. In the proposed work, a coordinated control strategy of PSSs and DFIG PODs has been proposed. This can be extended to include FACTS based damping controllers in this coordinated approach to further improve system damping and stability.
4. The proposed method for low frequency oscillation monitoring employs ANN along with synchrophasor measurements for oscillation monitoring. However, other AI based or hybrid methods like combination of Fuzzy and ANN, measurement based methods and ANN etc. may be investigated for possible improvement in accuracy and speed.
5. In the proposed PMU-ANN based real-time oscillation monitoring scheme other input feature such as voltage variations and speed variations can be compared for accuracy and speed. Also, the effect of delays in measurements through PMUs can be incorporated.
6. The proposed method can be extended and applied for voltage stability assessment of power system. Thus, a comprehensive tool for online voltage stability and small signal stability of power systems may be developed.
7. The proposed work may also be extended by proposing other preventive control methods like generator rescheduling to improve the system oscillatory stability.
8. The results of coherency analysis obtained in this thesis can be employed for applying suitable emergency control strategies for stability of the power system.

APPENDIX

The single-line diagram, line and bus data and other relevant data of test system considered for simulation of different techniques throughout this thesis is given below. Also, the optimized controller parameters result are given in this appendix.

A. IEEE 39-BUS, 10-GENERATOR NEW ENGLAND TEST SYSTEM

The simulations in this study are carried out on the IEEE-39 bus, 10-generator New England system. This transmission test system and its data are referred from [117]. The system has 10 generators, 12 transformers, 46 transmission lines. Bus no. 39 is taken as slack bus. It is 345 kV dynamic test system. The bus voltage magnitude limits are $V^{min} = 0.94$ p.u. and $V^{max} = 1.06$ p.u

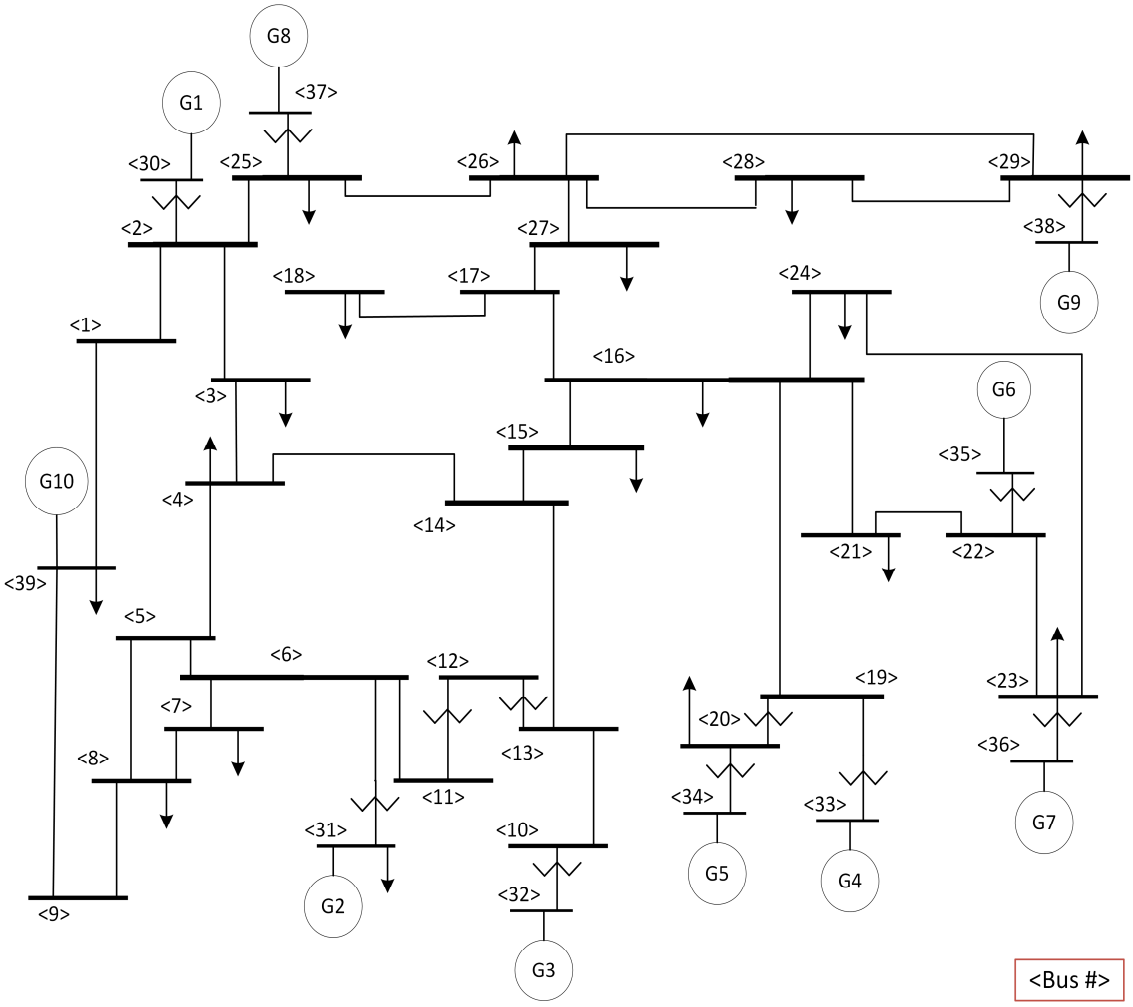

Fig. A.1. Single line diagram of IEEE 39-bus, 10-generator New England System

TABLE A.1
BUS DATA OF IEEE 39-BUS, 10-GENERATOR SYSTEM

Bus number	Active load, P_d (MW)	Reactive load, Q_d (MVAr)	V_m (p.u.)	V_θ (degrees)
1	97.60	44.20	1.0393836	-13.536602
2	0.00	0.00	1.0484941	-9.7852666
3	322.00	2.40	1.0307077	-12.276384
4	500.00	184.00	1.0044600	-12.626734
5	0.00	0.00	1.0060063	-11.192339
6	0.00	0.00	1.0082256	-10.408330
7	233.80	84.00	0.9983972	-12.755626
8	522.00	176.60	0.9978723	-13.335844
9	6.50	-66.60	1.0383320	-14.178442
10	0.00	0.00	1.0178431	-8.1708750
11	0.00	0.00	1.0133858	-8.9369663
12	8.53	88.00	1.0008150	-8.9988236
13	0.00	0.00	1.0149230	-8.9299272
14	0.00	0.00	1.0123190	-10.715295
15	340.00	153.00	1.0161854	-11.345399
16	329.00	32.30	1.0325203	-10.033348
17	0.00	0.00	1.0342365	-11.116436
18	168.00	30.00	1.0315726	-11.986168
19	0.00	0.00	1.0501068	-5.4100729
20	680.00	103.00	0.9910105	-6.8211783
21	284.00	115.00	1.0323192	-7.6287461
22	0.00	0.00	1.0501427	-3.1831199
23	247.50	84.60	1.0451451	-3.3812763
24	308.60	-92.20	1.0380010	-9.9137585
25	224.00	47.20	1.0576827	-8.3692354
26	139.00	17.00	1.0525613	-9.4387696
27	283.00	75.50	1.0383449	-11.362152
28	206.00	27.60	1.0503737	-5.9283592
29	285.50	26.90	1.0501149	-3.16987410
30	0.00	0.00	1.0499000	-7.3704746
31	9.20	4.60	0.9820000	0.0000000
32	0.00	0.00	0.9841000	-0.1884374
33	0.00	0.00	0.9972000	-0.19317445
34	0.00	0.00	1.0123000	-1.6311190
35	0.00	0.00	1.0494000	1.77650690
36	0.00	0.00	1.0636000	4.46843740
37	0.00	0.00	1.0275000	-1.5828988
38	0.00	0.00	1.0265000	3.8928177
39	1104.00	250.00	1.0300000	-14.535256

TABLE A.2
LINE DATA OF IEEE 39-BUS, 10-GENERATOR SYSTEM

Line number	From Bus	To Bus	Line Resistance (p.u)	Line Reactance (p.u)	Line Charging Susceptance (p.u)	MVA Rating
1	1	2	0.0035	0.0411	0.6987	600
2	1	39	0.0010	0.0250	0.7500	1000
3	2	3	0.0013	0.0151	0.2572	500
4	2	25	0.0070	0.0086	0.1460	500
5	2	30	0.0000	0.0181	0.0000	900
6	3	4	0.0013	0.0213	0.2214	500
7	3	18	0.0011	0.0133	0.2138	500
8	4	5	0.0008	0.0128	0.1342	600
9	4	14	0.0008	0.0129	0.1382	500
10	5	6	0.0002	0.0026	0.0434	1200
11	5	8	0.0008	0.0112	0.1476	900
12	6	7	0.0006	0.0092	0.1130	900
13	6	11	0.0007	0.0082	0.1389	480
14	6	31	0.0000	0.0250	0.0000	1800
15	7	8	0.0004	0.0046	0.0780	900
16	8	9	0.0023	0.0363	0.3804	900
17	9	39	0.0010	0.0250	1.2000	900
18	10	11	0.0004	0.0043	0.0729	600
19	10	13	0.0004	0.0043	0.0729	600
20	10	32	0.0000	0.0200	0.0000	900
21	12	11	0.0016	0.0435	0.0000	500
22	12	13	0.0016	0.0435	0.0000	500
23	13	14	0.0009	0.0101	0.1723	600
24	14	15	0.0018	0.0217	0.3660	600
25	15	16	0.0009	0.0094	0.1710	600
26	16	17	0.0007	0.0089	0.1342	600
27	16	19	0.0016	0.0195	0.3040	600
28	16	21	0.0008	0.0135	0.2548	600
29	16	24	0.0003	0.0059	0.0680	600
30	17	18	0.0007	0.0082	0.1319	600
31	17	27	0.0013	0.0173	0.3216	600
32	19	20	0.0007	0.0138	0.0000	900
33	19	33	0.0007	0.0142	0.0000	900
34	20	34	0.0009	0.0180	0.0000	900
35	21	22	0.0008	0.0140	0.2565	900
36	22	23	0.0006	0.0096	0.1846	600
37	22	35	0.0000	0.0143	0.0000	900
38	23	24	0.0022	0.0350	0.3610	600
39	23	36	0.0005	0.0272	0.0000	900

Continued …

TABLE A.2 (Continued …)
LINE DATA OF IEEE 39-BUS, 10-GENERATOR SYSTEM

Line number	From Bus	To Bus	Line resistance (p.u)	Line reactance (p.u)	Line Charging Susceptance (p.u)	MVA Rating
40	25	26	0.0032	0.0323	0.5310	600
41	25	37	0.0006	0.0232	0.0000	900
42	26	27	0.0014	0.0147	0.2396	600
43	26	28	0.0043	0.0474	0.7802	600
44	26	29	0.0057	0.0625	1.0290	600
45	28	29	0.0014	0.0151	0.2490	600
46	29	38	0.0008	0.0156	0.0000	1200

TABLE A.3
TECHNICAL LIMITS OF GENERATORS OF IEEE 39-BUS, 10-GENERATOR SYSTEM

Generator Number	Bus Number	P_G (MW)	Q_G (MVAr)	$P_{G,max}$ (MW)	$P_{G,min}$ (MW)	$Q_{G,max}$ (MVAr)	$Q_{G,min}$ (MVAr)
1	30	250	161.762	1040	0	400	140
2	31	677.87	221.574	646	0	300	-100
3	32	650	206.965	725	0	300	150
4	33	632	108.293	652	0	250	0
5	34	508	166.688	508	0	167	0
6	35	650	210.661	687	0	300	-100
7	36	560	100.165	580	0	240	0
8	37	540	-1.36945	564	0	250	0
9	38	830	21.7327	865	0	300	-150
10	39	1000	78.4674	1100	0	300	-100

TABLE A.4
DYNAMIC DATA OF GENERATORS OF IEEE 39-BUS, 10-GENERATOR SYSTEM

Generator Number	xd (pu)	x'd (pu)	T'do (sec)	xq (pu)	x'q (pu)	T'qo (sec)	H (sec)
1	1.00	0.310	10.2	0.69	0.31	1.50	4.2
2	2.95	0.697	6.56	2.82	0.697	1.50	3.03
3	2.49	0.531	5.70	2.37	0.531	1.50	3.58
4	2.62	0.436	5.69	2.58	0.436	1.50	2.86
5	6.70	1.320	5.40	6.2	1.32	0.440	2.6
6	2.54	0.500	7.30	2.41	0.50	0.400	3.48
7	2.95	0.490	5.66	2.92	0.49	1.50	2.64
8	2.90	0.570	6.70	2.8	0.57	0.410	2.43
9	2.10	0.570	4.79	2.05	0.57	1.96	3.45
10	0.20	0.060	7.00	0.19	0.060	0.700	50

TABLE A.5
AUTOMATIC VOLTAGE REGULATOR DATA OF IEEE 39-BUS, 10-GENERATOR SYSTEM

Generator Number	Exciter Type	K_A	T_A (sec.)	$V_{R,max}$ (p.u)	$V_{R,max}$ (p.u)	K_E	T_E (sec.)	T_F (sec.)
1	DC1	5	0.06	5	-5	-0.05	0.25	0.04
2	DC1	6.2	0.05	5	-5	0.63	0.41	0.06
3	DC1	5	0.06	5	-5	-0.02	0.50	0.08
4	DC1	5	0.06	5	-5	-0.05	0.50	0.08
5	DC1	40	0.02	10	-10	-0.04	0.785	0.03
6	DC1	5	0.02	5	-5	1	0.471	0.08
7	DC1	40	0.02	6.5	-6.5	1	0.73	0.03
8	DC1	5	0.02	5	-5	-0.05	0.528	0.09
9	DC1	40	0.02	10.5	-10.5	1	1.40	0.03
10	DC1	40	0.02	10.5	-10.5	1	1.60	0.04

TABLE A.6
POWER SYSTEM STABILIZER DATA OF IEEE 39-BUS, 10-GENERATOR SYSTEM

Generator Number	K	T_W	T_1	T_2	T_3	T_4	$V_{PSS,Max}$	$V_{PSS,Min}$
1	$1.0/120\pi$	10.0	5.0	0.60	3.0	0.50	0.2	-0.2
2	$0.5/120\pi$	10.0	5.0	0.40	1.0	0.10	0.2	-0.2
3	$0.5/120\pi$	10.0	3.0	0.20	2.0	0.20	0.2	-0.2
4	$2.0/120\pi$	10.0	1.0	0.10	1.0	0.30	0.2	-0.2
5	$1.0/120\pi$	10.0	1.5	0.20	1.0	0.10	0.2	-0.2
6	$4.0/120\pi$	10.0	0.5	0.10	0.5	0.05	0.2	-0.2
7	$7.5/120\pi$	10.0	0.2	0.02	0.5	0.10	0.2	-0.2
8	$2.0/120\pi$	10.0	1.0	0.20	1.0	0.10	0.2	-0.2
9	$2.0/120\pi$	10.0	1.0	0.50	2.0	0.10	0.2	-0.2

B. OPTIMIZED CONTROLLER PARAMETERS

TABLE B.1
OPTIMIZED PARAMETERS OF PSSS IN CASE 2

Controller	Case 2 (only PSS)		
	K	$T_{1,3}$	$T_{2,4}$
PSS1	20.6781	0.3715	0.0312
PSS2	20.5859	0.2437	0.0726
PSS3	11.4165	0.1968	0.0255
PSS4	43.2359	0.1573	0.1000
PSS5	46.5083	0.4456	0.1000
PSS6	09.1023	0.2543	0.0122
PSS7	31.3131	0.1000	0.0198
PSS8	01.8443	1.0000	0.0558
PSS9	50.0000	0.1096	0.0140

TABLE B.2
OPTIMIZED PARAMETERS OF PSSS & PODS IN CASE 3

Controller	Case 3 (PSS+POD)		
	K	$T_{1,3}$	$T_{2,4}$
PSS1	15.4179	1.0000	0.1000
PSS2	17.4032	0.6729	0.0841
PSS3	43.9731	0.1690	0.0455
PSS4	32.1774	0.1033	0.0393
PSS5	24.4541	0.3592	0.0919
PSS6	11.4271	0.4625	0.1000
PSS7	24.0759	0.1079	0.0272
PSS8	24.4410	0.3662	0.0428
PSS9	50.0000	0.2557	0.0400
POD1	10.2422	0.2029	0.0225
POD2	50.0000	0.6602	0.1000
POD3	06.9536	1.0000	0.0537

C. DFIG DATA

Nominal wind speed: 20 m/s; Blade length: 75 m; blade number: 3; air density: 1.225 kg/m3 ; inertia time constant = 3 s; gearbox ratio = 1/89; stator resistance = 0.01 p.u.; rotor resistance = 0.01 p.u.; stator reactance = 0.1 p.u.; rotor reactance = 0.08 p.u.; magnetizing reactance = 3 p.u.; number of poles = 4; voltage control gain = 10; power control time constant = 0.01; pitch control gain = 10; pitch control time constant = 3.

PUBLICATIONS

International Journals

[1] Abhilash Kumar Gupta, Kusum Verma and K. R. Niazi, "Dynamic impact analysis of DFIG-based wind turbine generators on low-frequency oscillations in power system", *IET Generation, Transmission & Distribution*, 2017, vol. 11, no. 18, pp. 4500-4510.

[2] Abhilash Kumar Gupta, Kusum Verma and K. R. Niazi, "Impact Analysis of DFIG Location on Low Frequency Oscillations in Power System", *The Journal of Engineering*, 2017, vol. 2017, no. 13, pp. 1413-1417.

[3] Abhilash Kumar Gupta, Kusum Verma and K. R. Niazi, "Robust Coordinated control for damping low frequency oscillations in high wind penetration power system", *International Transactions on Electrical Energy Systems*, 2019, vol. 29, no. 5, e12006. (https://doi.org/10.1002/2050-7038.12006)

[4] Abhilash Kumar Gupta, Kusum Verma and K. R. Niazi, "Wide area coordinated control for low frequency oscillations damping in a wind integrated power system", *The Journal of Engineering*, 2018. (doi: 10.1049/joe.2018.9315) (in press)

International Conferences

[1] Abhilash Kumar Gupta and Kusum Verma, "PMU-ANN based Real Time Monitoring of Power System Electromechanical Oscillations", in 1st IEEE International Conference on Power Electronics, Intelligent Control and Energy systems (ICPEICES 2016) , DTU Delhi, 4-6 July 2016.

[2] Abhilash Kumar Gupta, Kusum Verma and K. R. Niazi, "Real Time Intelligent Oscillatory Stability Monitoring and Coherent Groups Identification", in IEEE 7th Power India International Conference (PIICON 2016), Bikaner, 25-27 Nov. 2016.

[3] Abhilash Kumar Gupta, Kusum Verma and K. R. Niazi, "Intelligent Wide Area Monitoring of Power System Oscillatory Dynamics in Real Time", in IEEE 4th International Conference on Advanced Computing and Communication Systems (ICACCS 2017), Coimbatore, 6-7 Jan. 2017.

[4] Abhilash Kumar Gupta, Kusum Verma and K. R. Niazi, "Impact Analysis of DFIG Location on Low Frequency Oscillations in Power System", in 6th

International Conference on Renewable Power Generation (IET RPG 2017), China, 19-20 Oct. 2017.

[5] Abhilash Kumar Gupta, Kusum Verma and K. R. Niazi, "Contingency Constrained Optimal Placement of PMUs for Wide Area Low Frequency Oscillation Monitoring", in IEEE 7th International Conference on Power System (ICPS 2017), Pune, 21-23 Dec. 2017.

[6] Abhilash Kumar Gupta, Kusum Verma and K. R. Niazi, "Power system low frequency oscillations monitoring and generator coherency determination in real time", in IEEE PES ISGT 2018, Singapore, 22-25 May 2018.

[7] Abhilash Kumar Gupta, Kusum Verma and K. R. Niazi, "Wide area coordinated control for low frequency oscillations damping in a wind integrated power system", in 7th International Conference on Renewable Power Generation (IET RPG 2018), Denmark, 26-27 Sept. 2018.

[8] Abhilash Kumar Gupta, Kusum Verma and K. R. Niazi, "Wide-area PMU-ANN based monitoring of low frequency oscillations in a wind integrated power system", in IEEE 8th India International Conference on Power Electronics (IICPE 2018), Jaipur, 13-15 Dec. 2018.

[9] Abhilash Kumar Gupta, Kusum Verma and K. R. Niazi, "Real-time low frequency oscillations monitoring and coherency determination in a wind integrated power system", in Springer International Conference on Intelligent Computing Techniques for Smart Energy Systems (ICTSES 2018), Jaipur, 22-23 Dec. 2018.

REFERENCES

[1] R. Sodhi, and M. I. Sharieff, "Phasor measurement unit placement framework for enhanced wide-area situational awareness", *IET Gener. Transm. Distrib.*, vol. 9, no. 2, Jan. 2015, pp. 172-182.

[2] F. Aminifar, M. Fotuhi-Firuzabad, A. Safdarian, A. Davoudi, and M. Shahidehpour, "Synchrophasor measurement technology in power systems: panorama and state-of-the-art", *Access IEEE*, vol. 2, Jan. 2015, pp. 1607-1628.

[3] A. G. Phadke, "Synchronized phasor measurements in power systems", *IEEE Computer Applications in Power*, vol. 6, no. 2, April 1993, pp. 10-15.

[4] A. G. Phadke and J. S. Thorp, *Synchronized phasor measurements and their applications*, Springer, New York, 2008.

[5] R. Sodhi, S.C. Srivastava, and S.N. Singh, "Multi-criteria decision making approach for multistage optimal placement of phasor measurement units", *IET Gen. Trans. Distrib.*, vol. 5, 2011, pp. 181-190.

[6] M. Nazari-Heris, and B. Mohammadi-Ivatloo, "Application of heuristic algorithms to optimal PMU placement in electric power systems: an updated review," *Renew Sustain Energy Rev*., vol. 50, Oct. 2015, pp. 214–228.

[7] N. M. Manousakis , G.N. Korres & P. S. Georgilakis, "Taxonomy of PMU placement methodologies", *IEEE Trans. Power Syst.*, vol. 27, no. 2, 2012, pp. 1070 -1077.

[8] T. L. Baldwin, L. Mili, M. B. Boisen, and R. Adapa, "Power System Observability With Minimal Phasor Measurement Placement", *IEEE Trans Power Syst.*, vol. 8, no. 2, May 1993, pp. 707-715.

[9] S. Chakrabarti and E. Kyriakides, "Optimal placement of phasor measurement units for power system observability", *IEEE Trans. Power Syst.*, vol. 23, Aug. 2008, no. 3, pp. 1433–1440.

[10] B. Gou, "Generalized integer linear programming formulation for optimal PMU placement", *IEEE Trans. Power Syst.*, vol. 23, no. 3, Aug. 2008, pp. 1099–1104.

[11] D. Dua, S. Dambhare, R. K. Gajbhiye, and S. A. Soman, "Optimal multistage scheduling of PMU placement: An ILP approach", *IEEE Trans. Power Del.*, vol. 23, no. 4, Oct. 2008, pp. 1812–1820.

[12] S. Chakrabarti, E. Kyriakides, and D. G. Eliades, "Placement of Synchronized Measurements for Power System Observability", *IEEE Trans Power Del.*, vol. 24, no. 1, Jan. 2009, pp. 12-19.

[13] B. K. S. Roy , A. K. Sinha, and A. K. Pradhan, "An optimal PMU placement technique for power system observability", *Int. J. Elect.Power Energy Syst.*, vol. 42, no. 1, 2012, pp. 71 -77.

[14] B. Milosevic and M. Begovic, "Nondominated sorting genetic algorithm for optimal phasor measurement placement" , *IEEE Trans. Power Syst.*, vol. 18, no. 1, Feb. 2003, pp. 69–75.

[15] J. Peng, Y. Sun, and H. F.Wang, "Optimal PMU placement for full network observability using Tabu search algorithm", *Int. J. Elect. Power Energy Syst.*, vol. 28, no. 4, May 2006, pp. 223–231.

[16] R. F. Nuqui and A. G. Phadke, "Phasor measurement unit placement techniques for complete and incomplete observability", *IEEE Trans. Power Del.*, vol. 20, no. 4, Oct. 2005, pp. 2381–2388.

[17] C. Peng, H. Sun, and J. Guoa, "Multi-objective optimal PMU placement using a non-dominated sorting differential evolution algorithm", *Int. J. Elect. Power Energy Syst.*, vol. 32, no. 8, Oct. 2010, pp. 886–892.

[18] M. Hajian, A. M. Ranjbar, T. Amraee, and B. Mozafari, "Optimal placement of PMUs to maintain network observability using a modified BPSO algorithm", *Int. J. Elect. Power Energy Syst.*, vol. 33, no. 1, Jan. 2011, pp. 28–34.

[19] A. Ahmadi, Y. Alinejad-Beromi, and M. Moradi, "Optimal PMU placement for power system observability using binary particle swarm optimization and considering measurement redundancy", *Expert Syst. Appl.*, vol. 38, no. 6, Jun. 2011, pp. 7263–7269.

[20] F. Aminifar, C. Lucas, A. Khodaei, and M. Fotuhi-Firuzabad, "Optimal placement of phasor measurement units using immunity genetic algorithm", *IEEE Trans. Power Del.*, vol. 24, no. 3, Jul. 2009, pp. 1014–1020.

[21] M. Hurtgen and J.C. Maun, "Optimal PMU placement using iterated local search", *Int. J. Elect. Power Energy Syst.*, vol. 32, no. 8, Oct. 2010, pp. 857–860.

[22] T. T. Kim, and H. V. Poor, "Strategic protection against data injection attacks on power grids", *IEEE Trans. Smart Grid*, vol. 2, no. 2, Jun. 2011, pp. 326–333.

[23] R. F. Nuqui, A. G. Phadke, R. P. Schulz, and N. Bhatt, "Fast on-line voltage security monitoring using synchronized phasor measurements and decision trees", in *Proc. IEEE Power Eng. Soc. Winter Meeting*, vol. 3, 2001, pp. 1347–1352.

[24] F. Aminifar, A. Khodaei, M. Fotuhi-Firuzabad, and M. Shahidehpour, "Contingency-constrained PMU placement in power networks", *IEEE Trans. Power Syst.*, vol. 25, no. 1, Feb. 2010, pp. 516–523.

[25] D. Thukaram et al., "Real-time monitoring of critical nodes with minimal number of phasor measurement units", in *Proc. IEEE Int. Conf. Power Systems (ICPS'09)* , 2009, pp. 1–6.

[26] A. Pal, G. A. Sanchez-Ayala, V. A. Centeno, & J. S. Thorp, "A PMU placement scheme ensuring real time monitoring of critical buses of the network", *IEEE Trans. Power Del.*, vol. 29, no. 2, 2014, pp. 510–517.

[27] V. S. S. Kumar and D. Thukaram, "Approach for Multistage Placement of Phasor Measurement Units Based on Stability Criteria", *IEEE Transactions on Power Systems*, vol. 31, no. 4, 2016, pp. 2714-2725.

[28] M. Crow, M. Gibbard, et al., "Identification of Electromechanical Modes in Power Systems", *IEEE Power & Energy Society*, Special publication TP462, June 2012.

[29] H. Huang, Z. Xu, and W. Hua, "Estimation of interarea modes in large power systems", *Int. J. Electr. Power Energy Syst.*, vol. 53, Dec. 2013, pp. 196-208.

[30] P. Kundur, *Power System Stability and Control*, McGraw-Hill, New York, 1994.

[31] G. Rogers, *Power System Oscillations*, Kluwer Academic Publishers, Massachusetts, 2000.

[32] J. Ma, Z. Y. Dong, P. Zhang, "Comparison of BR and QR eigenvalue algorithms for power system small signal stability analysis", *IEEE Trans. Power Syst.*, vol. 21, no. 4, Nov. 2006, pp. 1848–1855.

[33] P. Kundur, G. J. Rogers, D. Y. Wong, L. Wang, and M. G. Lauby, "A comprehensive computer program package for small signal stability analysis of power systems", *IEEE Trans. Power Syst.*, vol. 5, no. 4, Nov. 1990, pp. 1076–1083.

[34] Z. Du, C. Li, and Y. Cui, "Computing interarea eigenvalues of power systems using inexact two-sided Jacobi–Davidson", *IEEE Trans. Power Syst.*, vol. 26, no. 4, Nov. 2011, pp. 2015–2022.

[35] R. Jalayer, and B.T. Ooi, "Estimation of electromechanical modes of power systems by transfer function and eigenfunction analysis", *IEEE Trans. Power Syst.*, vol. 28, no. 1, Feb. 2013, pp. 181–189.

[36] S. Ghosh, and N. Senroy, "The localness of electromechanical oscillations in power systems", *Int. J. Electr. Power Energy Syst.*, vol. 42, no. 1, Nov. 2012, pp. 306-313.

[37] F. R. S. Sevilla, and L. Vanfretti, "A small-signal stability index for power system dynamic impact assessment using time-domain simulations", in *Proc. IEEE/PES Power Systems Conf. Expo. (PSCE'14)*, 2014, pp. 1-5.

[38] U. Kerin, E. Lerch, and G. Bizjak, "Monitoring and reporting of security of power system low-frequency oscillations", *Electr Power Comp. Syst.*, vol. 38, no. 9, Jun. 2010, pp. 1047-1060.

[39] J.J. Sanchez-Gasca and J.H. Chow, "Performance Comparison of Three Identification Methods for the Analysis of Electromechanical Oscillations", *IEEE Trans. Power Syst.*, vol. 14, no. 3, August 1999, pp. 995–1002.

[40] J. W. Pierre, D. J. Trudnowski, and M. K. Donnelly, "Initial results in electromechanical mode identification from ambient data", *IEEE Trans. Power Syst.*, vol. 12, no. 3, Aug. 1997, pp. 1245–1251.

[41] D. S. Laila, A. R. Messina and B. C. Pal, "A Refined Hilbert–Huang Transform With Applications to Interarea Oscillation Monitoring", *IEEE Trans. Power Syst.*, vol. 24, no. 2, May 2009, pp.610-620.

[42] L.H. Hassan, M. Moghavvemi, H.A. Almurib, and O. Steinmayer, "Current state of neural networks applications in power system monitoring and control", *Int. J. Electr. Power Energy Syst.*, vol. 51, Oct. 2013, pp. 134-144.

[43] Y. Hsu , C. Chen and C. Su, "Analysis of electromechanical modes using an artificial neural network", *IET Gen., Transm., Distrib.*, vol. 10, no. 3, 1995, pp.1986 -1993.

[44] S.P. Teeuwsen, I. Erlich, and M.A. El-Sharkawi, "Small-Signal Stability Assessment based on Advanced Neural Network Methods", in *Proc. IEEE/PES General Meeting*, Toronto, Canada, July 2003.

[45] M.H. Velayati, N. Amjady, and S. A. Hosseini, "Prediction of Generators' Participation Factors and Oscillation Types for Dominant Oscillatory Modes of Power System", *Electr Power Components and Sys.*, vol. 43, no. 15, Sept. 2015, pp. 1727-1740.

[46] F. Sulla, E. Masback, and O. Samuelsson, "Linking damping of electromechanical oscillations to system operating conditions using neural networks", in *Proc. IEEE/PES Innovative Smart Grid Tech. Conf., Europe (ISGT-Europe)*, Oct. 12, 2014, pp. 1-6.

[47] P. McNabb, D. Wilson, and J. Bialek, "Classification of mode damping and amplitude in power systems using synchrophasor measurements and classification trees", *IEEE Trans. Power Syst.*, vol. 28, no. 2, May 2013, pp. 1988-1996.

[48] S.P. Teeuwsen, I. Erlich, M.A. El-Sharkawi, and U. Bachmann, "Genetic algorithm and decision tree-based oscillatory stability assessment", *IEEE Trans. Power Syst.*, vol. 21, no. 2, May 2006, pp. 746-753.

[49] O. Antoine, and J.C. Maun, "Inter-area oscillations: Identifying causes of poor damping using phasor measurement units", in *Proc. IEEE/PES General Meeting*, Jul. 2012, pp. 1-6.

[50] N. Zhou, J.W. Pierre, and D. Trudnowski, "A stepwise regression method for estimating dominant electromechanical modes", *IEEE Trans. Power Syst.*, vol. 27, no. 2, May 2012, pp. 1051-1059.

[51] D. Cai, P. Regulski, M. Osborne and V. Terzija, "Wide area inter-area oscillation monitoring using fast nonlinear estimation algorithm", *IEEE Trans. Smart Grid*, vol. 4, no. 3, Sep. 2013, pp. 1721-1731.

[52] C. Zheng, V. Malbasa, and M. Kezunovic, "Regression tree for stability margin prediction using synchrophasor measurements", *IEEE Trans. Power Syst.*, vol. 28, no. 2, May 2013, pp. 1978-1987.

[53] Y. Chompoobutrgool, and L. Vanfretti, "Identification of power system dominant inter-area oscillation paths", *IEEE Trans. Power Syst.*, vol. 28, no. 3, Aug. 2013, pp. 2798-2807.

[54] T. Van Rooyen, and J. Rens, "Real-time power system oscillation monitoring using synchrophasor measurements", in *Proc. IEEE PowerTech*, Eindhoven, Jun. 2015, pp. 1-6.

[55] N.R. Chaudhuri, and B. Chaudhuri, "Damping and relative mode-shape estimation in near real-time through phasor approach", *IEEE Trans. Power Syst.*, vol. 26, no. 1, Feb. 2011, pp. 364-373.

[56] N. Kakimoto, M. Sugumi, T. Makino, and K. Tomiyama, "Monitoring of interarea oscillation mode by synchronized phasor measurement", *IEEE Trans. Power Syst.*, vol. 21, no. 1, Feb. 2006, pp. 260-268.

[57] L. Dosiek, and J. W, Pierre, "Estimating electromechanical modes and mode shapes using the multichannel ARMAX model", *IEEE Trans. Power Syst.*, vol. 28, no. 2, May 2013, pp. 1950-1959.

[58] D. J. Trudnowski, "Estimating electromechanical mode shape from synchrophasor measurements", *IEEE Trans. Power Syst.*, vol. 3, no. 23, 2008, pp. 1188-1195.

[59] J. Ma, P. Zhang, H. J. Fu, B. Bo, and D. Y. Dong, "Application of phasor measurement unit on locating disturbance source for low-frequency oscillation", *IEEE Trans. Smart Grid*, vol. 1, no. 3, Dec. 2010, pp. 340-346.

[60] L. Chen, Y. Min, and W. Hu, "An energy-based method for location of power system oscillation source", *IEEE Trans. Power Syst.*, vol. 28, no. 2, May 2013, pp. 828-836.

[61] N. Al-Ashwal, D.H. Wilson, and M. Parashar, "Identifying Sources of Oscillations Using Wide Area Measurements", in *Proc. CIGRE Grid of the Future Symposium, US National Committee*, Paris, 2014.

[62] V. Rampurkar, F. Kazi, H. A. Mangalvedekar, and P. Pentayya, "Synchrophasor Based Oscillatory Mode Source Identification: A Case Study Indian Grid", in *Proc. 6th Int. Conf. Intelligent Syst., Modelling and Simulation (ISMS)*, Feb. 9, 2015, pp. 169-174.

[63] A. Vahidnia, G. Ledwich, E. Palmer and A. Ghosh, "Generator coherency and area detection in large power systems", *IET Gener. Transm. Distrib.*, vol. 6, no. 9, Sep. 2012, pp. 874–883.

[64] O. Gomez and M.A. Rios, "Real time identification of coherent groups for controlled islanding based on graph theory", *IET Generation, Transmission & Distribution*, vol. 9, no. 8, 2015, pp. 748-758.

[65] S. A. Siddiqui, K. Verma, K. R. Niazi, and M. Fozdar, "Real-Time Monitoring of Post-Fault Scenario for Determining Generator Coherency and Transient Stability through ANN", *IEEE Transactions on Industry Applications*, vol. 54, no. 1, 2018, pp. 685-692.

[66] H. You, V. Vittal, and X. Wang, "Slow coherency-based islanding", *IEEE Trans. on Power Systems*, vol. 19, no. 1, 2004, pp. 483-491.

[67] K. K. Anaparthi, B. Chaudhuri, N. F. Thornhill, and B. C. Pal, "Coherency identification in power systems through principal component analysis", *IEEE Trans. Power Syst.*, vol. 20, no. 3, Aug. 2005, pp. 1658-1660.

[68] M.A.M. Ariff, and B. C. Pal, "Coherency identification in interconnected power system—An independent component analysis approach", *IEEE Trans. Power Syst.*, vol. 28, no. 2, May 2013, pp. 1747-1755.

[69] X. Wang, V. Vittal, and G. Heydt, "Tracing generator coherency indices using the continuation method: A novel approach", *IEEE Trans. Power Syst.*, vol. 20, no. 3, Aug. 2005, pp. 1510–1518.

[70] K. Verma, and K. R. Niazi, "A coherency based generator rescheduling for preventive control of transient stability in power systems", *International Journal of Electrical Power & Energy Systems*, vol. 45, no. 1, 2013, pp. 10-18.

[71] R. Agrawal, and D. Thukaram, "Support vector clustering-based direct coherency identification of generators in a multi-machine power system", *IET Generation, Transmission & Distribution*, vol. 7, no. 12, 2013, pp. 1357-1366.

[72] Z. Lin, F. Wen, Y. Ding, and Y. Xue, "Wide-Area Coherency Identification of Generators in Interconnected Power Systems with Renewables", *IET Generation, Transmission & Distribution*, vol. 11, no. 18, 2017, pp.4444-4455.

[73] J. Wei, D. Kundur, and K. L. Butler-Purry, "A novel bio-inspired technique for rapid real-time generator coherency identification", *IEEE Transactions on Smart Grid*, vol. 6, no. 1, 2015, pp. 178-188.

[74] F. B. Alhasawi, J. V. Milanovic, "Ranking the importance of synchronous generators for renewable energy integration", *IEEE Transactions on Power Systems*, vol. 27, no. 1, 2012, pp. 416-423.

[75] W. Du, J. Bi, T. Wang, and H. Wang, "Impact of grid connection of large-scale wind farms on power system small-signal angular stability", *CSEE Journal of Power and Energy Systems*, vol. 1, no. 2, 2015, pp. 83-89.

[76] J. Quintero, V. Vittal, G. T. Heydt, and H. Zhang, "The impact of increased penetration of converter control-based generators on power system modes of oscillation", *IEEE Transactions on Power Systems*, vol. 29, no. 5, 2014, pp. 2248-2256.

[77] M. Jafarian, and A. M. Ranjbar, "Interaction of the dynamics of doubly fed wind generators with power system electromechanical oscillations", *IET Renewable Power Generation*, vol. 7, no. 2, 2013, pp. 89-97.

[78] H. T. Jadhav, and R. Roy, "A comprehensive review on the grid integration of doubly fed induction generator", *International Journal of Electrical Power & Energy Systems*, vol. 49, 2013, pp. 8-18.

[79] D. Gautam, V. Vittal, and T. Harbour, "Impact of increased penetration of DFIG-based wind turbine generators on transient and small signal stability of power systems", *IEEE Trans. on Power Systems*, vol. 24, no. 3, 2009, pp. 1426-1434.

[80] J. G. Slootweg, W. L. Kling, "The impact of large scale wind power generation on power system oscillations", *Electric Power Systems Research*, vol. 67, no. 1, 2003, pp. 9-20.

[81] D. Thakur, N. Mithulananthan, "Influence of constant speed wind turbine generator on power system oscillation", *Electric Power Components and Systems*, vol. 37, no. 5, 2009, pp. 478-494.

[82] B. Mehta, P. Bhatt, V. Pandya, "Small signal stability analysis of power systems with DFIG based wind power penetration", *International Journal of Electrical Power & Energy Systems*, vol. 58, 2014, pp. 64-74.

[83] M. Garmroodi, D. J. Hill, G. Verbič, and J. Ma, "Impact of Tie-Line Power on Inter-Area Modes with Increased Penetration of Wind Power", *IEEE Transactions on Power Systems*, vol. 31, no. 4, 2016, pp. 3051-3059.

[84] M. Jafarian, A. M. Ranjbar, “The impact of wind farms with doubly fed induction generators on power system electromechanical oscillations”, *Renewable Energy*, vol. 50, 2013, pp. 780-785.

[85] T. Knuppel, J. N. Nielsen, K. H. Jensen, et al., “Small-signal stability of wind power system with full-load converter interfaced wind turbines”, *IET Renewable Power Generation*, vol. 6, no. 2, 2012, pp. 79-91.

[86] G. Tsourakis, B. M. Nomikos, and C. D. Vournas, “Effect of wind parks with doubly fed asynchronous generators on small-signal stability”, *Electric Power Systems Research*, vol. 79, no. 1, 2009, pp. 190-200.

[87] E. Vittal, M. O'Malley, and A. Keane, “Rotor angle stability with high penetrations of wind generation”, *IEEE Transactions on Power Systems*, vol. 27, no. 1, 2012, pp. 353-362.

[88] E. Vittal, and A. Keane, “Identification of critical wind farm locations for improved stability and system planning”, *IEEE Transactions on Power Systems*, vol. 28, no. 3, 2013, pp. 2950-2958.

[89] A. J. Allen, M. Singh, E. Muljadi, and S. Santoso, “Measurement-based investigation of inter- and intra-area effects of wind power plant integration”, *International Journal of Electrical Power & Energy Systems*, vol. 83, 2016, pp. 450-457.

[90] W. Du, J. Bi, and H. F. Wang, “Small-signal angular stability of power system as affected by grid-connected variable speed wind generators-A survey of recent representative works”, *CSEE Journal of Power and Energy Systems*, vol. 3, no. 3, 2017, pp. 223-231.

[91] M. Singh, A. J. Allen, E. Muljadi, V. Gevorgian, Y. Zhang, and S. Santoso, “Interarea oscillation damping controls for wind power plants”, *IEEE Transactions on Sustainable Energy*, vol. 6, no. 3, 2015, pp. 967-975.

[92] Y. Mishra, S. Mishra, M. Tripathy, et al., “Improving stability of a DFIG-based wind power system with tuned damping controller”, *IEEE Transactions on Energy Conversion*, vol. 24, no. 3, 2009, pp. 650-660.

[93] M. Edrah, K. L. Lo, and O. Anaya-Lara, “Reactive power control of DFIG wind turbines for power oscillation damping under a wide range of operating conditions”, *IET Generation, Transmission & Distribution*, vol. 10, no. 15, 2016, pp. 3777-3785.

[94] H. Golpira, H. Bevrani, and A. H. Naghshbandy, “An approach for coordinated automatic voltage regulator–power system stabiliser design in large-scale interconnected power systems considering wind power penetration”, *IET Generation, Transmission & Distribution*, vol. 6, no. 1, 2012, pp. 39-49.

[95] K. Elkington, and M. Ghandhari, “Non-linear power oscillation damping controllers for doubly fed induction generators in wind farms”, *IET Renewable Power Generation*, vol. 7, no. 2, 2013, pp. 172-179.

[96] D. Ke, and C. Y. Chung, “Design of Probabilistically-Robust Wide-Area Power System Stabilizers to Suppress Inter-Area Oscillations of Wind Integrated Power Systems”, *IEEE Transactions on Power Systems*, vol. 31, no. 6, 2016, pp. 4297-4309.

[97] T. Surinkaew, and I. Ngamroo, “Robust power oscillation damper design for DFIG-based wind turbine based on specified structure mixed H2/H∞ control”, *Renewable Energy*, vol. 66, 2014, pp. 15-24.

[98] H. Huang, and C. Y. Chung, “Coordinated damping control design for DFIG-based wind generation considering power output variation”, *IEEE Trans. on Power Systems*, vol. 27, no. 4, 2012, pp. 1916-1925.

[99] A. E. Leon, J. M. Mauricio, A. Gómez-Expósito, et al., “Hierarchical wide-area control of power systems including wind farms and FACTS for short-term frequency regulation”, *IEEE Transactions on Power Systems*, vol. 27, no. 4, 2012, pp. 2084-2092.

[100] A. E. Leon, and J. A. Solsona, “Power oscillation damping improvement by adding multiple wind farms to wide-area coordinating controls”, *IEEE Trans. on Power Systems*, vol. 29, no. 3, 2014, pp. 1356-1364.

[101] T. Surinkaew, and I. Ngamroo, “Hierarchical Co-ordinated wide area and local controls of DFIG wind turbine and PSS for robust power oscillation damping”, *IEEE Transactions on Sustainable Energy*, vol. 7, no. 3, 2016, pp. 943-955.

[102] T. Surinkaew, and I. Ngamroo, “Two-level coordinated controllers for robust inter-area oscillation damping considering impact of local latency”, *IET Generation, Transmission & Distribution*, vol. 11, no. 18, 2017, pp. 4520-4530.

[103] J. Zuo, Y. Li, D. Shi, et al., "Simultaneous robust coordinated damping control of power system stabilizers (PSSs), static var compensator (SVC) and doubly-fed induction generator power oscillation dampers (DFIG PODs) in multimachine power systems", *Energies*, vol. 10, no. 4, 2017, pp. 565.

[104] C. Zhang, D. Ke, Y. Sun, et al., "Coordinated Supplementary Damping Control of DFIG and PSS to Suppress Inter-Area Oscillations with Optimally Controlled Plant Dynamics", *IEEE Transactions on Sustainable Energy*, vol. 9, no. 2, 2018, pp.780-791.

[105] A. H. M. A. Rahim, I. O. Habiballah, "DFIG rotor voltage control for system dynamic performance enhancement", *Elect. Power Syst. Res.*, vol. 81, no. 2, 2011, pp. 503–509.

[106] J. L. Domínguez-García, O. Gomis-Bellmunt, F. D. Bianchi, and A. Sumper, "Power oscillation damping supported by wind power: A review", *Renewable and Sustainable Energy Reviews*, vol. 16, no. 7, 2012, pp. 4994-5006.

[107] X. Zhang, C. Lu, S. Liu, and X. Wang, "A review on wide-area damping control to restrain inter-area low frequency oscillation for large-scale power systems with increasing renewable generation", *Renewable and Sustainable Energy Reviews*, vol. 57, 2016, pp. 45-58.

[108] A. Heniche, and I. Karnwa, "Control loops selection to damp inter-area oscillations of electrical networks", *IEEE Trans. Power Syst.*, vol. 17, no. 2, May 2002, pp. 378-384.

[109] M. M. Farsangi, Y. H. Song and K. Y. Lee, "Choice of FACTS device control inputs for damping interarea oscillations", *IEEE Trans. Power Syst.*, vol. 19, no. 2, May 2004, pp. 1135-1143.

[110] S. Ray, B. Chaudhuri and R. Majumder, "Appropriate signal selection for damping multi-modal oscillations using low order controllers", in *Proc. IEEE/PES General Meeting- Conversion and Delivery of Electrical Energy 21st Century*, Jul. 20-24, 2008, pp.1-7.

[111] Y. Zhang and A. Bose, "Design of Wide-Area Damping Controllers for Interarea Oscillations", *IEEE Trans. Power Syst.*, vol. 23, no. 3, Aug. 2008, pp. 1136-1143.

[112] A. Heniche and I. Kamwa, "Assessment of two methods to select wide-area signals for power system damping control", *IEEE Trans. Power Syst.*, vol. 23, May 2008, pp. 572-581.

[113] L. P. Kunjumuhammed, R. Singh and B. C. Pal, "Robust signal selection for damping of inter-area oscillations", *IET Gener. Transm. Distrib.*, vol. 6, no. 5, May 2012, pp. 404-416.

[114] Y. Li, C. Rehtanz, S. Rüberg, L. Luo and Y. Cao, "Assessment and choice of input signals for multiple HVDC and FACTS wide-area damping controllers", *IEEE Trans. Power Syst.*, vol. 27, Nov. 2012, pp. 1969-1977.

[115] L. P.Kunjumuhammed, and B. C. Pal, "Selection of feedback signals for controlling dynamics in future power transmission networks", *IEEE Transactions on Smart Grid*, vol. 6, no. 3, 2015, pp. 1493-1501.

[116] M. A. Pai, *Energy Function Analysis for Power System Stability*, Norwell, MA: Kluwer, 1989.

[117] C. Canizares, T. Fernandes, *et al.*, "Benchmark Systems for Small-Signal Stability Analysis and Control", Technical Report, *IEEE PES*, Aug. 2015, pp. 66-72.

[118] The Math Works, Inc., MATLAB programming, 2015.

[119] F. Milano, "An open source power system analysis toolbox", *IEEE Transactions on Power Systems*, vol. 20, no. 3, 2005, pp. 1199-1206.

[120] J. Paserba, P. Kundur, J. Sanchez-Gasca and E. Larsen, *Small signal stability and power system oscillations, Electric Power Engineering Handbook*, IEEE Press, 2001, pp. 20 -34.

[121] M. J. Basler, and R. C. Schaefer, "Understanding Power-System Stability", *IEEE Transactions on Industry Applications*, vol. 2, no. 44, 2008, pp. 463-474.

[122] F. Milano, "Documentation for PSAT version 2.1.8", January 6, 2013.

[123] F. Milano, *Power system modelling and scripting*, Springer Science & Business Media, 2010.

[124] M. Henderson, W. Henson, J. Norden, et al., "ISO New England Wind Integration Study", in *Proc. IEEE Power and Energy Society General Meeting*, 2011, pp. 1-6.

[125] Ian A. Hiskens, and A. Magnus, "Analysis of the Nordel power grid disturbance of January 1, 1997 using trajectory sensitivities", *IEEE Transactions on Power Systems*, vol. 14, no. 3, 1999, pp. 987-994.

[126] B. Sapkota, and V. Vittal, "Dynamic VAr planning in a large power system using trajectory sensitivities", *IEEE Transactions on Power Systems*, vol. 25, no. 1, 2010, pp. 461-469.

[127] Y. Del Valle, G. K. Venayagamoorthy, S. Mohagheghi, J. C. Hernandez, and R. G. Harley, "Particle swarm optimization: basic concepts, variants and applications in power systems", *IEEE Transactions on evolutionary computation*, vol. 12, no. 2, 2008, pp.171-195.

[128] S. Mirjalili, S. M. Mirjalili, and A. Lewis, "Grey wolf optimizer", *Advances in Engineering Software*, vol. 69, 2014, pp. 46-61.

[129] S. Mirjalili, and A. Lewis, "The whale optimization algorithm", *Advances in Engineering Software,* vol. 95, 2016, pp. 51-67.

[130] Y. Zhang, J. Zhou, Y. Zheng, Y. Xu, "Control optimisation for pumped storage unit in micro-grid with wind power penetration using improved grey wolf optimiser", *IET Generation, Transmission & Distribution*, vol. 11, no. 13, 2017, pp. 3246-3256.

Brief Bio-Data of the Author

Mr. Abhilash Kumar Gupta received his B.Tech. degree in Electrical Engineering from Rajasthan Technical University, Kota, Rajasthan, India in 2012, and M.Tech. degree in Electrical Engineering (Control Systems) from National Institute of Technology Patna, India in 2014. He completed his PhD in Electrical Engineering from Malaviya National Institute of Technology Jaipur, Rajasthan, India in June 2019. His research interests includes power system stability and control, Wide Area Monitoring and Control of power system, AI applications to power system and grid integration of renewables. He is Graduate Student Member of IEEE, USA and Member IET, UK.